KENS REPORT XVII

2009-2010

KENS REPORT XVII
High Energy Accelerator Research Organization

KENS REPORT XVII

2009-2010

High Energy Accelerator Research Organization
KENS

KENS REPORT XVII

2009-2010

PREFACE

The year of 2009 and 2010 were mostly dedicated to the construction of neutron instruments at J-PARC and were also the starting point of user programs. J-PARC commenced on providing neutrons with 120kW of its power comparable to the world-class pulsed neutron facility ISIS in 2009. By the end of 2010, the operational power of accelerator attained to over 200kW, which is still a fifth of scheduled full power but already the world leading pulsed neutron and muon source. Five instruments construction (as KEK beamlines) had been completed and some of those started user programs. In addition to these early scheduled instruments, three new installations of beamlines are planned. These construction and research activities in KENS are based on S-type projects of Institute of Materials Structure Science (IMSS). 11 projects have been approved by KENS-PAC in 2009 and each proposal is valid for 2-5 years under proposed period. Each project is annually assessed their total activities and achievements by KENS-PAC. Here we review S-type project scientific and instrumental activities as *KENS Report XVII (2009-2010)*.

In the end of the fiscal year of 2010 (March 2011), we had disaster of the *world-class* earthquake, and KEK also had not small damages at both Tokai and Tsukuba area. However, we are now refurbishing parts of the accelerator, beamline systems, instruments, and buildings to provide proper scientific research field. And we are further developing our instrument suite in J-PARC through constructing new instruments and beamlines. Finally, we are looking forward to further great science will be back here in KENS.

May 2011
Editor of KENS-Report XVII

Tetsuya YOKOO

CONTENTS

FACILTY REPORT

S-TYPE REPORT

KENS REPORT XVII

2009-2010

FACILITY REPORT

Neutron Science Laboratory

H.Seto

Head of KENS Neutron Science Division (KENS), Institute of Materials Structure Science, High Energy Accelerator Research Organization

1. From KENS Facility

The Inter-University Research Program

In FY2010, 11 special (S-type) proposals and 36 general proposals were accepted as part of the Inter-University Research Program on pulsed neutron science. General proposals to use the KENS beamlines were discussed at the J-PARC/MLF Neutron Science Program Advisory Committee; the scientific merit of these proposals was assessed. They were approved by the Neutron Science Program Advisory Committee (KENS-PAC) in IMSS. The S-type proposals, aiming at construction, development and maintenance of a neutron instrument for scientific research will be evaluated at the KENS-PAC in IMSS, and the funding has been approved for 3-5 years. The 5 accepted S-type research projects relate to existing neutron science instruments; the Super High Resolution Powder Diffractometer (SuperHRPD), High Intensity Total Scattering Diffractometer (NOVA), High Resolution Chopper Spectrometer (HRC), High Performance Neutron Reflectometer with a Horizontal Sample Geometry (ARISA-II/SOFIA), and the Neutron Optics and Physics (NOP). The S-type research project led by T. Fukunaga at Kyoto University has begun construction of a new diffractometer to perform in-situ investigation of Li-ion battery materials under the NEDO project. K. Ohyama at Tohoku University will construct a polarization chopper spectrometer in collaboration with KEK. M. Hino at Kyoto University have developed resonance type neutron spin echo spectrometers, and started designing at BL06. The development of other S-type projects will also start to be aimed at contributing to the improvement of future neutron science instruments.

2. Science at KENS

2.1 2D-Ising-like critical behavior in mixtures of water and organic solvent including antagonistic salt or ionic surfactant

The effect of an antagonistic salt, composed from hydrophilic cations and hydrophobic anions, on the phase behavior and nanoscale structure of a mixture of D_2O and 3-methylpyridine (3MP) was investigated by small-angle neutron scattering (SANS). The addition of the antagonistic salt, namely sodium tetraphenylborate ($NaBPh_4$), induces the shrinking of the two-phase region in contrast to the case in which a normal (hydrophilic) salt is added. The SANS profile of the mixture with D_2O and 3MP without salt can be well explained by the Ornstein-Zernike function below the phase separation point. The critical indices are the values of 3D-Ising behavior. On the other hand, the SANS profiles from mixtures with the antagonistic salt deviate from the Ornstein-Zernike function owing to the existence of a long-range periodic structure, which is induced by the coupling of solvation effect and critical concentration fluctuation. With increasing salt concentration, the critical exponents change from the values of 3D-Ising and approach those of 2D-Ising. These results suggest that the concentration fluctuation of the mixture of solvents is limited to a quasi two-dimensional space by the periodic structure induced by the adding the salt. The same behaviors were also observed in mixtures composed of water, 3MP, and ionic surfactant such as SDS and AOT.

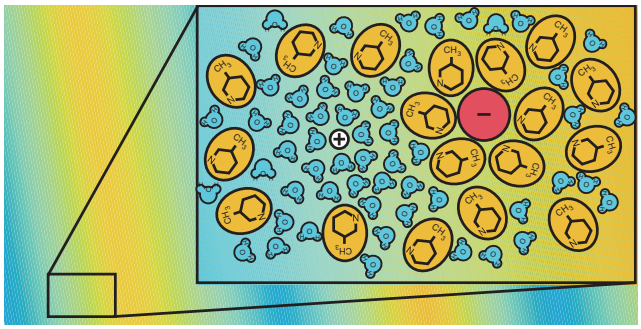

Fig. 1: Schematic picture of the periodic structure induced by the coupling of solvation effect and critical concentration fluctuation.

2.2 Structural and Hydrogen Desorption Properties of Aluminum Hydride

Aluminium trihydride (AlH_3, alane) is of interest as a possible hydrogen storage material because of its high gravimetric and volumetric hydrogen densities (10.1 mass% and 149 kgH^2/m^3, respectively) and its simple hydrogen desorption reaction of AlH_3 to Al ($AlH_3 \rightarrow$ Al

$+ 3/2H_2$) at 370–470K. Recently, it is revealed *in situ* microscopic observations and *in situ* X-ray photoelectron spectroscopy that AlH_3 particles (size 100 nm–1 mm) are covered by Al_2O_3 layer (thickness 3–5 nm) and, at room temperature, the hydrogen desorption reaction is prevented by the oxide layer on the surface of AlH_3; reaction begins only when the layer breaks up by thermal volume expansion of the underlying bulk AlH_3. The layer apparently forms after thermal desorption of the solvated ether from AlH_3–etherate, which is prepared by the following reaction between $LiAlH_4$ and $AlCl_3$ in ether solution.

$$3LiAlH_4 + AlCl_3 + n[(C_2H_5)_2O] \rightarrow 4AlH_3{-}n[(C_2H_5)_2O] + 3LiCl \rightarrow 4AlH_3 + 3LiCl + n[(C_2H_5)_2O]$$

To obtain precise structural information regarding the surface layer, we performed high-intensity neutron diffraction measurements by the high-intensity total diffractometer, NOVA, using 120 kW spallation neutron source in J-PARC and Rietveld analysis of α-AlD_3. The diffraction profiles show small diffraction peaks in addition to the peaks of α-AlD_3 in Fig. 2. These lattice spacing values for neutron and X-ray diffraction profiles are close to those of χ-Al_2O_3 (corresponding to 101–107% of the values in the literature). Therefore, the present result suggests that χ-Al_2O_3 forms on the surface of AlH_3 (AlD_3) by desorption of solvated ether. Furthermore, the short-range order (0.18 ± 0.021 nm for Al–O; 0.28 ± 0.058 nm for O–O; 0.32 ± 0.055 nm for Al–Al) of amorphous Al_2O_3 suggested by electron-energy-loss spectroscopy (EELS) may be observed under diffraction peaks of the crystal structures in Fig. 2.

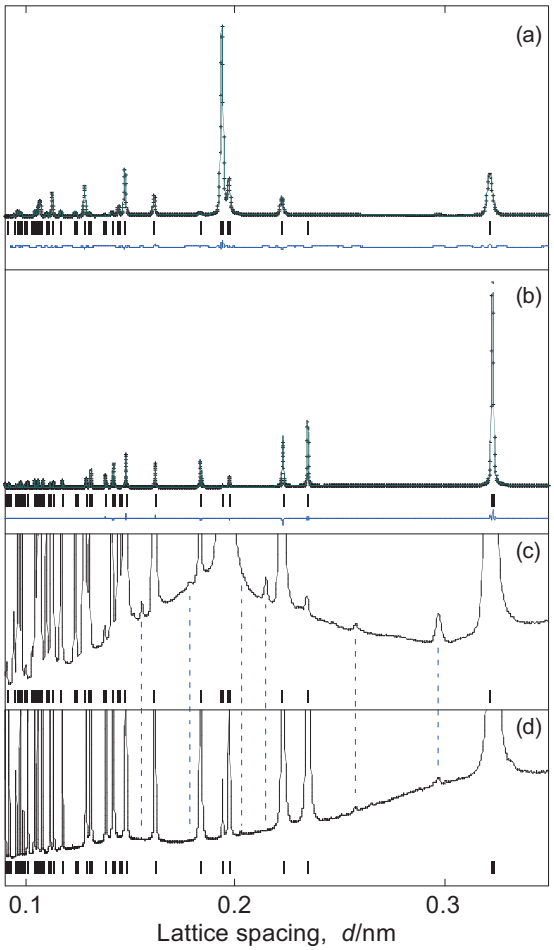

Fig. 2: High-intensity (a) neutron diffraction profile of α-AlD_3 and (b) X-ray diffraction profile of α-AlH_3 in linear scale. Rietveld refinement results: observed (cross), calculated (line), and residual (line below vertical bars) diffraction profiles. Tick marks show Bragg-reflection positions of α-AlD_3 and α-AlH_3. Vertical enlargements by 70 times of the diffraction profiles are shown in (c) for (a) α-AlD_3, and in (d) for (b) α-AlH_3, respectively. Positions except for α-AlD_3 and α-AlH_3 are shown by dashed lines.

2.3 Crystal Structure of a fast ionic conductor CuI

Copper iodide (CuI) shows two phase transitions at 440°C ($\beta - \alpha$) and 390°C ($\gamma - \beta$), and at the high-temperature α–phase, it shows fast-ion conductivity. We measured the time-of-flight (TOF) neutron powder diffraction data and synchrotron radiation X-ray diffraction (XRD) data and the extended x-ray absorption fine structure (EXAFS) data. We obtained crystal structural information of the both α– and γ–phases by Rietveld analyses of TOF and XRD data combined with the maximum-entropy-method (MEM), and local structural information by means of the pair distribution function (PDF) combined with the reverse Monte Carlo (RMC) simulation as well as EXAFS analyses.

The PDF analysis revealed the new split peaks in the partial pair correlation of Cu–Cu at $r = 2.47$ and 2.72 Å in the α–phase that correspond to the Cu – Cu diagonally distance between nearest neighboring tetrahedral corner ($32f - 32f$ sites in Fm-3m) and between tetrahedral center ($8c - 32f$ sites) such as represented by the split Cu site model. In the γ–phase, a better fit for EXAFS data was obtained with the split model than the non-split model, indicating the displacement of a copper atom to an iodine atom. The bond length difference of Cu – I pairs increased gradually with increasing temperature in the γ–phase. This suggests that a structural phase transition from γ–CuI to β–CuI does not occur suddenly at a certain temperature.

3. The J-PARC Project

Introduction

The user program started in December 2008, and in November 2009, the accelerator has been operated at 120kW from November 2009. In November 2010, the beam power increased over 200 kW and operated until the disaster on March 11, 2011. The 200 kW

stable operation has inspired both instrumental scientists and users, because experiments with small-size samples and/or higher resolution experiments are available. The 200 kW operation has also resulted in the increase in the number of users as well as the speed-up of the commissioning of instruments. Twelve instruments are operating in conjunction with the neutron beam and have started the user programs or are in the commissioning stages. Additional six instruments are under construction.

The Neutron International Advisory Committee (NIAC-2) was held from February 28 to March 2, 2011 in Tokai. The current status of neutron instruments and devices, management of experimental halls, the user program and support system, international activities and collaborations, and future plans were presented by members of MLF and then reviewed by the committee.

Neutron Optics and Physics (NOP)

The NOP beam line is under commissioning for the preparation of an experiment for the measurement of the neutron lifetime using the polarized beam branch. We measure both incident neutrons and decayed electrons using a time projection chamber (TPC). To reduce the background events efficiently, we have developed a spin flip chopper (SFC) system. Fig. 3 (left) shows the setup of a test experiment. The developed SFC and a prototype TPC are installed in the polarized beam branch. Using the unpolarized beam branch, we have produced mechanically decelerated ultra-cold neutrons (UCN) for the test measurement of optical devices and detectors for future measurement of the neutron electric dipole moment. We developed a Doppler shifter to decelerate very-cold neutrons from the unpolarized beam branch. Fig. 3 (right) shows the developed Doppler shifter. Using the low divergence beam branch, we are developing a multilayer interferometer for a pulsed neutron source and a new type of neutron spin echo system.

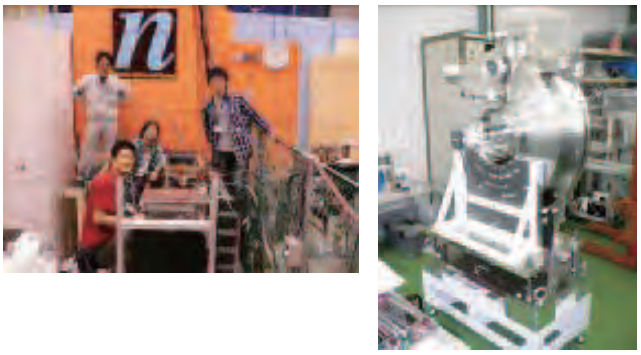

Fig. 3: left: NOP members setting up the experiment. right: the developed Doppler shifter.

Super High Resolution Powder Diffractometer (SuperHRPD)

Since SuperHRPD achieves the world best resolution of $\Delta d/d = 0.035\%$ in 2008, continuous development has been proceeding. In the summer of 2009, a new SuperHRPD chamber was installed in order to 1) improve the S/N ratio, 2) to achieve better resolution and 3) increase intensity. The new chamber consists of a backward bank with 384 (80 % of total) one-dimensional ^{3}He position-sensitive detectors (PSD's), a 90 degree bank with 288 PSD's (50 %), and a low-angle bank with 144 PSD's (30 %). In June, 2010, a MLF standard DAQ system was installed for the first time.

All parameters necessary for data correction were obtained twice through the two-times on-beam commissioning soon after the new chamber was installed and after the MLF standard DAQ system was installed. For the old DAQ system, it was confirmed data from the three banks were successfully analyzed with a newly developed software, Z-Rietveld. For the new DAQ system, backward bank data were successfully analyzed with Z-Rietveld. Z-Rietveld is now delivered to more than 100 users.

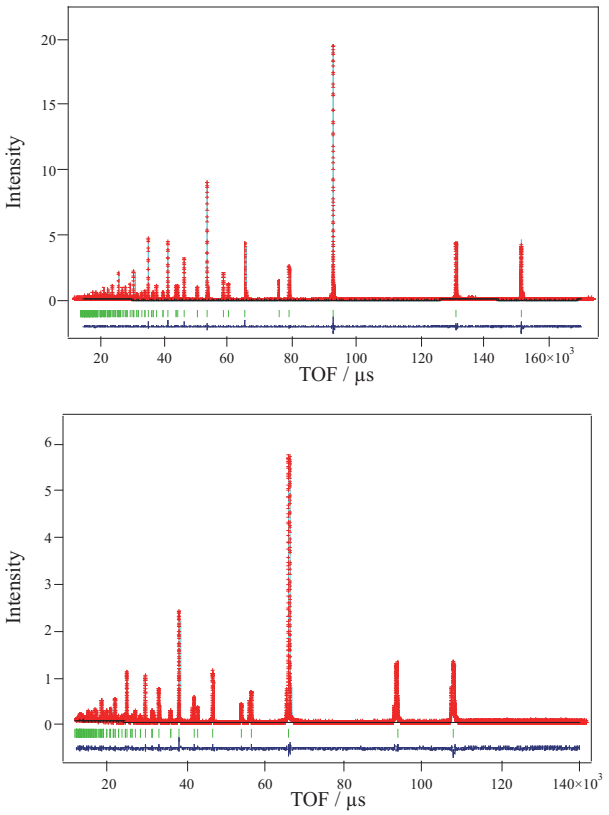

Fig. 4: Rietveld analyses of NIST Silicon data obtained with the backward bank and the 90 degree bank.

The High Resolution Chopper Spectrometer (HRC)

To study condensed-matter dynamics over a wide energy-momentum space with high resolution, we con-

structed the HRC at BL12 at J-PARC/MLF, under the collaboration between the University of Tokyo and KEK. With the construction nearly completed, we proceeded to characterize the HRC. We confirmed that, under limited conditions, the neutron intensity and energy resolution of the HRC agree well with the design values.

After the confirmation of the performance of the HRC, first, we measured magnetic excitations in the one-dimensional antiferromagnet $CsVCl_3$ at 20 K above the Néel temperature (T_N = 13.3 K), where the one-dimensional nature is dominant. It took 56 hours for the sample and 24 hours for the empty scan at 120 kW of proton-beam power. The intensity from the sample subtracted from the data for the empty scan is indicated in Fig. 5. We clearly observed the dispersion curve of the antiferromagnetic excitations starting at the magnetic zone center around $q \sim 1$ Å^{-1}, the excitations near the magnetic zone boundary near $q \sim 1.5$ Å^{-1}, and $E = 75$ meV, and the weak branch from the zone boundary to the nuclear zone ($q \sim 2$ Å^{-1}). This experiment indicates that the overall excitations can be clearly observed in 56 hours, which is expected to be reduced to only 7 hours when operating at full power (1 MW) at J-PARC. On the HRC, the counting rate is greatly improved by using long PSDs, and the energy and the momentum resolutions are also improved by intensities integrated within a PSD after correcting the energy transfers at the positions of detected neutrons with high-positional-resolution PSDs. As the result, the dispersion curve including the weak-intensity parts was clearly observed.

Also, inelastic neutron scattering experiments in a three-dimensional system MnP, which is a ferromagnetic intermetallic compound below T_C = 291 K, was performed. The dispersion relationship of ferromagnetic magnons in the energy momentum space exhibits a parabolic surface whose apex is on the reciprocal lattice point. Scattering intensities are observed on the ring crossing between the scanning surface of the detectors and the parabolic dispersion surface. The ring centered at (020) that is shown in Fig. 6 is the magnon intensity. Phonons also exist in the same position, so magnons could be separated from phonons by comparing the data at the paramagnetic state at 300 K.

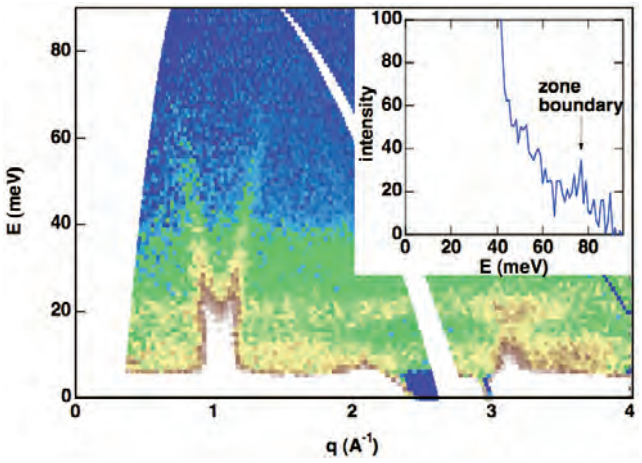

Fig. 5: Excitation spectrum in $CsVCl_3$ observed at 20 K with E_i = 100 meV on the HRC.

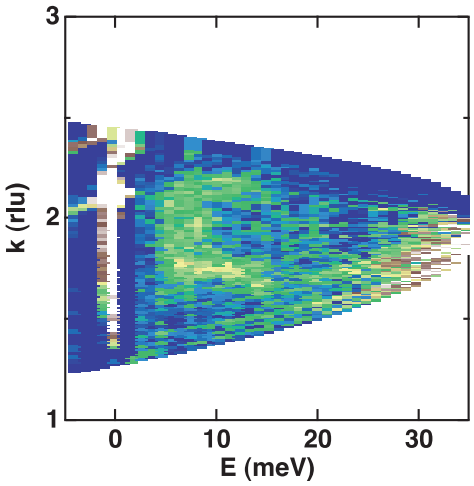

Fig. 6: Excitation spectrum in MnP observed at 60 K on the HRC.

The High Performance Neutron Reflectometer with a Horizontal Sample Geometry (ARISA-II/SOFIA)

Neutron reflectometry is one of the powerful tools for investigating the surface and interfacial structures of materials in the spatial range from nm to sub-μm. Because hydrogen and deuterium atoms have different scattering lengths for neutrons, this method can distinguish deuterated materials from normal ones in a mixture of soft-condensed matters, such as polymer blends, bio-mimic membranes, and so on. Furthermore, the high transmissivity of neutrons to materials enables us to probe deeply-buried interfaces such as solid/liquid interfaces in a non-destructive way.

ARISA-II was a horizontal-type neutron reflectometer at BL16, J-PARC/MLF. This reflectometer utilizes main components of ARISA reflectometer relocated from the KENS facility for temporal use, and has been in operation at J-PARC/MLF from 2008. In 2011, a newly developed T0 chopper and Ni/C mirror were installed to reduce background by fast and slow neutrons. Thanks to the upgrades, the S/N ratio has improved by one order of magnitude, and the observable reflectivity reaches 10^{-7}, which is a standard value for world-class neutron reflectometer at pulsed neutron source. Additionally, we replaced the main components relocated from Tsukuba campus with the brand-new ones by the support of JST/ERATO grant. In order to introduce incident neutron beam to free surface such as liquid/air interface, BL16 have two downward beam-

Fig. 7: Picture of the new reflectometer SOFIA from behind.

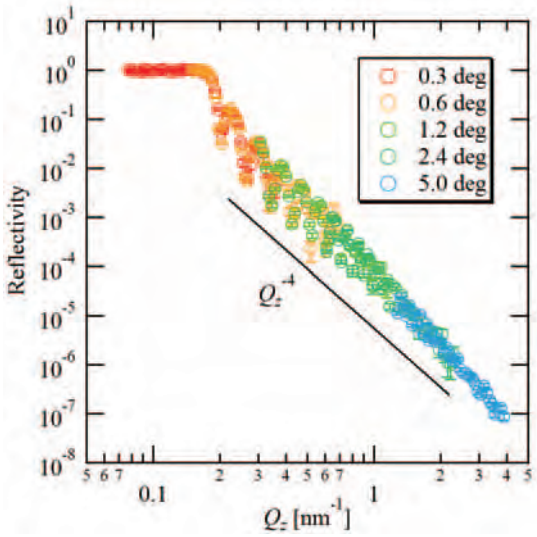

Fig. 8: Specular reflection of deuterated polystyrene thin film on Si substrate.

lines with different angle. By the installation of the new components, we could utilize both the beamlines for the first time. Figures 7 and 8 show the new reflectometer and typical reflectivity plot measured with new components. Due to the replacement of the new components, we renamed the reflectometer as SOFIA (SOFt Interface Analyzer).

The High Intensity Total Scattering Diffractometer (NOVA)

In FY2010, evaluation of instrument performance of the High Intensity Total diffractometer (NOVA) at BL21 was progressed. By performing neutron diffraction of various samples including liquids and amorphous, reliabilities of hardware and software have been confirmed. As a total diffractometer, high-Q value measurement of static structure factor, S(Q), is quite essential to obtain pair correlation function, g(r). It is confirmed that the statistical accuracy of S(Q) of

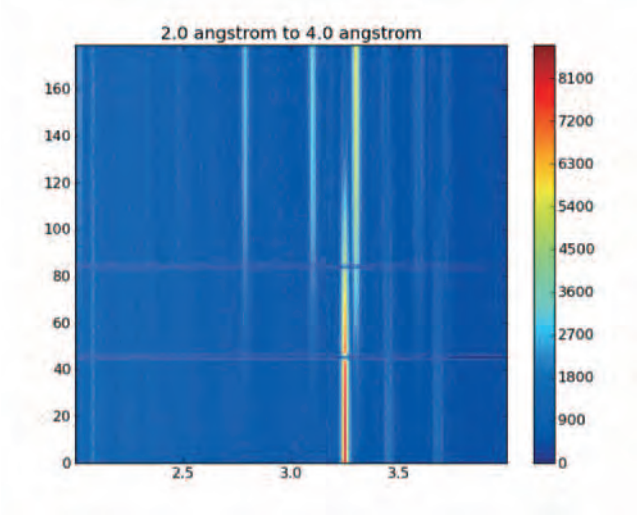

Fig. 9: A test measurement of time-transient phenomena on NOVA. Increasing of temperature according to time, the changing of diffraction pattern of $Li^{11}BD_4$ was successfully observed.

NOVA is the best in the world. Also, since the neutron intensity is very high, one-second measurement is feasible on NOVA. This means NOVA is powerful for time-transient phenomena. Figure 9 shows an example of time-transient measurement. With increasing of temperature according to time, the structure of a hydrogen storage material ($Li^{11}BD_4$) was changed from the low temperature phase to the high temperature one. Besides these high-performance of NOVA as a high-intensity neutron diffractometer, equipment's for hydrogen study has been fabricated and installed: 1) sample exchanger which can load 10-samples, 2) equipment for an in-situ experiment for H_2/D_2 gas atmosphere (max pressure is 10 MPa and temperature range is 50K $\sim$ 473K), and 3) a furnace of vanadium foil heater (room temperature to 1373 K). The performance of the in-situ gas equipment as pressure-composition-temperature (PCT) measurement was confirmed and neutron diffraction of $LaNi_5$-D_x was just successfully measured in the end of FY2010. With Fermi chopper, inelastic scattering experiments were performed on NOVA. With this device, R&D studies of incoherent-inelastic corrections of hydrogen atoms will be progressed to improve accuracy of hydrogen position information. It is expected that full-scale research of hydrogen storage materials will be starting soon. NOVA is supported by a NEDO project "Advanced Fundamental Research Project on Hydrogen Storage Materials (Hydro-Star)".

4. Device R&D

KENS DAQ Electronics

A neutron pulse-by-pulse recording, which is widely used in MLF/J-PARC, is expected for new method of

measurements such as observation of transient phenomena by pulsed neutron. In such measurements time sequential sample environment conditions are also necessary to know. We have developing an electronics module for event-recording such environment conditions, so called TrigNET. The TrigNET has fast and slow analog inputs and digital inputs, and generate event data based on spectrometer's local time. Figure 10 shows a prototype of the TrigNET. The board also has a fast data transfer technique by a network based on the SiTCP.

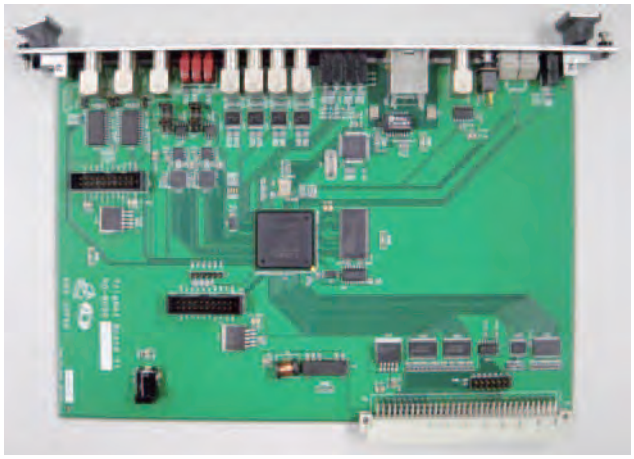

Fig. 10: The prototype of TrigNET module.

Most neutron scattering experiments, ^{3}He-gas position sensitive detectors (PSD) have been widely used. In general, gas counters are not good suited for high count rate detection, because of a property of long recovery time of gas counter. In high intensity neutron scattering experiments, the property limits a detection rate of neutrons. Therefore, new neutron detector alternate in ^{3}He PSD is required. The MPPC, multi pixel photon counter, is a new photon counting device which is consist of many avalanche photodiode (APD) pixels and is operated in room temperature. 1-dimensinal (1-D) neutron detector using MPPC has been developing. A principle of the detector is as follows, a neutron was detected by boron scintillator and scintillation light was spread in a grass, then diffused light was detected by several MPPC. The outputs of MPPCs were connected in series via registers, so total charge was divided into both ends. Figure 11 shows the prototype of 64 cells MPPC 1-D neutron detector. The average detection resolution was deduced as 2.8mm, and detection efficiency was 28 % compared with ^{3}He PSD by the neutron beam test.

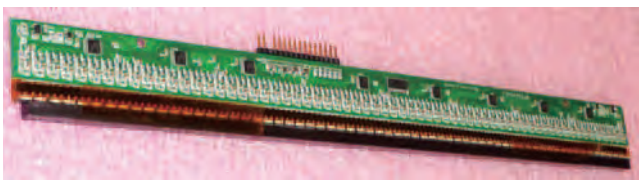

Fig. 11: The prototype of MPPC 1-D neutron detector.

Neutron Choppers

At KEK, T0 choppers and Fermi choppers have been developed under the collaboration between the Neutron Science Division (KENS) and the Mechanical Engineering Center (MEC). The T0 chopper is a key device to reduce the background noise that originates from high-energy neutrons emitted during neutron production. We developed and successfully installed the T0 chopper on the HRC at BL12 at J-PARC/MLF. Figure 12 (upper) shows the TOF spectrum from the standard vanadium sample detected at the PSD array with the T0 chopper rotating at 100 Hz, and with the T0 chopper off and the blade removed from the beamline. A Fermi chopper was operated to generate a monochromatic neutron beam. Since the collimation of the Fermi chopper is coarse, the neutron beam passes through the Fermi chopper every half turn, then many peaks appear. The neutron energy of the peak at TOF = 2000 μs corresponds to a neutron energy of 0.5 eV.

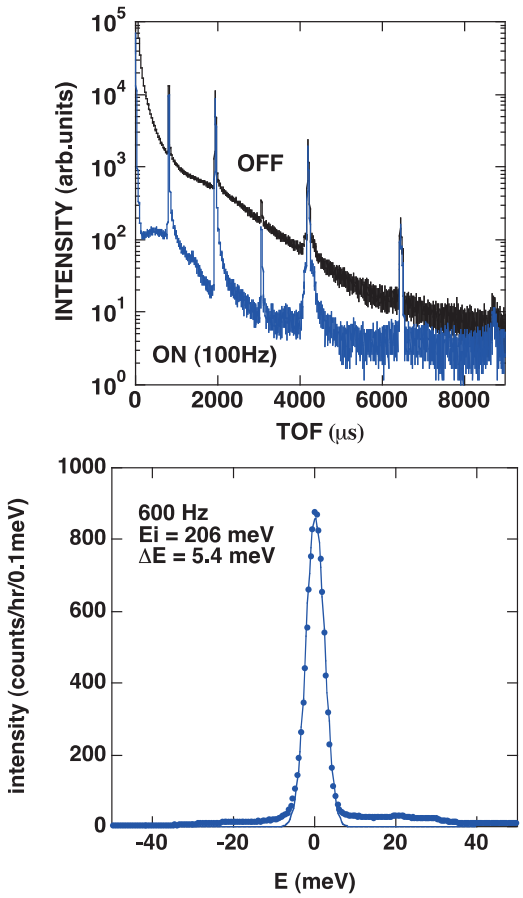

Fig. 12: Performance of neutron choppers developed at KEK. Upper: Effect of noise reduction by T0 chopper for the HRC. Lower: The energy spectrum of the monochromatic neutron beam from the Fermi chopper for the HRC.

We successfully reduced the background noise at neutron energies near 0.5 eV by two orders of magnitude. This indicates that inelastic neutron scattering experiments that require the detection of very small signals can be conducted on the HRC. Also, we developed and successfully installed the Fermi chopper on the HRC. Figure 12 (lower) shows the energy spectrum of the elastic scattering from the vanadium standard sample with operating the Fermi chopper at 600 Hz, and the width of the peak represents the energy resolution. We confirmed that the observed energy resolution well agrees with the design value. The Nishikawa Prize was awarded to this R&D works by the Foundation for High Energy Accelerator Science.

KENS REPORT XVII

2009-2010

S-TYPE REPORT

BL12: High Resolution Chopper Spectrometer (HRC)

S.Itoh, T.Yokoo, S.Satoh, S.Yano[1], D.Kawana, T.J.Sato[2], T.Masuda[2] and H.Yoshizawa[2]

Institute of Materials Structure Science, High Energy Accelerator Research Organization (KEK), Tsukuba 305-0801
[1]Graduate School of Science and Engineering, Aoyama Gaguin University, Sagamihara 252-5258
[2]The Institute for Solid State Physics, The University of Tokyo, Tokai 319-1106

The High Resolution Chopper Spectrometer (HRC) was installed at BL12 beamline at MLF, J-PARC, under the collaboration between the High Energy Accelerator Research Organization (KEK) and the University of Tokyo [1]. HRC delivers high-resolution and relatively high-energy neutrons for a wide range of studies on the dynamics of materials, and three types of experiments can be considered for HRC, as indicated in Fig. 1. The first technique targets high-resolution experiments in a conventional energy momentum space (region A in Fig. 1). This experimental condition is useful for simultaneously determining a dispersion relation of excitations and details of the dynamical structure factor. The second technique aims to access the first Brillouin zone by using low-angle detectors and high-energy neutrons (region B). Observation of ferromagnetic spin waves from a polycrystalline sample becomes possible and should be useful for material development. The third technique opens the possibility of accessing eV region (region C). Dispersive excitations up to a sub-eV energy region can be observed by using single-crystal samples. Electronic excitations are expected to be observed if eV neutrons are utilized.

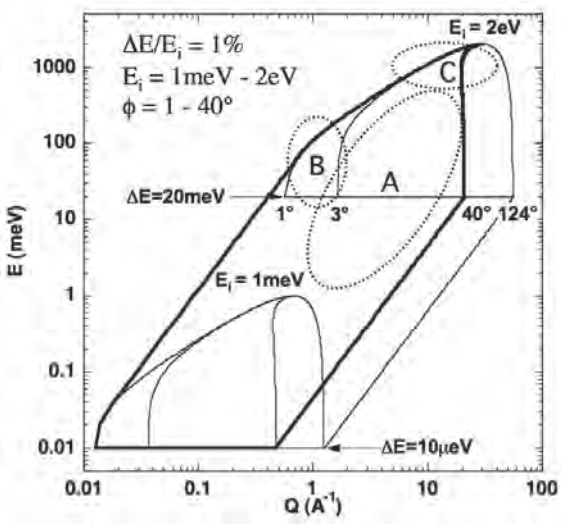

Fig. 1: Energy-momentum space for three techniques of high-resolution experiments A, B, and C proposed for HRC.

On a chopper spectrometer, a neutron beam is monochromatized by a Fermi chopper and then incident on a sample to be investigated. The neutrons scattered from the sample are detected by a neutron detector placed at a certain scattering angle. The energy transfer and momentum transfer from the neutron to the sample are determined by measuring the time-of-flight (TOF) and the scattering angle of the detected neutron. The Fermi chopper consists of a slit package inserted to a cylinder rotating in synchronization with the production timing of pulsed neutrons. Neutrons pass through the slit package when it rotates to a position of the slit parallel to the incident neutron beam, and the slit-open time (chopper-open time) determines the energy resolution of the spectrometer. High energy neutrons from the pulsed neutron source are scattered and moderated within the spectrometer, resulting in a large amount of background noise. A T0 chopper reduces this noise by blocking the incident neutron beamline at around time zero. Also, to increase the neutron flux, a supermirror guide tube is mounted in the primary flight path.

A schematic layout of HRC is illustrated in Fig. 2. The size parameters are $L_1 = 15$ m (the distance between the neutron source and the sample), $L_2 = 4$ m (the distance between the sample and the detector), and $L_3 = 1$ m (the distance between the Fermi chopper and the sample). HRC at BL12 facesthe decoupled moderator, which has an area of 100 mm × 100 mm, and the maximum sample size is assumed to be 50 mm × 50 mm. In this geometrical condition, the energy resolution is estimated to be $\Delta E/E_i = 2.5\%$ (E_i: incident neutron energy) for the optimum condition where the chopper-open time Δt_{ch} is equal to the pulse width Δt_m, and the incident beam divergence is estimated to be $\Delta\phi = 5$ mrad. The energy resolution can be improved when $\Delta t_{ch} < \Delta t_m$, with a concomitant reduction in the peak neutron intensity. For $\Delta E/E_i = 1\%$, the peak neutron intensity is 75% of that for the optimum condition, which we consider to be an acceptable tradeoff.

A supermirror guide tube was installed in the primary flight path at the shutter section (m = 3), the biological shielding section (m = 3.65) and the down

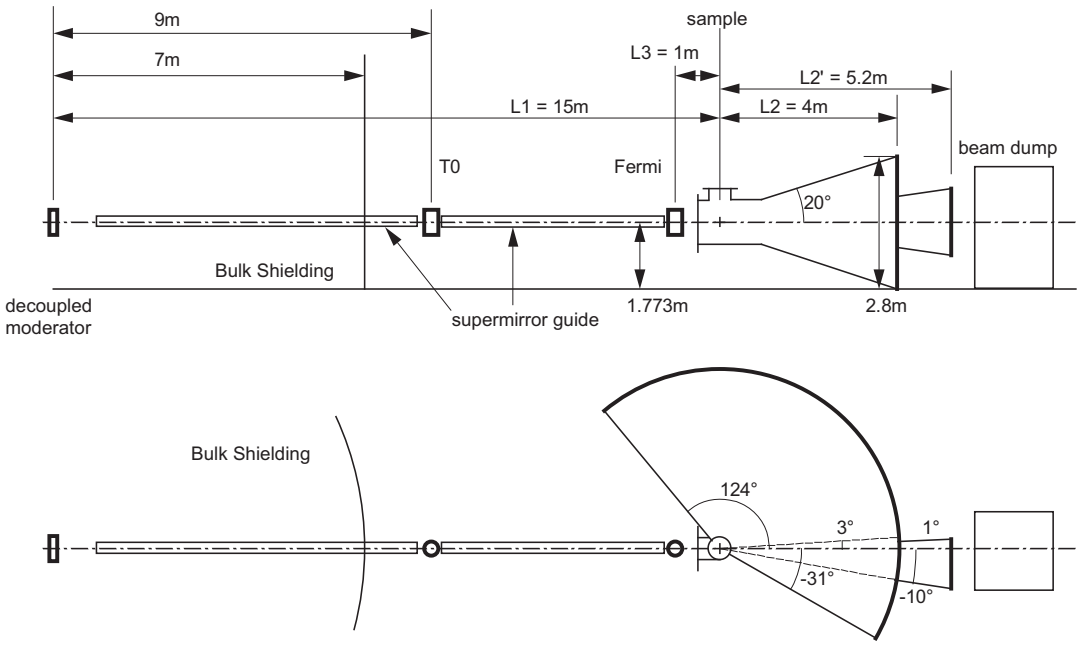

Fig. 2: Schematic layout of HRC.

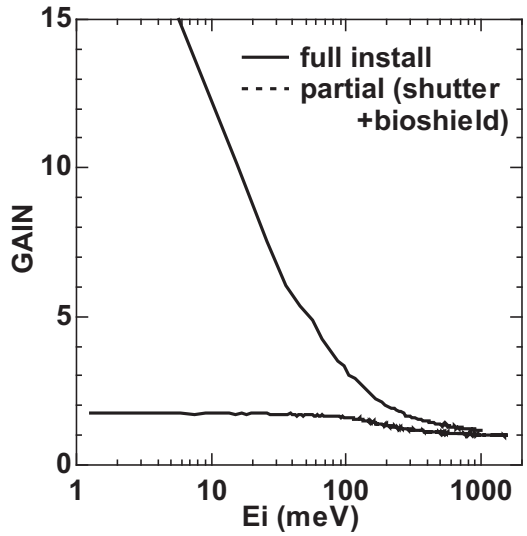

Fig. 3: Calculated flux gain of the guide tube on HRC. In the measurements in Figs. 5 (a) – (c), the guide tube was partially installed (dashed line).

stream section (m = 4), where m is the ratio of the critical wave number for the supermirror to that for natural nickel. The m values were determined by the financial budgets provided. The energy dependence of the flux gain of the guide tube was calculated by McStas, a large gain is expected, as shown in Fig. 3.

A T0 chopper [2] was installed 9 m from the neutron source. At this position, the beam cross section is 76 mm × 76 mm. The size of the T0 chopper blade is 78 mm × 78 mm, which includes a ±1 mm margin for the beam cross section. The length of the blade along the beamline is 300 mm, and the blade is made of Inconel X 750, which was chosen for its mechanical strength and radiation properties. When the blade center is initially centered on the beamline, it takes 408 μs for the blade to be removed from the beam cross section, and this occurs at a 100 Hz rotational frequency and for a 300 mm rotational radius. The rotational axis is parallel to and under the beamline. Under these conditions, HRC accepts neutrons with energy less than 2.5 eV. The margin of ±1 mm corresponds to a phase-control accuracy of ±5 μs at 100 Hz. We developed a phase control system which reduces the fluctuations in the rotational period down to 1 μs (FWHM) at 100 Hz at an off beam environment. Also, the fluctuations during beam time were measured to be approximately 3 μs (FWHM) at any rotational frequency. The observed fluctuations meet the requirement demanded by a phase-control accuracy within ±5 μs.

A newly developed Fermi chopper [3] is installed at L_3 = 1 m. We tried to develop the Fermi chopper by modifying a turbo molecular pump (TMP) with a magnetic bearing system. First, the TMP blade was replaced by the slit package, and we could rotate up to 600 Hz by the TMP controller. Next, we tried to design the phase control system of the Fermi chopper synchronized with the production timing of pulsed neutrons. We could drive the motor of this system by an external power supply and just by using the TMP controller as a magnetic bearing controller. Finally, we successfully developed the phase control system. Based on the developments, we produced the first model of the Fermi chopper made in Japan. The commercially available composites made of boron fibers were used for the slit materials. In this actual system, we confirmed

the phase control accuracy less than 0.1 μs (FWHM) at 600 Hz against the timing of the external trigger at an off beam environment. A shifting mechanism of two Fermi choppers was also developed in order to select one of the choppers or white beam condition.

We mounted 2.8 m (effective length) PSDs (position sensitive detectors) inside the vacuum scattering chamber. Although it was possible to install detectors from -31° to 124° in scattering angle, the detectors cover at present only from -10° to 40° because of the recent limitations in He-3 gas supplies. Therefore, the installed detector area is only 30% of the entire area. In the main detector area from 3° to 40°, 128 PSDs (effective length: 2.8 m, diameter: 0.75 inch, He-3 gas pressure: 1.8 MPa) were mounted inside the vacuum chamber for conventional experiments. At low angles from -10° to 1°, 123 shorter PSDs (0.8 m, 0.5 inch, 2 MPa; 0.6 m, 0.5 inch, 2 MPa; 0.6 m, 1 inch, 1 MPa; used at KENS or newly acquired) were mounted; some at $L_2 = 4$ m and the rest at $L_2 = 5.2$ m at the lowest angles. These detectors are for experiments involving low-angle inelastic neutron scattering.

The data acquisition (DAQ) system for HRC is illustrated in Fig. 4. Signals generated at a PSD are amplified by preamplifiers and sent to a readout module called NEUNET. When a neutron is captured at PSD n_{det}, the charge generated at both ends of the PSD is digitized and converted to digital pulse heights Q_1 and Q_2 by an analog-to-digital converter (ACD) in the NEUNET where, in an ideal case, the position u of the detected neutron within the PSD is given by $u = L_D Q_2/(Q_1+Q_2)$ with the PSD length L_D. A timing signal from the accelerator defining $t = 0$ is delivered by a GATENET to NEUNETs and the TOF of the detected neutron (t) is determined at the NEUNET. The timing signal is gated by the device status, which is the phasing status of the Fermi chopper and the T0 chopper with respect to the timing, the temperature of the sample, etc. Thus, the GATENET does not forward the timing signal to the NEUNET unless the device status indicates that all devices are operational. For detection

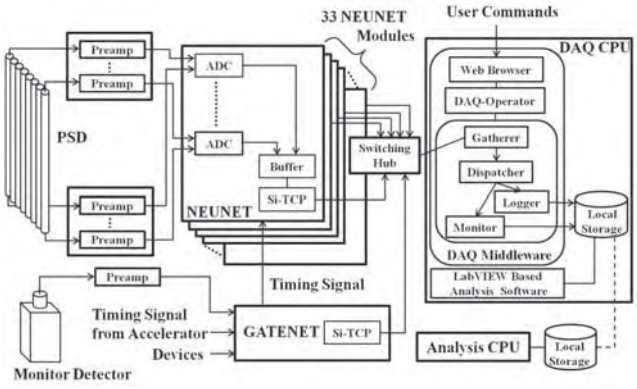

Fig. 4: DAQ system installed on HRC.

of a single neutron, the set $\{n_{det}, Q_1, Q_2, t\}$ is generated as an event datum (8 bytes/event) on the NEUNET. Event data can be accessed through a computer network with SiTCP. In addition, event data from the monitor detectors can be accessed at the GATENET module through the computer network with SiTCP. One NEUNET, which uses the VME standard, controls 8 PSDs. A 19-inch VME rack can contain up to 20 NEUNETs for 160 PSDs. On HRC, 251 PDSs are controlled by 33 NEUNETs, and a GATENET is also mounted on the VME rack. The event data are transferred by the computer network from the NEUNETs to the central processing unit (CPU). We prepared a CPU (POWER MASTER Server A8452 from System Works Co.) as the CPU for the DAQ system (DAQ CPU), and installed Scientific Linux 5.4 as well as the DAQ middleware. Via the DAQ-Middleware, the DAQ-Operator configures the DAQ system and controls some DAQ-Components that control processes in the DAQ system. User commands such as begin/end of the data acquisition can be sent to the DAQ system through a web-browser user interface.

To evaluate the HRC performance, a vanadium standard sample was mounted at the sample position on HRC. A monochromatic neutron beam with the Fermi chopper or a white neutron beam without the Fermi chopper was incident on the sample, and the scattered neutrons were detected with the array of 128 PSDs located at scattering angles between 3° and 40°. A monitor detector was located at 13.4 m from the neutron source (just upstream of the Fermi chopper). The neutron intensities detected by the monitor and that detected by the PSD array for the white beam are plotted in Figs. 5(a) and 5(b). The observed intensities were in good agreement with the calculations in the absolute values within a factor. Figure 5(c) shows the elastic scattering energy spectrum from the vanadium standard sample and detected by the PSD array for the incident neutron energy of $E_i = 203$ meV, with the optimum chopper (which provides roughly $\Delta t_{ch} = \Delta t_m$) at 600 Hz, as a function of the energy transfer. We chose $E_i = 203$ meV because the neutron transmission through the optimum chopper shows a maximum at 200 meV. The solid line is a calculated spectrum without any adjustable parameters. The energy resolution from the observed energy width was obtained to be $\Delta E = 5.2$ meV by a Gaussian fit to the observed spectrum, and therefore $\Delta E/E_i = 2.5\%$. At $E_i = 203$ meV, the absolute magnitude of the neutron intensity for a monochromatic beam agreed with the calculation, and also it was confirmed that $\Delta E/E_i = 2.5\%$ in the energy resolution as designed for the optimum condition. Assuming the optimum condition ($\Delta E/E_i = 2.5\%$ with $\Delta t_{ch} = \Delta t_m$) for any E_i, the neutron flux for inelastic neutron scattering experiments at the sample position with a 1 MW proton beam for full installation of the guide tube is estimated as shown in Fig. 5(d).

The T0 chopper is a key device to reduce the background noise that originates from high-energy neutrons emitted during neutron production. Figure 6(a) shows the TOF spectrum observed at the PSD array from the standard vanadium sample with the T0 chopper running at the rotational frequency of 100 Hz, and with the T0 chopper off and the blade removed from the beamline. The sloppy chopper was used as the Fermi chopper and operated at 600 Hz. Since the slit width of the sloppy chopper is coarse, the neutron beam passes through the sloppy chopper every half turn, then many peaks appear. The neutron energy of the peak at TOF = 2000 μs corresponds to 0.5 eV. We successfully reduced the background noise at neutron energies near 0.5 eV by two orders of magnitude. This indicates that inelastic neutron-scattering experiments that require the detection of very small signals can be conducted on HRC. Figure 6(b) shows the dependence of the T0 chopper transmission on the TOF spectrum obtained from the standard vanadium sample and detected at the PSD array with the white neutron beam. We confirm that the transmission recovers below 2.5 eV of the neutron energy at 100 Hz, as designed. The energy for 50% transmission at 100 Hz is 10 eV, and then neutrons with energies up to several eV can be used with only a slight reduction in neutron intensities.

After the confirmation of the performance of HRC, first, we measured magnetic excitations in the one-dimensional antiferromagnet $CsVCl_3$ at 20 K above the Néel temperature (T_N = 13.3 K), where the one-dimensional nature is dominant. It took 56 hours for the sample and 24 hours for the empty scan at 120 kW of proton-beam power. The intensity from the sample subtracted from the data for the empty scan is indicated in Fig. 7. We clearly observed the dispersion curve of the antiferromagnetic excitations starting at the magnetic zone center around q $\sim$ 1 Å^{-1}, the excitations near the magnetic zone boundary near q $\sim$ 1.5 Å^{-1}, and E = 75 meV, and the weak branch from the zone boundary to the nuclear zone (q $\sim$ 2 Å^{-1}). This experiment indicates that the overall excitations can be clearly observed in 56 hours, which is expected to be reduced to only 7 hours when operating at full power (1 MW) at J-PARC. On HRC, the counting rate is greatly improved by using long PSDs, and the energy and the momentum resolutions are also improved by intensities integrated within a PSD after correcting the energy transfers at the positions of detected neutrons with high-positional-resolution PSDs. As the result, the dispersion curve including the weak-intensity parts was clearly observed.

Also, inelastic neutron scattering experiments in a three-dimensional system MnP, which is a ferromagnetic intermetallic compound below T_C = 291 K, were performed. The dispersion relationship of ferromagnetic magnons in the energy momentum space exhibits a parabolic surface whose apex is on the reciprocal lattice point. Scattering intensities are observed on the ring crossing between the scanning surface of the detectors and the parabolic dispersion surface. The ring centered at (020) shown in Fig. 8 is the magnon intensity. Phonons also exist in the same position, so magnons could be separated from phonons by comparing the data at the paramagnetic state at 300 K.

In summary, the construction of HRC is nearly complete except for the coverage of the PSD array and we have characterized its performance. We confirmed

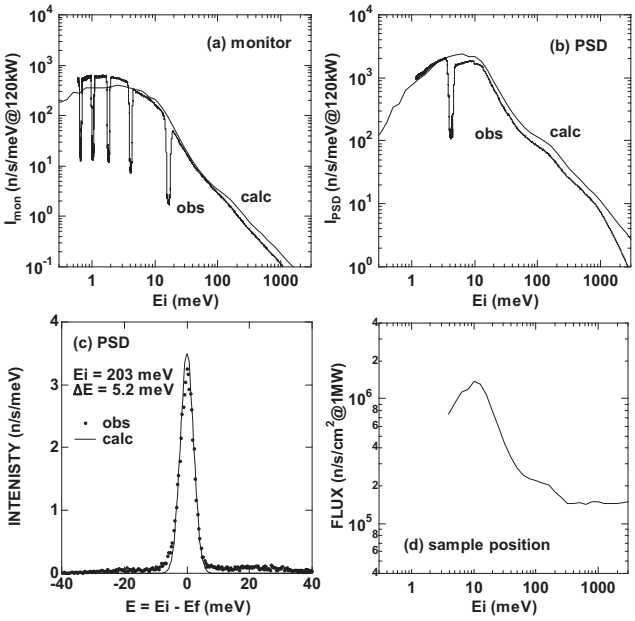

Fig. 5: Neutron intensities at the monitor (a) and at the PSD array (b) for white neutron beam. The dips in the observed data are caused by the operation of the T0 chopper. (c) Elastic-scattering energy spectrum at PSD array for vanadium standard sample with E_i = 203 meV. (d) Expected neutron flux at sample position for the optimum condition $\Delta E/E_i$ = 2.5% for 1 MW proton beam.

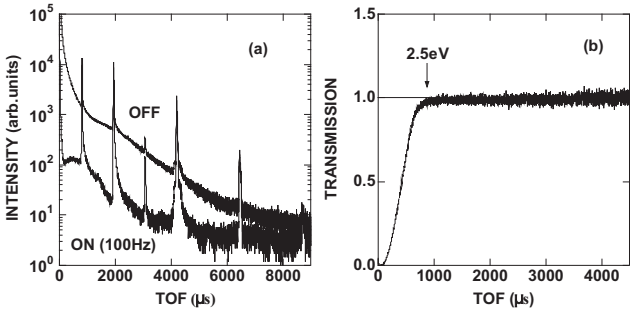

Fig. 6: (a) Background noise reduction for monochromatic neutron beam. The TOF spectra with operating the T0 chopper at 100 Hz (ON) and without operation (OFF) are indicated. (b) TOF dependence of the transmission at 100 Hz measured with the white neutron beam.

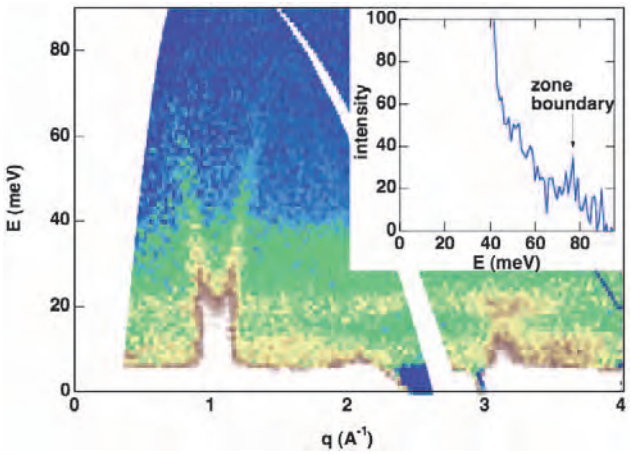

Fig. 7: Excitation spectrum in $CsVCl_3$ observed at 20 K with E_i = 100 meV on HRC. The inset shows the energy spectrum observed at a detector whose scan trajectory passes through the magnetic zone boundary.

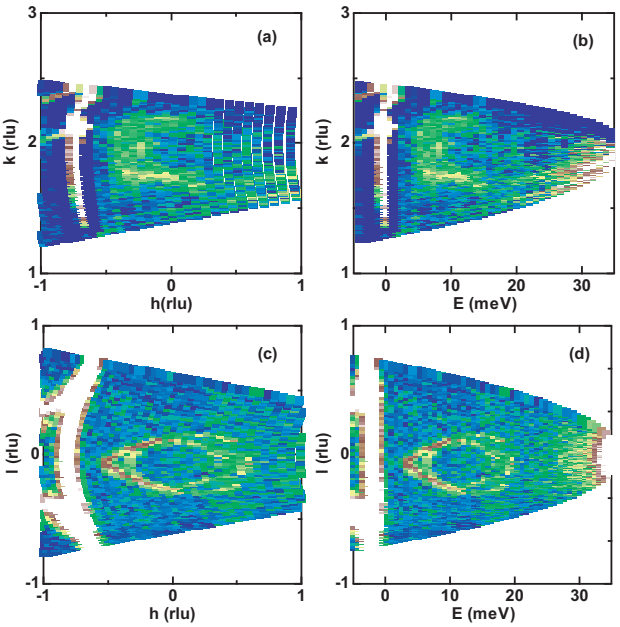

Fig. 8: Excitation spectrum in MnP observed at 60 K with E_i = 35.8 meV on HRC: (a) (h, k) plane with l = 0, (b) (h, E) plane with l = 0, (c) (h, l) plane with k = 0, and (d) (l, E) plane with k = 0.

that, under limited conditions, the neutron intensity and the energy resolution were in good agreement with the design values. Also, we verified the data analysis process by visualizing excitations in one- and three-dimensional single-crystal magnetic systems in inelastic neutrons scattering experiments.

References

1) S. Itoh, T. Yokoo, S. Satoh, S. Yano, D. Kawana, J. Suzuki and T. J. Sato, Nucl. Instr. Meth. Phys. Res. **A 631** (2011) 90.
2) S. Itoh, K. Ueno, R. Ohkubo, Y. Funahashi, H. Sagaheshi, T. Yokoo, T. J. Sato, T. Otomo and S. Satoh, ICANS XIX (2010) IP121.
3) S. Itoh, K. Ueno, T. Yokoo, Y. Funahashi, T. Kamiyama, H. Sato, N. Miyamoto, Y. Kiyanagi, T. J. Sato, T. Otomo and S. Satoh, ICANS XIX (2010) IP120.

Time of Flight Neutron Diffractometer Dedicated to Structural Biology

T.Chateke, Y.Morimoto, K.Kusaka*, I.Tanaka*, N.Niimura*

Research Reactor Institute, Kyoto University, 2 Asashironishi, Kumatori, Osaka, 590-0494, Japan.
**Frontier Research Center for Applied Atomic Sciences, Ibaraki University, 162-1 Shirakata, Tokai, Ibaraki, 319-1106, Japan*

In this study, we have designed a new-type of time-of-flight (TOF) neutron diffractometer dedicated to neutron protein crystallography (NPC), and estimated its performance from diffraction experiments using the IBARAKI biological crystal diffractometer (iBIX). [1)]

Last year, we had designed the Neutron Structural Biology Diffractometer (NSBD) to be installed at J-PARC. [2)] Hydrogen atom (H) and its cation (H^+) regulate various biological functions via hydrogen bonds and electrostatic interaction. Moreover, water molecules (H_2O) surrounding biomolecules form cluster structures, which contribute to information transfer and stabilization of the three-dimensional structure of biomolecules. Consequently, in order to understand biological phenomena, it is essential to determine the positions of the H and H^+ in biomolecules. NPC is one of important techniques for determining H and H^+, because NPC has the capacity of detecting H and H^+ even at medium resolutions. There are three neutron diffractometers for NPC in Japan; monochromatized neutron diffractometers BIX-3, BIX-4 and TOF diffractometer iBIX. iBIX is the most powerful among these diffractometers, because the high flux of the pulsed neutron beam is available. We have planed NSBD as the second diffractometer for NPC. iBIX belongs to Ibaraki prefecture in Japan, and it is mainly used for industrial purposes, and hence, its utilization in academics is limited. Moreover, iBIX is used both for researches on small molecules and large molecules; therefore, it is not suitable for the measurement of a large lattice dimension. On the other hand, the main aim of NSBD is an inter-university research, and the specification of NSBD is specialized for large crystal lattices of biomacromolecules.

The predicted performance of NSBD is summarized in Table 1. The NSBD would support large lattices and high resolution. These values correspond to those found in 96.3% and 94.8% of X-ray crystallographic analyses of macromolecules, respectively. The experimental measurement time was estimated to be one week, and diffraction experiments of more than 20 protein crystals per year could be carried out. Moreover, The NSBD would ensure so large space around the sample (5 m^2) that various optional devices could be installed in the experiment. Schematic diagrams of the diffractometer are shown in Fig. 1. The NSBD, like iBIX, is equipped with a super-mirror guide tube. The tube is curved so that the sample is protected from radiation damage, which is caused by burst gamma ray. The tail cutter is located at a distance of 8 m from the moderator; it selects neutrons with wavelengths between 1.5 and 4.2 Å. The temporal resolution of the pulsed neutron beam is improved because the distance between the moderator and the sample is large (L_1 = 60 m). The NSBD consists of neutron image detectors composed of wavelength-shifting fiber (WLSF); these detectors are used in iBIX. The WLSF has a two-dimensional sensor. WLSFs are arranged such that they resemble a fan. The distance from the sample to each detector (L_2) is 600 mm, which is selected so that the spatial resolution is guaranteed to be sufficient for identifying diffractions from large lattices. In addition, the large experimental area enables us to include various optional equipments such as a dynamic polarized pro-

Table 1: The predicted performance of NSBD.

Diffractometer	NSBD	iBIX (J-PARC)
Max. unit cell	200 Å	135 Å
d_{min}	1.4 Å	0.7 Å
Crystal size	0.5×0.5×0.5 mm^3	1.0×1.0×1.0 mm^3
Experimental time	1 week	1 week
Experimental area	5 m^2	0.6 m^2
Equipment	PPM	cooling device

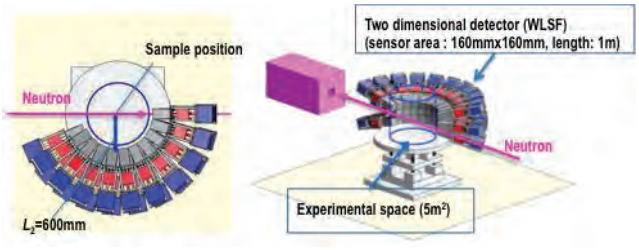

Fig. 1: Schematic views of NSBD.

ton device (described in the later).

In order to estimate the performance of NSBD, it is essential to evaluate those of iBIX as the comparison. In FY2010, four NPC experiments were carried out using iBIX. Ribonuclease A (RNaseA) and human hemoglobins (Hb) were carried out by our group. RNase A was the first protein used in iBIX. The volume of RNase A crystal was 4.7 mm^3, and the power of J-PARC was 120 kW. Fourteen WLSF detectors were used in this experiment. Fig. 2 shows an example of neutron diffraction image recorded on WLSF. In order to collect the complete data set of RNase A, 66 frames were taken with different orientations of the crystal. A total experimental time was 15.7 d.

Previously, a NPC experiment of RNase A was carried out using monochromatized neutron diffractometer BIX-4 at the reactor JRR-3M.[3)] These two experiments were compared in Table 2. Although the volume of crystal was 1/3 the size of BIX-4 and the power of J-PARC was 1/8 of the maximum and the number of available detectors were 14, iBIX demonstrated approximately the same performance as BIX-4, and the results would suggested that the performance of the iBIX would be dozens of times of BIX-4 as expected.

We have estimated the performance of NSBD from those of iBIX. The efficiencies of guide tube, band width and solid angle of detectors are 80-90%, 85% and 56% of iBIX, respectively. The total performance is calculated to be 40%. If the number of detectors (30) becomes twice (60), The performance is improved to be 80%. Assuming that a crystal has mmm symmetry and its volume is 1 mm^3, the NSBD can collect one neutron data set with completeness of 90% for 3.25 d.

Recently, we carried out NPC experiments of Hb using iBIX. Two kinds of Hb crystals were used; adult human deoxyhemoglobin obtained from PEG solution (deoxyHb-PEG) and adult human carbomonoxyhemoglobin (COHb). Previously, crystals of deoxyHb-PEG were tested using BIX-4 and Protein Crystallography Station (PCS) at LANSCE. Only poor diffraction images could be obtained using BIX-4, and ∼3.5 Å diffraction images could be obtained using PCS (100 kW), while iBIX could provide 3.0-3.5 Å diffraction images, indicating the present performance of iBIX comparative to PCS. An amazing result was obtained from COHb (Fig. 3, left). We found diffractions at 2.4 Å resolution on the diffraction image (Fig. 3, right). The present result showed the capability of iBIX, which can measure a crystal of a larger unit cell than the estimated one. The nominally maximum length is 135 Å for iBIX, meanwhile the length of the c-axis of the crystal of COHb was 196.4 Å. Neighboring diffraction spots around 2.4 Å resolution can be separated in case of this crystal, indicating that iBIX can support larger crystal lattices (∼200 Å) if the effective resolution is medium.

Table 2: The comparison between iBIX and BIX-3.

Diffractometer	iBIX	BIX-4
$V_{crystal}$	4.7 mm^3	14 .0 mm^3
Source	J-PARC (120 kW)	JRR-3M (20 MW)
Effective Res.	1.7 Å	1.7 Å*
Experimental time	15.7 d	32d

* d_{min} was 1.4 Å. The effective resolution was estimated to be 1.7 Å, because of low completeness in the high resolution shell.

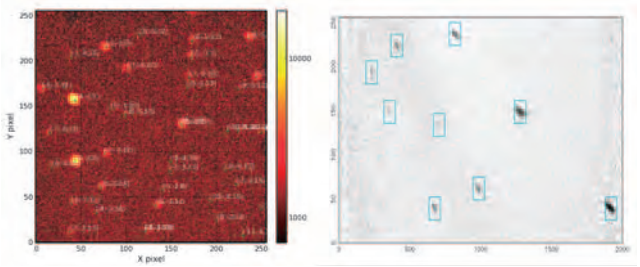

Fig. 2: Neutron diffractions of RNase A obtained by iBIX.

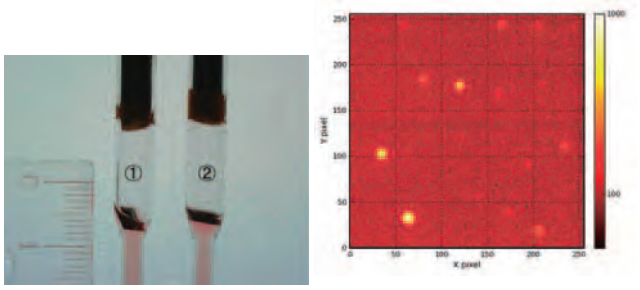

Fig. 3: Crystals of COHb (left) and neutron diffractions of COHb (right).

The present study showed iBIX could support large crystal lattices (∼200 Å) in case of crystals of normal quality (2-2.5 Å). NSBD is expected to support 300 Å for such a case. However, crystals having large lattices usually give weaker reflections than those of small lattices. In order to guarantee NPC experiments for a large crystal lattice, some improvements of neutron diffraction techniques would be necessary.

One of promising new techniques for NPC is proton polarization method (PPM). Nearly all NPC experiments were carried out using deuterated crystals, because H has a large neutron incoherent-scattering cross section and a lower neutron scattering length than a deuterium atom (D). However, there always remains the question of whether or not the deuteration affects the folding structure of the protein, because the living cells that produce the protein never live in nature in a D_2O environment for so long.

PPM is one of answers to this question. The effec-

tive coherent scattering length of H, as a function of the polarization, P, of its nuclear spin, is given by the following equation:

$b = (-0.275+1.46P)\cdot 10^{-12}$ cm

When the proton is not polarized, P equals 0, and $b^{(0)} = -0.375\cdot 10^{-12}$ cm. When the proton is 100 % polarized and the polarization is parallel to the neutron, P equals 1, and $b^{(++)} = 1.085\cdot 10^{-12}$ cm. When the proton is 100 % polarized but the polarization is anti-parallel to the neutron, P equals -1, and $b^{(+-)} = -1.835\cdot 10^{-12}$ cm. Thus it is seen that the effective coherent-scattering lengths of H atoms with parallel and anti-parallel spins, relative to the neutron polarization, are very different from each other. If this nature could be exploited, it would be a unique way to determine the position of the H atoms in proteins.

In PPM, ideally, H in all of protein molecules in a single crystal must be polarized. This technique has been already successfully realized in the case of insulators and reported. A small amount of paramagnetic centers is added to the sample. In a moderately strong magnetic field of 2.5 T at temperatures less than 100 mK at least, microwave irradiation will polarize the nuclear spins. Secondly, the neutron beam must be polarized parallel to the protein protons and then used to make a typical diffraction experiment. Thirdly, the neutron polarization must be reversed, and another diffraction experiment should be made. The technique of producing polarized neutrons is well established.

The polarization of protons in protein molecules in solution has been tried successfully. However, the polarization of protons in protein molecules in a single crystal has never been tried yet. The remaining significant hurdles are, (1) how to dope the crystal with paramagnetic materials, which are essential to initialize the polarization of protons, and (2) how to realize the cooling of a protein crystal at 100 mK. In this study, we carried out the preliminary experiment of obtaining the doped crystal. 2,2,6,6-tetramethylpiperidine-1-oxyl (TEMPO) was used as paramagnetic centers. 3.75-30 mM TEMPO was added in crystallization solution of hen-egg-white-lysozyme (HEWL) and ribonuclease A (RNase A). There are no apparently differences in microscope between crystals obtained from solutions with/without TEMPO. Mass spectroscopy showed the presence of TEMPO in the TEMPO-doped HEWL crystals. X-ray crystallographic analyses show no electron density of TEMPO, indicating that the nonlocalizational presence of TEMPO in the crystals. The second hurdle might be overcome by the development of the technique of high-pressure cooling of protein crystals. Further preliminary experiments would be necessary to realize PPM in NPC.

In the present study, we carried out neutron diffraction experiment of protein crystals using iBIX, and estimated the performance of NSBD that we have designed as a next neutron diffractometer for NPC. The NSBD would work with good performance as we expected, however further improvement would be necessary for an efficient neutron experiment for crystals having large lattices. PPM would be a plausible candidate for such improvement. We concluded that a next-generation neutron diffractometer for NPC would be a TOF-PPM type.

References

1) I. Tanaka *et al.*, Acta Crystallogr. **D66** (2010) 1194-1197.
2) T. Chatake *et al.*, Seibutsubutsuri **50**, suppl. 2 (2010) S4.
3) D. Yagi *et al.*, Acta Crystallogr. **D65** (2009) 892-899.

Studies of Neutron Optics for Physics Researches

Y.Arimoto[a], N.Higashi[a], T.Ino[a], K.Mishima[a], T.Morishima[a], S.Muto[a], H.M.Shimizu[a,f,i,j,*], K.Taketani[a], N.L.Yamada[a], T.Yoshioka[a,1], T.Shima[b], H.Funahashi[c], M.Bleuel[d,2], M.Hino[d], Y.Kawabata[d], M.Kitaguchi[d], M.Ichikawa[e], Y.Iwashita[e], T.Kanaya[e], S.Nakamura[e], Y.Tajima[e], H.Tongu[e], M.Yamada[e], H.Fujioka[f], S.Imajo[f], T.Nagae[f], T.Tanimori[f], S.Tasaki[g], K.Asahi[h], K.Hirota[i], K.Ikeda[i], J.Ju[i], A.Makinouchi[i], H.Ohmori[i], Y.Otake[i], H.Sato[i], Y.Seki[i], H.Sunaga[i], Y.Yamagata[i], Y.Yamagata[i], A.Yoshimi[i], F.Hiraga[j], H.Iwasa[j], H.Iwashita[j], T.Kamiyama[j], Y.Kiyanagi[j], H.Oide[k], H.Otono[k], S.Yamashita[k], G.Ichikawa[l], Y.Kamiya[l], S.Kawasaki[l,3], S.Komamiya[l], T.Ebisawa[m], R.Maruyama[m], T.Oku[m], K.Sakai[m], T.Shinohara[m], J.-i.Suzuki[m,4], D.Yamazaki[m], K.Niita[n], S.J.Kennedy[o], K.Andersen[p], P.Geltenbort[p], B.Guerard[p], G.Manzin[p], J.M.Carpenter[q], J.Lal[q], B.J.Micklich[q], R.Pynn[r]

[a]*High Energy Accelerator Research Organization (KEK), 1-1 Oho, Tsukuba, Ibaraki 305-0801, Japan*
[b]*Research Center for Nuclear Physics, Osaka University, Ibaraki, Osaka 567-0047, Japan*
[c]*Institute for the Promotion of Excellence in Higher Education, Kyoto University, Yoshida, Kyoto 606-8501, Japan*
[d]*Research Reactor Institute, Kyoto University, Kumatori, Osaka 590-0494, Japan*
[e]*Institute for Chemical Research, Kyoto University, Gokasho, Uji, Kyoto 611-0011, Japan*
[f]*Faculty of Science, Kyoto University, Kitashirakawa, Kyoto 606-8502, Japan*
[g]*Faculty of Engineering, Kyoto University, Yoshida, Kyoto 606-8502, Japan*
[h]*Department of Physics, Tokyo Institute of Technology, 2-12-1 O-Okayama, Meguro, Tokyo 152-8551, Japan*
[i]*RIKEN, 2-1 Hirosawa, Wako, Saitama 351-0198, Japan*
[j]*Faculty of Engineering, Hokkaido University, Sapporo, Hokkaido 060-8628, Japan*
[k]*International Center for Elementary Particle Physics, University of Tokyo, Hongo, Bunkyo, Tokyo 113-0033, Japan*
[l]*Faculty of Science, University of Tokyo, Hongo, Bunkyo, Tokyo 113-0033, Japan*
[m]*Japan Atomic Energy Agency, Tokai, Ibaraki 319-1195, Japan*
[n]*Research Organization for Information Science and Technology, Tokai, Ibaraki 319-1106, Japan*
[o]*Bragg Institute, Australian Nuclear Science and Technology Organisation, Lucas Heights, NSW 2234, Australia*
[p]*Institut Laue Langevin, 6 rue Jules Horowirz, BP 156 - 38042 Grenoble Cedex 9, France*
[q]*Argonne National Laboratory, Argonne, IL 60439, USA*
[r]*Center for Exploration of Energy and Matter, Indiana University, Bloomington, IN 47408, USA*

1. Introduction

Neutron optics is a powerful tool to increase the utilization efficacy of neutrons to enhance the sensitivity in fundamental physics and material researches. A neutron beamline "Neutron Optics and Physics (NOP)" has been constructed at the port BL05 of the Materials and Life-science research Facility (MLF) of the JPARC [1]. It is under commissioning for the study of neutron optics and fundamental physics. Applications of developed optical devices to material researches are also in progress.

*Corresponding author.
[1]Present address: Faculty of Science, Kyushu University, 6-3-1 Hakozaki, Fukuoka 812-8581, Japan
[2]Present address: Reactor Institut Delft, TU Delft, Mekelweg 15, 2629 JB Delft, The Netherlands
[3]Present address: High Energy Accelerator Research Organization (KEK)
[4]Present address: Research Center for Neutron Science and Technology, Comprehensive Research Organization for Science and Society, Tokai, Ibaraki 319-1106, Japan

2. J-PARC/MLF BL05

The BL05 beamline views the coupled moderator. A shutter and a biological shield are in the regions of L = 2.3–4.3m and L = 4.3–7.2m, respectively, where L is the distance from the moderator. Supermirrors of m = 2 with a cross section of 100mm×110mm are installed in the shutter and biological shields are transporting neutrons into the inlet of beam benders. A pre-position shield covers the region of L = 7.2 – 12m. The beam benders are installed in the void space inside the preposition shield having height and width of 2 m and 1 m, respectively. The benders with the curvature radii of approximately 100 m distribute cold neutrons into three beam branches: the low-divergence beam branch, unpolarized beam branch and polarized beam branch. The interiors of beam benders are filled with helium gas. Fast neutrons are absorbed in the beam dump placed in the region of L = 12 – 16 m. The bent neutrons are transported into beam holes penetrating the beam dump and measuring approximately 15cm×15cm. The configuration of the NOP beamline is shown in Fig. 1.

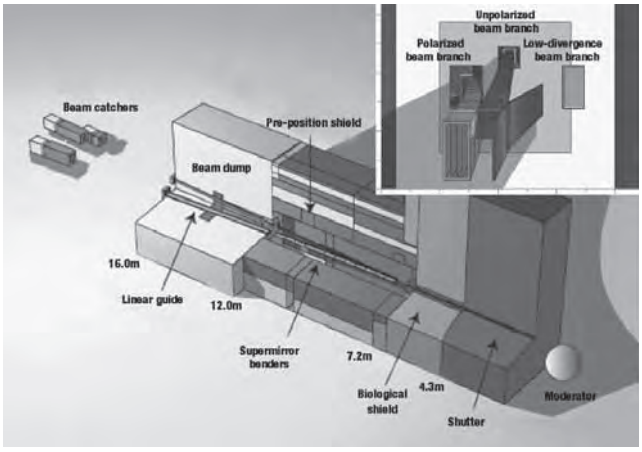

Fig. 1: Schematic view of the configuration of the NOP beamline for the study of neutron optics and fundamental physics at the beam port BL05.

2.1. Low-divergence Beam Branch

The low-divergence beam branch is designed for the multilayer neutron interferometry. Two supermirrors of m = 3 are installed to transport neutrons slower than 1.2×10^3 m s^{-1} with the density of 1.8×10^6 cm^{-2} μsr^{-1} s^{-1} MW^{-1}. A multilayer interferometer with spatially separated paths was successfully demonstrated for the steady beam from the reactor neutron source [2]. Further development to accept the pulsed beam is in progress. Additionally, an extension to the energy region of the very-cold neutrons (VCN) is also in progress. A possibility of unknown medium-range force searches is under discussion [3, 4] in the VCN interferometry [5].

This beam branch was applied as the test port for the MIEZE-type spin echo and also for the study of specularity of the neutron reflection on the surface of neutron mirrors [6]. The installation of the MIEZEtype spin echo at the J-PARC is in progress at the port BL06.

2.2. Polarized Beam Branch

The polarized beam branch is designed for the study of the neutron decay. A multichannel magnetic supermirror bender with $m = 2.8$ is installed to provide polarized neutrons. The length of the bender is 4.5 m and the cross section is 10 cm×4cm. The bent neutrons are designed to be transported by an $m = 2$ straight guide in the region of $L = 12 - 16$ m, which has not been installed yet. After the completion of the additional guide installation and alignment, the flux of 4.0×10^8 cm^{-2} s^{-1} MW^{-1} and polarization of 99.8% can be obtained for the neutron energy of larger than 1.5 meV [7, 8]. Currently a measurement of the neutron lifetime is under development.

[5] Improved search for the medium-range force in the detection of quantum mechanical height distribution of gravitationally confined ultracold neutrons (UCN) is in progress by using a μm-level CCD-based UCN imager [5].

We measure the decay rate by counting decayed electrons using a time projection chamber (TPC). The detection gas contains the diluted ^{3}He and the incident neutron number is measured by counting the protons produced through the ^{3}He(n,p)^{3}H reaction. To reduce the background events efficiently, we have developed a spin flip chopper (SFC) [9]. The Fig. 2 shows the experimental setup at the beginning of the R&D phase of the SFC and TPC. The developed SFC and a TPC are currently at the commissioning phase.

Fig. 2: Installation of a spin flip chopper for the measurement of neutron lifetime at the polarized beam branch of the NOP beamline.

2.3. Unpolarized Beam Branch

The unpolarized beam branch is designed as a versatile beam branch. A measurement of angular distribution of scattering cross section is planned to for the search of unknown medium range interactions between neutrons and neutral atoms. A five-channel supermirror bender is installed to bend neutrons upward with a curvature radius of 100 m. The length of the bender is 4 m and the cross section is 5 cm×4cm. The bent neutrons are designed to be transported by a $m = 2$ straight guide in the region of $L = 12 - 16$ m, which has not been installed yet. A neutron flux of 1.2×10^9 cm^{-2} s^{-1} MW^{-1} is expected after the completion of the additional guide installation and alignment.

Currently, a principle-proof experiment of the time-focusing of ultracold neutrons (UCNs) is in preparation at the unpolarized beam branch [10]. The time-focusing can be applied as an efficient transport of pulsed UCNs, which is proposed for the measurement of neutron electric dipole moment at J-PARC. We have successfully produced ultra cold neutrons (UCN) for the principleproof experiment [11]. The very cold neutrons contained in the cold neutron beam are converted to UCN by the Doppler shift on the reflection by a moving mirror. The Doppler shifter is shown in Fig. 3. It is designed to decelerate the $v \sim 140$ m s^{-1} neutrons to

UCNs with the multilayer mirror, which has the m-value of $m = 10$.

Fig. 3: Doppler shifter installed at the unpolarized beam branch of the NOP beamline for the study of neutron optics and fundamental physics at the beam port BL05. A moving multilayer mirror of $m = 10$ is installed to convert very cold neutrons ($v \sim$140m s^{-1}) to ultracold neutrons by the Doppler shift.

3. Applications of Neutron Optics

3.1. Magnetic Lens

A high spin polarization of cold neutrons has been demonstrated by using quadrupole magnets, which had been studied for the suppression of the halo component around the spot image on the focal plane in the magnetic focusing SANS (Small Angle Neutron Scattering) [12]. A precision determination of the neutron spin polarization at the level of 10^{-4} has been studied in the VCN region by using the precisely calculable spin selectivity [13, 14].

Suppression of the chromatic abberation is necessary to apply the magnetic lens to SANS with pulsed neutron beam. Two types of the abberation suppression methods have been studied. One of them is the combination of static magnets and spin flippers to adjust the effective focal length as a function of the neutron time-of-flight [15]. This method is currently applied in the magnetic focusing function employed in the SANS instrument currently under construction at the port BL15 of J-PARC/MLF. The other is the synchronization of the field strength and the neutron time-of-flight [16, 17]. This method has been intensively developed after the successful demonstration of focusing VCNs using the variable permanent sextupole magnet synchronized with the VCN time-of-flight [18, 19]. The total length of focusing SANS instrument in the VCN region can be suppressed since the focal length of magnetic lens is remarkably short. In addition, larger scattering angles of VCN remain in small-q regions, which implies that more neutrons can be delivered to small samples the on-sample focusing. Further study of the focusing SANS is in progress using a chopped VCN beam at the PF2-VCN at the Institut Laue Langevin [20, 21, 22].

3.2. Compound Refractive Lens

A short-distance 2-dimensional focusing of the cold neutron beam has been demonstrated using a stack of Fresnel-shape compound refractive lenses formed on thin films of per-fluoropolymer [23].

3.3. Neutron Sources at Users' Sites

The improved target moderator assembly, optics and detectors introduces an enhancement of neutron utilization efficacy to enable a practical use of small-scale and medium-scale neutron sources. Such small sources can be installed on the users' site. Practical applications of such sources have been proposed and are currently planned [24, 25].

Acknowledgement

This work was partially supported by the Creative Scientific Research Grant (no.19GS0210) of the Japan Society for Promotion of Science and the S-type Research Program (no.2009S03) of the Institute of Material Structure Science of KEK.

References

[1] K. Mishima *et al.*, Nucl. Instrum. Methods Phys. Res. **A600** (2009) 342.
[2] Y. Seki *et al.*, J. Phys. Soc. Jpn. **79** (2010) 124201.
[3] V.Gudkov, G.L.Greene, H.M.Shimizu, Nucl. Instrum. Methods Phys. Res. **A611** (2009) 153.
[4] V.Gudkov, H.M.Shimizu, G.L.Greene, Phys. Rev. C **83** (2011) 025501.
[5] G.Ichikawa *et al.*, IEEE Nuclear Science Symposium Conference Record (2009) Article Number 5402255, pages 1619.
[6] M.Kitaguchi *et al.*, Physica B (in press).
[7] T.Ino *et al.*, Physica B (in press).
[8] Y.Arimoto *et al.*, Physica B (in press).
[9] K.Taketani *et al.*, Nucl. Instrum. Methods Phys. Res.

A634 (2011) 134.

[10] H. M. Shimizu *et al.*, Nucl. Instrum. Methods Phys. Res. **A634** (2011) 25.

[11] S.Imajo, Master thesis, Faculty of Science, Kyoto University, Mar. 2011.

[12] T.Oku *et al.*, Measurement Science and Technology **19** (2008) 034011.

[13] K.Taketani *et al.*, Physica B **404** (2009) 2643.

[14] T. Yoshioka *et al.*, Nucl. Instrum. Methods Phys. Res. **A634** (2011) 17.

[15] T.Oku *et al.*, Nucl. Instrum. Methods Phys. Res. **A600** (2009) 100.

[16] Y.Iwashita *et al.*, Nucl. Instrum. Methods Phys. Res. **A586** (2008) 73.

[17] H.Iwashita *et al.*, Nucl. Instrum. Methods Phys. Res. **A600** (2009) 129.

[18] Y.Iwashita *et al.*, IEEE Trans. Appl. Supercond. **18** (2008) 957 (art. no. 4497936)

[19] M.Yamada *et al.*, Physica B **404** (2009) 2646.

[20] M.Bleuel *et al.*, Physica B **404** (2009) 2629.

[21] Y.Iwashita *et al.*, IEEE Trans. Appl. Supercond. **20** (2010) 842.

[22] M. Yamada *et al.*, Nucl. Instrum. Methods Phys. Res. **A634** (2011) 156.

[23] T.Ino *et al.*, Nucl. Instrum. Methods Phys. Res. **A634** (2011) 94.

[24] J.Ju *et al.*, Proceedings of the 19th meeting on the International Collaboration on Advanced Neutron Sources, March 8-12, 2010, Grindelwald, Switzerland.

[25] Y.Iwashita *et al*,, Nucl. Instrum. Methods Phys. Res. **A634** (2011) 97.

Minifocusing SANS Instrument Development for J-PARC

M.Furusaka, T.Miyata, S.Takeda, Y.Oba*, M.Ohnuma*, S.Goko, N.L.Yamada**, N.Torikai***, F.Fujita, A.Homma, M.Sugiyama****, T.Fujiwara*****, H.Takahashi*****

Graduate School of Engineering, Hokkaido University, Kitaku Kita-13 Nishi-8, Sapporo, Hokkaido 060-8628, Japan
**X-Ray Physics Group, Quantum Beam Unit, National Institute for Materials Science 1-2-1 Sengen, 305-0047 Tuskuba, Japan*
***Neutron Science Laboratory, KEK (High Energy Accelerator Research Organization), 203-1 Shirakata, Tokai, Naka 319-1106, Japan*
****Graduate School of Engineering, Mie University, Tsu, Mie-ken 514-8507, Mie, Japan*
*****Kyoto Research Reactor Institute, Kyoto University, Kumatori, Sennan-gun, Osaka 590-0494 JAPAN*
****** Department of Nuclear Engineering and Management, The University of Tokyo, 7-3-1 Hongo, Bunkyo-ku, Tokyo 113-8656, Japan*

Research activities using neutron scattering techniques are strongly hampered by its limited availability of neutron sources, instruments or the machine-time there. We need a very large facility to perform neutron scattering research, at either a research reactor or an accelerator driven neutron source, and the number of such facilities in the world is rather limited. Also true is the number of instruments at such facilities. As a result, getting machine time of one of such instruments is generally limited; often they are oversubscribed by a factor of three or more. Also, there is a kind of prejudice that neutron scattering is a technique only for selected researchers or simply many researchers or engineers do not know what neutrons can do and the way to access one of these facilities.

We are now developing compact focusing small-angle neutron scattering instruments (mini focusing SANS, mfSANS), where many of such modules can be installed at beamlines at a large facility. If it becomes available, opportunities to use SANS instruments would become extremely high, or one can perform a high-profile experiment that requires very long machine time. In the latter case, one can perform parallel measurements using many of such instrument modules.

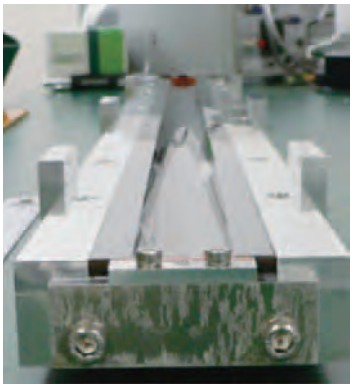

Fig. 1: An ellipsoidal mirror with 2.5 Qc supermirror coating. The major radius of the ellipsoid is 1250 mm and minor radius was 20 mm. The overall length of the mirror was 900 mm and only about 1/6 of the circle is covered.

By using a neutron-focusing mirror, like the ellipsoidal mirror we are developing, we can make very compact SANS instruments that suit the above purposes, in total length of 2 to 4 m. Also the performance of such instruments should be nearly the same as one of the conventional pinhole SANS instruments (PH-SANS) in theory, if we could make the sample size the same. The goal of this S-type project is to develop mfSANS instruments suitable to install many of such instruments at one of the J-PARC beamlines. To realize the purpose, we need to develop three main components. Focusing mirrors, a beam branching technique and detectors suitable to focusing instruments.

For the mirror, we are now testing an ellipsoidal mirror at the JRR-3 research reactor of Japan Atomic Energy Agency (JAEA), which is shown in Fig. 1. Although the surface finish of the mirror was worse than planned because of the machine trouble when fabricating the mirror, the performance of it was acceptable. We could successfully measure SANS in a steel sample that has nanoscopic structures in it as shown in Fig. 2.

We are also developing a Kirkpatrick-Baez (KB) type focusing mirror using the Hokkaido University electron linac based pulsed cold neutron source (HUNS). We used conventional 2 Q_c supermirrors on float-glass substrates and push them gently against precisely machined frames to form elliptical surfaces. We used two different focal lengths to form the KB mirror arrangement, 1.7m for vertical mirror and 1.05m for horizontal one. We successfully obtained a focused beam as shown in Fig. 3 and SANS in an iron nano powder sample.

Beam bending device is the most difficult one to develop of all the necessary components. Since J-PARC is a pulsed cold neutron source, it would be

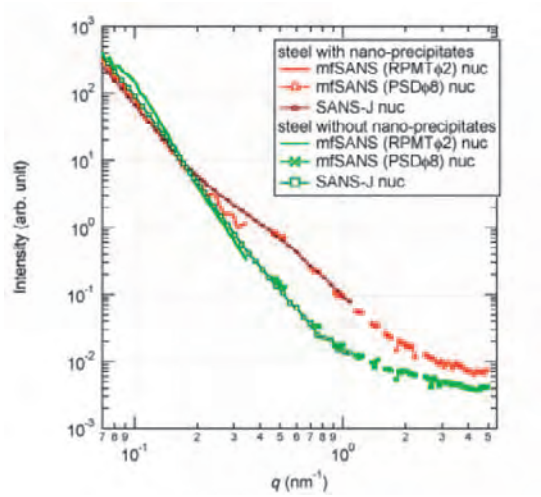

Fig. 2: Steel sample that have nano-precipitates and without them. A 0.5 T magnetic field was applied to the sample to separate magnetic and chemical component of the scattering. The red curve below 0.3 nm^{-1} shows low-Q part of the scattering obtained by mfSANS at JRR-3 and the Q-range 0.4 to 5 nm^{-1} by the intermediate-angle detector bank of it. The black curve shows the SANS measured by the SANS-J instrument at JRR-3. Both data are consistent. The lower curve and markers show scattering from steel sample without nano-precipitate. The green curve below 0.3 nm^{-1} shows data obtained by low angle detector bank (RPMT detector) of the mfSANS and green markers by intermediate-angle one. Also shown is a scattering obtained by SANS-J.

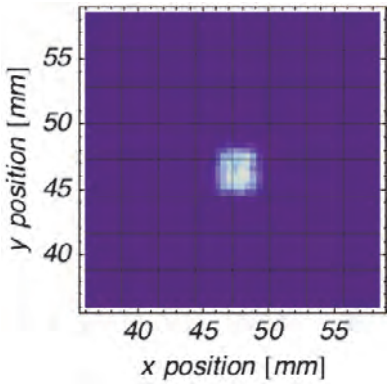

Fig. 3: Image of the focused beam using a KB mirror setup. The incident beam size of the slits were 2mm, both for vertical and horizontal directions.

better to be able to measure Bragg scattering as well as usual SANS. Also the incident neutron spectrum has a peak at around $k_i = 0.25$ nm^{-1} ($\lambda = 0.25$ nm) in the wavenumber presentation, therefore it is desirable to use neutrons from the wavelength close to it. On the other hand, we need to bend a beamline by about 0.1 rad to branch and place an mfSANS module along the main beamline with acceptable transmission efficiency. If we limit the smallest λ to 0.6 nm, it is feasible by using a bender, but it is almost impossible to transport neutrons close to 0.25 nm. Anyway, the only way to accomplish this seems to us to use a stack of silicone wafers of 0.1-0.2 mm thick with nickel coating on them. Fortunately, we are developing a bent perfect silicone crystal monochromator using a stack of silicone wafers of 0.5 mm, and the same technology would be applicable to develop a bender device. We successfully develop a way of bending wafers that have 120 mm in length to the radius of 700 mm, result in 0.17 rad bending.

We are now using a ZnS scintillation detector coupled with a 5 inch position sensitive photomultiplier tube (Hamamatsu photonics K.K. made R3292). The whole system together with a data acquisition electronics based on VME modules and National Instruments Corporation made LabView based control software can be obtained from Japan Neutron Optics Inc. It is a very convenient system, with the position resolution of less than 1 mm, count rate of 17 kpps at 10% dead time, but detecting efficiency is not so high, about 20%.

We are now developing a new type of micro strip gas counter (MMSGC), which should have higher detecting efficiency, higher counting rate, but slightly worse position resolution of about 2mm.

References

K. Hirota *et al.*, Development of a neutron detector based on a position-sensitive photomultiplier, Physical Chemistry Chemical Physics **7** (2005) 1836-1838.

Development of a High Resolution Powder Diffractometer SuperHRPD

S.Torii*, T.Kamiyama*, M.Yonemura*, T.Surya Panca Putra*, J.Zhang*, P.Miao*, T.Muroya*, R.Tomiyasu*, T.Morishima*, S.Sato*, H.Sagehashi*, Y.Noda**

*High Energy Accelerator Research Organization, Tokai-mura, Naka-gun 319-1106
**Tohoku University, Aoba-ku, Sendai 980-8577

1. Motivation

At KENS, we had developed TOF neutron powder diffractometers (NPD's), Vega [1] and Sirius [2,3], with the best resolution of $\Delta d/d = 0.3$ % and 0.15 %, respectively, at backward detectors bank. Total flight paths of Vega and Sirius were 20 m and 40 m, respectively. Sirius was the world first TOF NPD with a long supermirror guide tube. Both Vega and Sirius had been operated until the KENS shutdown in 2006.

There are variety of demands for neutron powder diffractometers such as better resolution, more intensity (small samples and/or short time measurement) and wide Q range, *etc.*[4, 5]. *In situ* measurements under various sample environments are strongly required for the application of NPD. Motivated by the requirements, three NPD's with different resolution and intensity, SuperHRPD (Super high resolution powder diffractometer), iMATERIA (Ibaraki materials design diffractometer) and NOVA (High intensity total scattering diffractometr), were planned in the beginning of J-PARC. Special purpose NPD's, Takumi (Engineering diffractometer), PLANET (High pressure diffractometer) and SPICA (Special environment diffractometer) were also proposed. PLANET is under commissioning, SPICA will accept neutron beam in December, 2011, and the four others are in operation. Here we describe SuperHRPD.

SR powder diffractometers (SR-XRD) and advanced analysis methods have developed rapidly in the past 10 years. In SR-XRD, the use of high luminosity and short wavelength X-ray as well as high resolution results in the best statistic data and well-resolved structure factors with wide Q range of measurements. Advanced analysis methods like the maximum entropy method enables us to extract structural information from tiny changes in diffraction patterns. The combination of high resolution and *ab initio* structural calculation opens new opportunity in pharmaceuticals development. The newly developed functional materials as the results of nano-science tend to have large unit cell volumes which can be fully solved only by high resolution powder diffractometers. The advanced analyses realized or will be realized in SR-XRD are in most cases applicable to NPD data, but the limited statistics and the instrumental resolution of most existing instruments impede the breakthrough of NPD. This confinement would be expected to be removed in NPD's at advanced facilities. Then, we proposed and developed a high-resolution powder diffractometer with $\Delta d/d = 0.03$ %, which is compatible with that of the best SR diffractometer.

2. Design and Construction of SuperHRPD

2.1 Moderator

The lower repetition rate of J-PARC (25Hz) than that of ISIS TS-I (50 Hz) and SNS (60 Hz) is advantageous for NPD because a wide dynamical range is attainable with limited loss of neutrons. To widen further the wavelength range of SuperHRPD at BL08, the shorter flight path is preferable than, for example, 100 m of ISIS-HRPD, which requires development of a high resolution moderator [4]. The high resolution moderator is also requested to satisfy, for accurate crystal structure analyses, the symmetrical pulses with less tails. We have chosen a decoupled poisoned hydrogen moderator; hydrogen moderator is better than water moderator at energy region lower than 100 meV because narrow & symmetrical pulse region extends to longer-wavelength range. Demands on S/N above 100 meV to be better than 1.5 - 2 order lead to the preferred decoupling energy of 1 eV with Ag-In-Cd alloy (AIC) [4, 6, 7]. As for the poisoning material, on the other hand, the choice of Cd results in the shift of symmetrical region to the shorter wavelength region, and narrower and more symmetrical Δt at $\lambda > 1$ Å will be attained by selecting 20 mm depth in average (25 mm at the deepest). Although poisoning energy is larger in Cd, peak intensity is not so different. Detailed comparison between designed performance and experimental results is being examined.

2.2 Beamline design & suppermirror guide

SuperHRPD consists of tapered iron collimators in biological shields, 82.6 m supermirror guide tube with

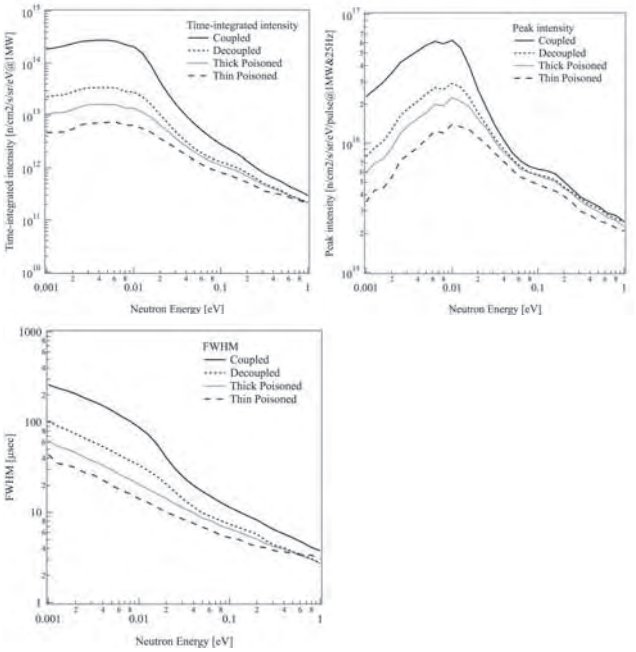

Fig. 1: Calculated specification for MLF moderators. For high resolution realization, we selected a thin poisoned decoupled moderator.

m = 3 starting at 7.145 m, disk choppers, beamline monitors, slits, a sample chamber with the sample position at 94.2 m, detectors, various neutron shields and beamstop. To install this long flight path instrument, the construction of a beamline building (MLF SuperHRPD BL building) with 4 m (H) x 3 m (W) x 50 m (L) and a SuperHRPD experimental hall (MLF SuperHRPD building) with 7 m (H) x 10 m (W) x 13 m (L) were started in July and completed by the end of December, 2007 (Fig. 2). The design, installation and alignment of the guide tube system were carefully executed because of an expected ground settlement and earthquake. It is noted elliptical guide was examined but not adopted because the unequal sinking might deteriorate neutron transmission.

The supermirror guide tube is composed of a 31.245 m curved guide part (5.55 m, 1.695 m plus 24.0 m with 0.11 m gap for the second disk chopper at 12.75 m) with a cross section of 25 mm (W) x 75 mm (H), and 51.4 m straight guide part with a cross section of 25 mm (W) x 55 mm (H) between the instrument and the moderator. The radius of curvature of the curved part is 5 km. Here, the guide tube cross sections are different to minimize the effect of unequal subsidence of the MLF main building and that of the beamline building: with the present guide tube design, 10 % loss of intensity at most by the 10 mm difference in height due to subsidence [8]. We also envisioned that unequal floor sinking might complicate the guide-tube re-alignment. Then we minimized the number of pedestals connecting guide tubes and the floor; three units of guide tubes

Fig. 2: The east building for BL08 (SuperHRPD).

(typically one unit is 2 m) were located inside a metal jacket with 6 m length, which is placed on a long steel rail. The rail is connected with the floor with small number of pedestals. In principle, we only have to adjust 5 pedestals in 80 m guide tube when re-alignment.

2.3 Disk choppers

The flight path as long as 100 m causes overlap of pulsed neutron. Under 25Hz operation, only the wavelength window of about 1.6 Å can be utilized. Therefore, in SuperHRPD, 5Hz mode of 1/5 thinned-out operation is adopted to be the basic TOF duration, resulting in the wavelength window of about 8.0 Å. SuperHRPD can realize various operation modes by the combination of three disk choppers (DC's) located at two positions. The three disk choppers were designed so as to prevent frame overlap and to utilize the wide wavelength; DC1 is at 7.1 m with an opening angle of 31.2°, and DC2 and DC3 are at 12.75 m with 94.9°. DC2 and DC3 are usually counter rotating to speed up beam opening and closing.

2.4 Construction

We proceeded with the construction project of SuperHRPD in two phases because initial budget was limited while early start up of the general user program was requested. We decided to utilize recycled components from both Vega and Sirius in "Phase-I", and gradually to replace them with new ones. In the "Phase-I", we concentrated on beamline components including guide tubes, shielding, choppers, *etc.* and started up quickly by using a vacuum chamber of Sirius, and ^{3}He position sensitive detectors (PSD's) and electronics of both Sirius and Vega. Close-cycle-refrigerators, furnaces and an automatic sample changer with 10 samples were also recycled.

In the "Phase-II", after the careful R&D studies on large thin windows of a vacuum chamber (Fig. 3), we constructed a new SuperHRPD chamber and replaced the Sirius chamber with the new one in summer of 2009

(Fig. 4). The new chamber was developed so as to improve S/N and to achieve better resolution as well as intensity. During the process of the R&D studies on large thin windows of the vacuum chamber and manufacture of whole chambers, we tried to develop local industries in Ibaraki prefecture. A small and medium-sized enterprise group, JSS (the J-PARC Support Study Group), in Ibaraki prefecture was organized and devoted to develop the chamber. The new chamber consists of a vacuum sample chamber with capacity of about 1 m^3, and gas-filled scattering banks around it. In the design concept of a new chamber, a detector solid angle was increased, d-range / Q-range was expanded, and also choices of high-intensity mode and high resolution mode were implemented by varying incident collimations. To cover this large detector solid angle, about 1500 one-dimensional ^{3}He PSD's of 1/2 inch in diameter can be installed in the backward bank, 90 degree bank, and low-angle bank; at present, 320, 192 and 192 PSD's are installed, respectively. In future, high resolution detector will replace parts of detectors in the backward bank. The 'on-beam commissioning' of all detectors at the new SuperHRPD was completed in autumn, 2009, and general user program restarted with this new chamber. Instrumental parameters are shown in Table I.

2.5 Sample environment

The setup of the auto sample changer for 10 samples is completed and its control system has been linked with the data acquisition system. Then, the usual room temperature measurements are fully automated. Low

Table I: Instrumental parameters for SuperHRPD.

Moderator	Poisoned decoupled hydrogen moderator
Primary flight path L_1	94.2 m
Curved guide	31.245 m ($m = 3$, $r = 5$ km)
Straight guide	51.4 m ($m = 3$)
Position for disk choppers	7.1 m (single), 12.75 m (double)
backward bank	
2θ	$150^\circ \leq 2\theta \leq 175^\circ$
L_2	2.0 - 2.3 m
d-range	0.3 - 4.0 Å
Best Resolution $\Delta d/d$	0.035%
at $2\theta \approx 172^\circ$	
90 degree bank	
2θ	$60^\circ \leq 2\theta \leq 120^\circ$
L_2	2.0 - 2.3 m
d-range	0.4 - 7.5 Å
Resolution $\Delta d/d$	0.4 - 0.7 %
low-angle bank	
2θ	$10^\circ \leq 2\theta \leq 40^\circ$
L_2	2.0 - 4.5 m
d-range	0.6 - 45 Å
Resolution $\Delta d/d$	0.7 - 3.0 %

L_2 is the scattered flight path.

Fig. 3: R&D studies on large thin windows of the vacuum chamber. In order to increase a detector solid angle, a thin window was directly screwed with many bolts.

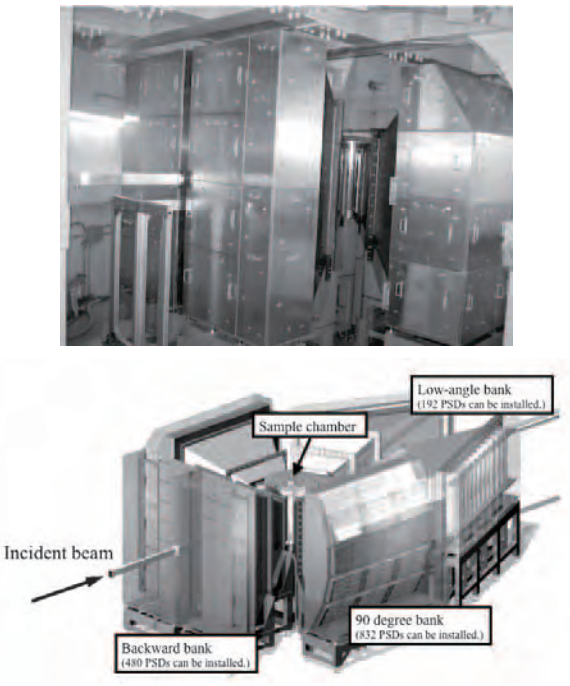

Fig. 4: A photograph (upper figure) and a 3D illustration (lower figure) of the new SuperHRPD chamber, which was installed in summer of 2009. About 1500 PSD detectors can be installed in SuperHRPD diffractometer.

temperature measurement environments are also advanced, and the setup of two cryostats is progressing now; a 5K refrigerator under operation will be connected with the new data collection system soon and a 1 K refrigerator will be introduced soon. The high temperature measurement using a vanadium electric furnace is also available up to 1000 °C. In the future, installations of other sample environment such as a high field magnet, *etc.* are planned.

3. Commissioning of SuperHRPD

The first powder diffraction pattern at J-PARC for an iron steel block (both α-Fe and γ-Fe is included) was recorded on May 31 with 500 shots of neutrons (0.2kW, 25 min.). Although optimization of a beam slit system was not complete, the Bragg peaks of α-phase and γ-phase can be clearly separated (Fig. 5).

June 21, 2008, we had succeeded in achieving the best resolution among all NPD in the world, and a part of detector had achieved $\Delta d/d = 0.035$ %. Fig. 6 shows a comparison of two Bragg peaks measured by SuperHRPD and the Sirius diffractometer at KENS; the FWHM shows a three-fold improvement in SuperHRPD and the tails of the Bragg peaks observed in Sirius were not observed in SuperHRPD, resulting in a 10-fold improvement in the 1/10-width with very symmetrical peak profile. This success was achieved by the long-term R&D work for the high resolution decoupled poisoned moderator by the moderator group to attain the desired resolution within the 100 m flight path. This characteristic is very effective for both precise crystal structure analyses of complicated materials with large unit cells and the detection of tiny structural distortions. It is emphasized that development of the high resolution moderator with less tails in profile is successful.

The comparison between Si single crystal data and simulation result is carried out and the result is shown in Fig. 7. This simulation was calculated using Monte Carlo simulation code McStas[9]. These peak profiles have been reproduced to reflect the simulation results for each wavelength region.

We measured some sealed standard samples filled with powder to check the "time focusing" procedure, as well as to verify the capability of SuperHRPD as a high resolution NPD. In Fig. 8, the diffraction pattern of Si powder (NIST SRM 640c) and its Rietveld analysis result with Z-Rietveld [10] is shown. Z-Rietveld is Rietveld analysis software and one of the powder diffraction data analysis software suits, Z-Code, which had been developed by us. As the result, an excellent fitting was obtained, and the chi-square value of the fitting was as low as 1.30.

Although we are still using old PSDs of the Sirius diffractometer with the 1 cm pixel size, it is worth to evaluate the present resolution in the high resolution

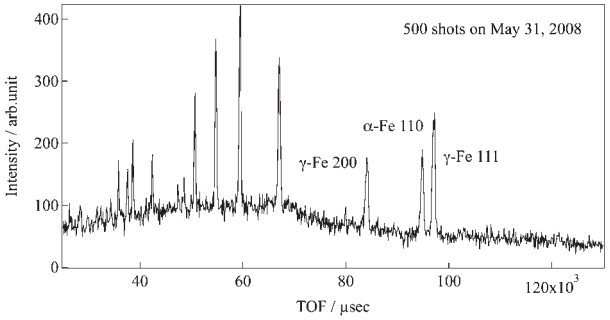

Fig. 5: The first diffraction pattern at J-PARC/MLF: iron steel block.

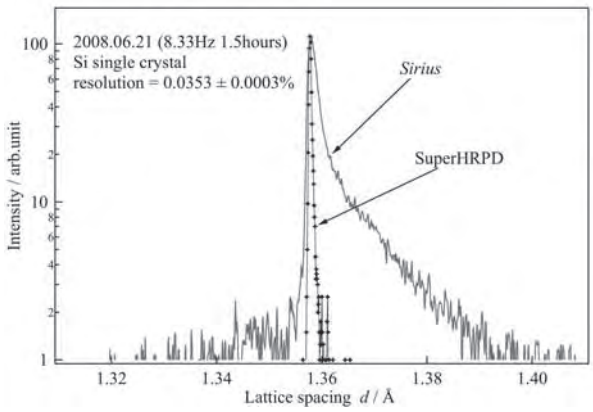

Fig. 6: The 400 reflection of Si measured by SuperHRPD. For accurate crystal structure analyses, the symmetrical pulses with less tails are quite important.

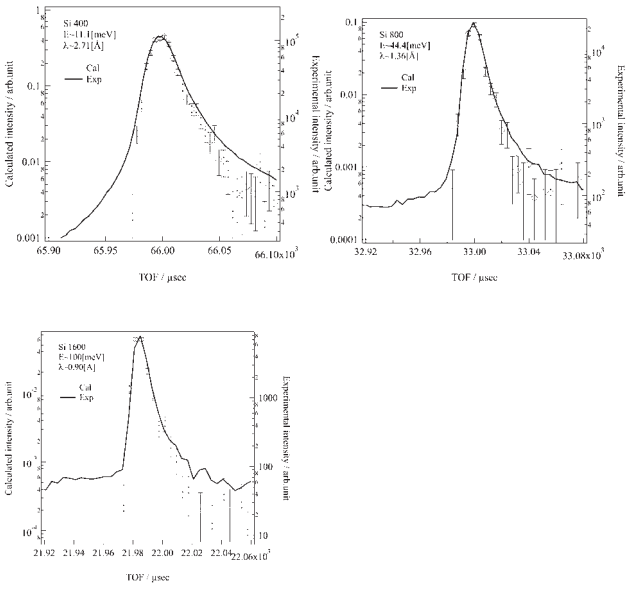

Fig. 7: The comparison between Si single crystal data and simulation results. Markers: calculated data. Lines: experimental data.

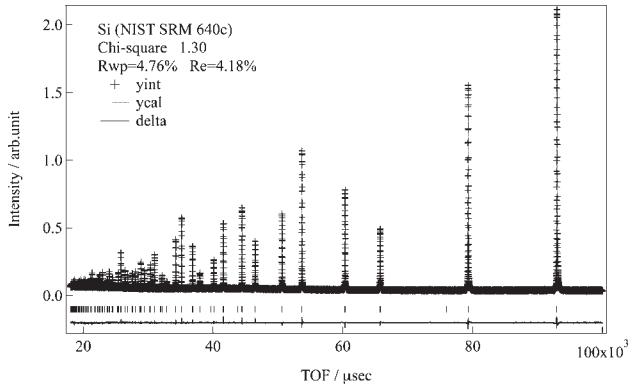

Fig. 8 Rietveld analysis result of Si powder using Z-Code.

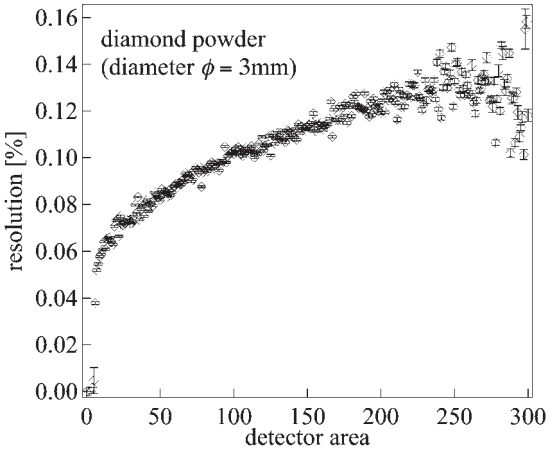

Fig. 9: A detector area dependency of the resolution. When the value of the horizontal axis is smaller, a scattering angle of detector area becomes higher.

mode with the diamond powder sample. Fig. 9 shows a detector area dependence of the resolution. It was shown that the resolution $\Delta d/d$ better than 0.06 % was realizable by limiting the detector area as well as using sample holder of diameter 3 mm.

4. Conclusion

We have completed the construction of SuperHRPD and started user programs. While the development including the introduction of various sample environments such as a 1K cryostat and a high-field magnet are still on going, we have started to utilize SuperHRPD in order to detect tiny structural changes which are not detectable with conventional NPD.

References

1) T. Kamiyama, K. Oikawa, N. Tsuchiya, M. Osawa, H. Asano, N. Watanabe, M. Furusaka, S. Satoh, I. Fujikawa, T. Ishigaki and F. Izumi: Physica B **213&214** (1995) 875.
2) S. Torii, T. Kamiyama, K. Mori, K. Oikawa, S. Itoh, M. Furusaka, S. Satoh, S. Ikeda, F. Izumi and H. Asano : J. Phys. Chem. Solids **60** (1999) 1583.
3) T. Kamiyama, S. Torii, K. Mori, K. Oikawa, S. Itoh, M. Furusaka, S. Satoh, T. Egami, F. Izumi, and H. Asano, Materials Science Forum, **321-324** (2000) 302-307.
4) T. Kamiyama and K. Oikawa: Proc. of ICANS-XVI, Deusseldorf-Neuss, Germany, May **12-15** (2003) 309.
5) T. Ishigaki, A. Hoshikawa, M. Yonemura, T. Morishima, T. Kamiyama, R. Oishi, K. Aizawa, T. Sakuma, Y. Tomota, M. Arai, M. Hayashi, K. Ebata, Y. Takano, K. Komatsuzaki, H. Asano, Y. Takano, T. Kasao, Nuclear Instruments and Methods in Physics Research **A 600** (2009) 189-191.
6) M. Harada, M. Teshigawara, N. Watanabe, T. Kai and Y. Ikeda: Proc. ICANS-XVI. **2** (2003) 697.
7) M. Harada, S. Saito, M. Teshigawara, M. Kawai, K. Kikuchi, N. Watanabe, Y. Ikeda: Proc. ICANS-XVI. **2** (2003) 677.
8) K. Oikawa, F. Maekawa, M. Tamura, M. Harada,T. Kato, Y. Ikeda, K. Niita, Proc. of ICANS-XVII, **1** (2006) 139-145.
9) K. Lefmann, K. Nielsen: Neutron News 10/3 (1999) 20.
10) R. Oishi, M. Yonemura, Y. Nishimaki, S. Torii, A. Hoshikawa, T. Ishigaki, T. Morishima, K. Mori, T. Kamiyama: Nucl. Instr. and Meth., **600**(1) (2009) 94.

Fundamental Research of Hydrogen Storage Mechanism with High-Intensity Total Diffractometer

T.Otomo[a], K.Suzuya[b], M.Misawa[a], N.Kaneko[a], H.Ohshita[a], K.Ikeda[a], M.Tsubota[a], T.Seya[a], T.Fukunaga[c], K.Itoh[d], M.Sugiyama[c], K.Mori[c], Y.Kameda[e], T.Yamaguchi[f], K.Yoshida[f], K.Maruyama[g], Y.Kawakita[b], S.Shamoto[h], K.Kodama[h], S.Takata[b], S.Satoh[a], S.Muto[a], T.Ino[a], H.M.Shimizu[a], T.Kamiyama[a], S.Ikeda[a], S.Itoh[a], Y.Yasu[i], K.Nakayoshi[i], H.Sendai[i], S.Uno[i], M.Tanaka[i], K.Ueno[j]

[a]*Neutron Science Division, High Energy Accelerator Research Organization (KEK),Tsukuba, Ibaraki 305-0801, Japan*
[b]*J-PARC center, Japan Atomic Energy Agency (JAEA), 2-4 Shirane Shirakata, Tokai-mura, Naka-gun, Ibaraki 319-1195, Japan*
[c]*Research Reactor Institute, Kyoto University, 2 Asashiro-Nishi, Kumatori-cho, Sennan-gun, Osaka 590-0494, Japan*
[d]*Graduate School of Education, Okayama University, 1-1-1 Tsushima-naka, Kita-ku, Okayama, Okayama 700-8530, Japan*
[e]*Faculty of Science, Yamagata University, Koshirakwa, Yamagata, Yamagata 990-8560, Japan*
[f]*Department of Chemistry, Fukuoka University, Nanakuma, Johnan, Fukuoka 814-0180, Japan*
[g]*Graduate School of Science and Technology, Niigata University, 8050 Igarashi, Nishi-ku, Niigata, Niigata 950-2181, Japan*
[h]*Quantum Beam Science Directorate, Japan Atomic Energy Agency (JAEA), 2-4 Shirane Shirakata, Tokai-mura, Naka-gun, Ibaraki 319-1195, Japan*
[i]*Institute of Particle and Nuclear Studies, High Energy Accelerator Research Organization (KEK), 1-1 Oho, Tsukuba, Ibaraki 305-0801, Japan*
[j]*Mechanical Engineering Center, High Energy Accelerator Research Organization (KEK), 1-1 Oho, Tsukuba, Ibaraki 305-0801, Japan*

1. Overview of FY2010

In FY2010, evaluation of instrument performance of the High Intensity Total diffractometer (NOVA) at BL21 was progressed. Addition to instrument components of T0 chopper, Fermi chopper, *in-situ* sample environments such as hydrogen gas atmosphere, vanadium foil heater had been tested on NOVA. By performing neutron diffraction of various samples including liquids and amorphous, reliabilities of hardware and software have been confirmed. Since it was confirmed that one-second measurement is feasible, NOVA is expected to be powerful diffractometer for time-transient phenomena. Besides these commissioning, hydrogen storage materials studies were started on NOVA and general user experiments were performed in FY2010.

2. Design concepts of NOVA

Total scattering is a technique that had been developed for liquid and amorphous materials studies [1, 2] and is now widely used to observe non-crystalline features in variety materials including crystalline [3]. Total scattering instruments measure static structure factor, $S(Q)$, in wide-Q and real-space pair correlation function, $g(r)$, will be obtained by Fourier transformation of $S(Q)$. This is one of the technique to analyze every atomic correlation.

$$g(r)=1+\frac{1}{2\pi^2\rho r}\int_{Qmin}^{Qmax} Q(S(Q)-1)\sin(Qr)dQ \qquad (1)$$

where,

$$Q = 4\pi \sin\theta/\lambda. \qquad (2)$$

It is essential to measure $S(Q)$in a wide Q-range since the r -resolution of $g(r)$is inverse-proportional to $Qmax$. Therefore, smaller λ_{min} is desired for total diffractometers. This is the reason why total scattering technique has been developed at pulsed neutron facilities and recently at third generation synchrotron sources.

Hydrogen absorption and desorption cause structural changes of host material such as large distortion of lattice (∼30%), phase transition and amorphization. Even in crystalline hydrogen storage materials, order and disorder structure coexists.

To adapt neutron total scattering to hydrogen storage materials, a neutron total diffractometer, NOVA, was constructed at J-PARC to observe hydrogen storage materials. It is aimed to extract of variety of structural information such as hydrogen-hydrogen correlation even in disordered phase. One of the most prominent features of NOVA is the ability to analyze structures of amorphous and liquids structure as well as crystalline structure.

NOVA was constructed at J-PARC to observe hydrogen storage materials. As a total diffractometer, NOVA covers a wide momentum transfer range, 0.01 Å^{-1} $\leq Q \leq$ 100 Å^{-1} in one measurement by utilizing a wide neutron wavelength, 0.12 Å $\leq \lambda \leq$ 8.3 Å and a wide detector angle range, 0.7 deg $\leq \theta \leq$ 170 deg. This

wide- Q measurement ability is also useful for meso-structure and nearest atomic correlation simultaneously. NOVA consists of 5 detector banks as depicted in Fig. 1. To utilize short wavelength neutron effectively, shortest moderator to sample distance (L1) was chosen as 15 m by taking account the thickness of neutron shields (iron and concrete) and spaces for beam line devices such as disk chopper for longer-wavelength neutron elimination and T0 chopper for bast neutron elimination. The decoupled moderator (supercritical H_2) was chosen because the neutron pulse width was sufficient to realize better than 0.5 % resolution at back scattering bank with the short L1. Since it is actually shortest as powder diffractometer at J-PARC, NOVA can be recognized as very intense powder diffractometer. Based on the high neutron flux of J-PARC, real-time observation of non-equilibrium state is feasible. The designed resolution of NOVA were listed in Table 1.

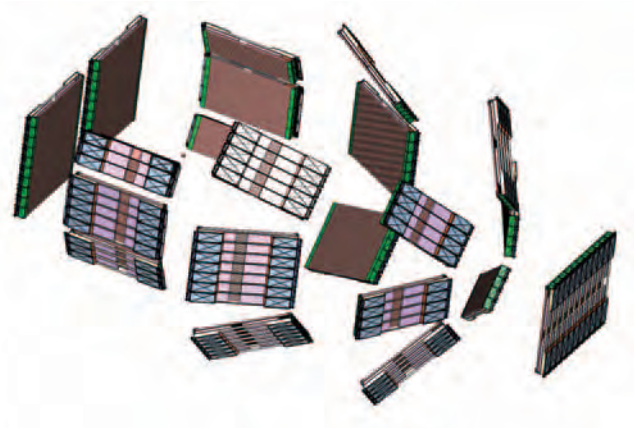

Fig. 1: Five detector banks of NOVA.

3. Commissioning of NOVA

3.1. Data Acquisition System

Detector acquisition of NOVA is neutron-capture event data recording as well as other instruments at MLF [4]. For 900 ^{3}He position sensitive neutron detectors, conversion parameters to obtain positions in detectors from pulse hight had been optimized. Each detector tube (1/2 inch in diameter and 300 mm of effective length) contains 20 bar ^{3}He gas. A gas electron multiplier (GEM) detector had been developed as incident neutron monitor of NOVA [5]. It is a two dimensional position sensitive detector with Boron converter and very high counting rate of $\sim$1 MHz. At sample position of NOVA, neutron flux will be 5 x 10^8 neutron/ sec. The efficiency of the GEM monitor was chosen as 0.1% therefore it can count the neutron flux with minimum loss of statistics. High statistics of incident neutron wavelength dependenth $I_0(\lambda)$ is important to correct one of the wavelength dependent factor. The stability of GEM monitor is now confirming under actual usage conditions. Addition to the incident monitor, GEM monitor for transmitted neutron was fabricated in 2010 and installed downstream of small-angle neutron detector.

3.2. Data Reduction

Reduction of measured event data is as follows. Based on data analysis framework of MLF (Manyo-lib) [6], software for $S(Q)$has been developed.

1. Histograming: Conversion from event data to Time- Of-Flight histogram
2. Pixel merging: Merging of pixel that resolution and $Q(d)$ range are equivalent.
3. Correction: Wavelength dependent factors, delay time of neutron production, multiple scattering, incoherent scattering cross section and background.
4. Merging: Merging of all spectra to one $S(Q)$.

Addition to those basic reduction, self-term correction will be developed. Also, easy-to-use histograming software, which can optimize TOF bin size and pixel size according to statistical accuracy, is under consideration.

3.3. Choppers for neutron beam control

T0 chopper and Fermi chopper were fabricated in 2009 and commissioned in 2010. Figure 2 shows choppers of NOVA. From upper side of the picture, i.e. from near side to neutron moderator, disk chopper, Fe collimeter, T0 chopper and Fermi chopper can be seen. Except the Fermi chopper, these devices are used for reducing background of ^{3}He detectors. The Fermi chopper is optionally used for inelastic experiment at NOVA.

Fig. 2: Choppers of NOVA. From the top (near to the neutron-source), disk chopper, T0 chopper and Fermi chopper.

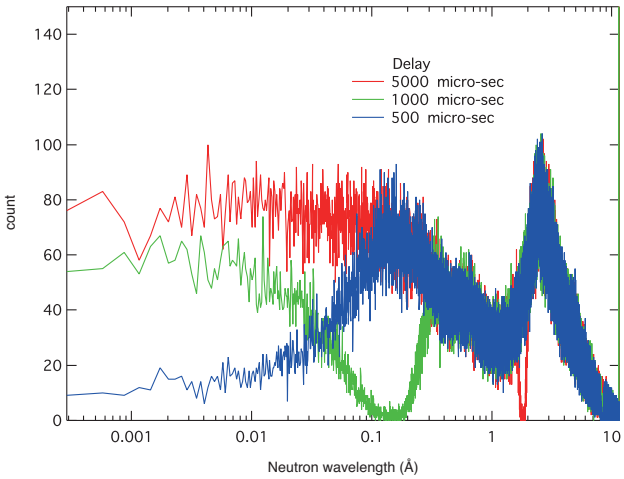

Fig. 3: Phasing test of T0 chopper.

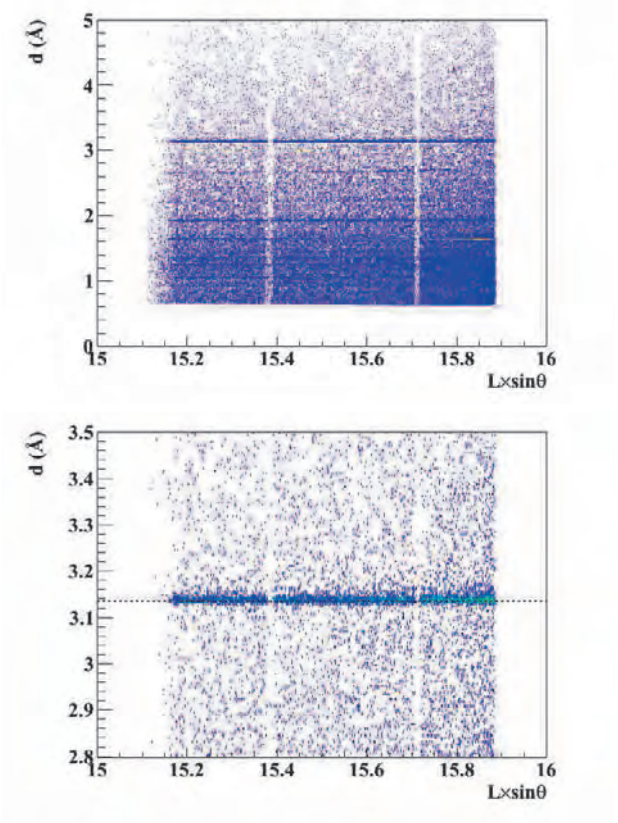

Fig. 4: Resolution of bs-bank.

T0 chopper consists of 30 cm thickness inconel blade to prevent bast neutron going to downstream. To achieve 100 Å^{-1}, shortest wavelength of neutron is 0.12 Å. Shorter wavelength than 0.12 Åmay penetrate into shields and come to neutron detector after moderation. It is background for neutron diffraction but the most efficient way is to eliminate at upper stream of the instrument. Figure 3 shows the result of phase optimization of T0 chopper. By choosing 500 μsec for the delay time, T0 chopper eliminate bast neutron nicely. Inelastic experiment with the Fermi chopper was also performed. Since the event data recording system of data acquisition had been adapted at MLF, multi-Ei measurement is also available on NOVA. It is able to use multiple incident neutron energy for inelastic measurement with a phasing parameter optimized for one incident energy. By using softwares developed by chopper group of MLF, recoil effect of hydrogen containing materials will be examined. This is aiming at establishing self-term correction of $S(Q)$for hydrogenous materials.

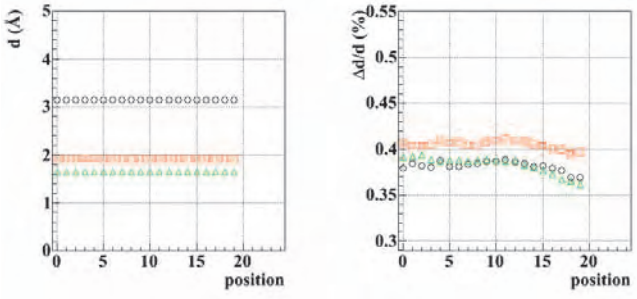

Fig. 5: Resolution of bs bank.Triangles: Si (311), recangles:Si (220) peaks, circles:Si (111).

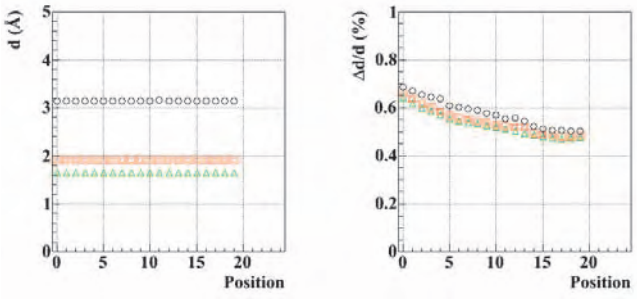

Fig. 6: Resolution of 90-deg. bank. Triangles: Si (311), recangles: Si (220) peaks, circles:Si (111).

3.4. Resolution and Intensity of NOVA

The resolution of NOVA was checked by a standard sample (NIST Si powder 640C). Firstly, every event data assigned its detected position and based on the position, Lsinθ calculated and d-space value.

$$d = \frac{3.956t}{2L\sin\theta} \quad (3)$$

where, d is d-spcae (Å), t is time-of-flight (μsec), L is total neutron flight pass length (m) and 2θ is scattering angle (radian). Then all the event were plotted d-space vs. $L\sin\theta$. A result of the back scattering bank of this procedure was depicted in Fig. 4. At each $L\sin\theta$ value, Δd/d values were estimated by fitting with Gaussian (Fig. 5 and Fig. 6). While Δd/d of 90-deg bank is consistent with designed value, Δd/d of back-scattering bank is larger than the designed value in Table 1. This inconsistency might be caused by pixel merging process.

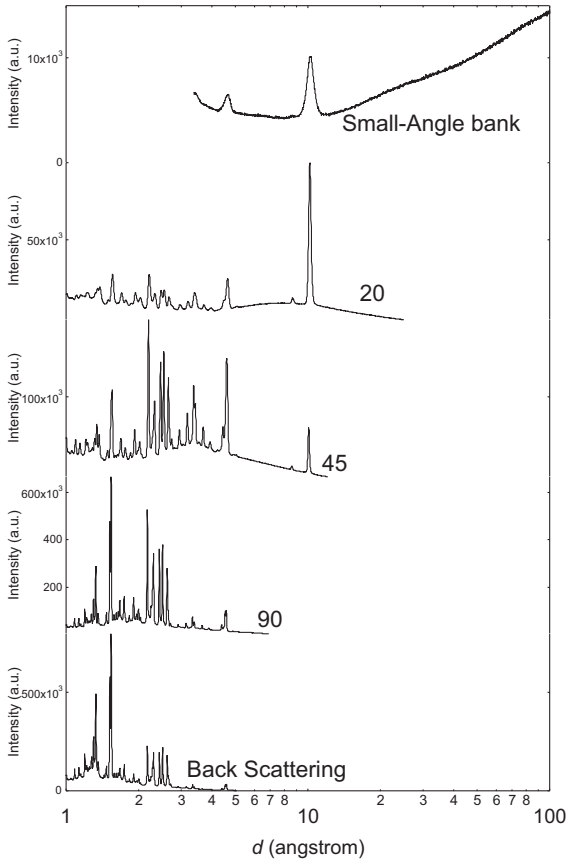

Fig. 7: Wide Q-range measurement of NOVA.

3.5. Q-range

Figure 7 depicted the measured scattering profile of a standard sample (NIST, mica). In this case, pixels of each detector bank were merged into one profile in d-space by similar way as time-focusing: one nominal pixel was chosen to fix d-space (x-axis). This is the reason why Q-ranges of each bank are narrower than the values in Table 1.

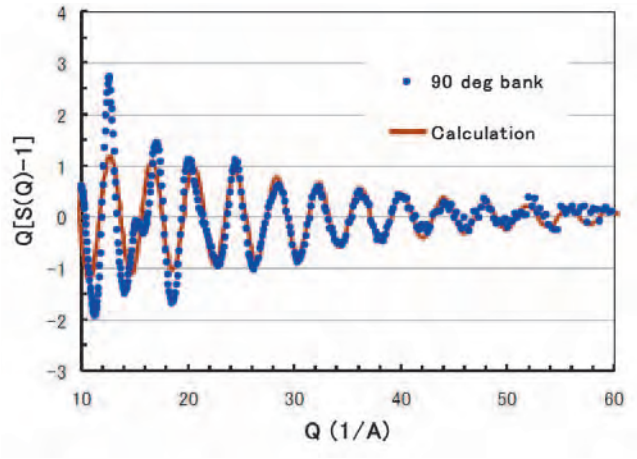

Fig. 8: High-Q measurement of silica glass on NOVA. Solid line shows the calculated result with eq. 4

3.6. Accuracy at high Q-range

Statistical accuracy at high Q-range is crucial since it directory affects $g(r)$. This is clear because Q is multiplied to ($S(Q)$-1) (Eq. 1:). In Fig. 8, Q ($S(Q)$-1) of silica glass (SiO_2) was depicted as well as calculation of Si-O partial correlation. Based on Eq. 4, the coordination number of Oxygen around Silicon and Si-O distance were decided as 3.85 and 1.605 Å, respectively. This is consistent with most reliable data obtained by ISIS-LAD diffractometer (the coordination number is 3.85, the distance is 1.608 Å). Also, the data of NOVA is quite consistent to calculated curves of Si-O correlation upto 60 Å^{-1}. This means NOVA is the best diffractometer to measure high-Q range.

$$Q(S(Q)-1) = 2c_{Si}c_O \frac{b_{Si}b_O}{\langle b\rangle^2} N_{SiO} \frac{\sin(r_{SiO}Q)}{r_{SiO}} \exp\left(-\frac{Q^2 l^2_{SiO}}{2}\right) \quad (4)$$

Table 1: Resolution of each detector bank of NOVA. L2 corresponds to sample to detector distance.

Detector bank	2θ [deg]	L2 [m]	Q-resolution [%]	Q-range [Å^{-1}] (d-range [Å])
small-angle	10 ∼ 20	4	7 (4 ∼ 50)	0.01 ∼ 8 (0.8 ∼ 628)
20-deg	12.6 ∼ 28	2.8 ∼ 3.0	2.5 (1.7 ∼ 3.9)	0.2 ∼ 26 (0.2 ∼ 31)
45-deg	33 ∼ 57	1.7 ∼ 1.9	1.2 (0.9 ∼ 1.5)	0.4 ∼ 50 (0.1 ∼ 16)
90-deg	72 ∼ 108	1.2 ∼ 1.3	0.6 (0.5 ∼ 0.7)	1 ∼ 82 (0.08 ∼ 6.3)
back-scattering	135 ∼ 170	1.0 ∼ 1.4	0.3 (0.3 ∼ 0.35)	1.4 ∼ 100 (0.06 ∼ 4.5)

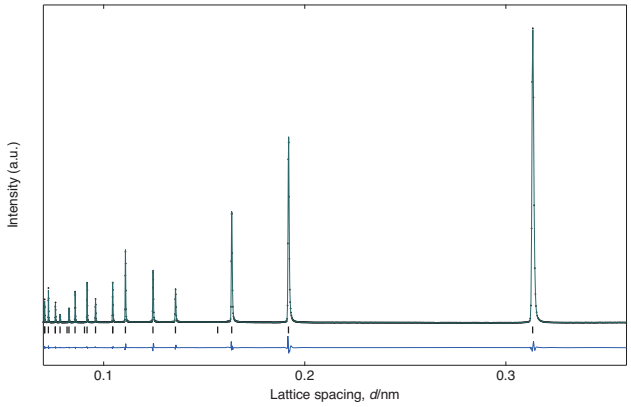

Fig. 9: Rietveld refinement of Si measured by back-scattering bank: observed (cross), calculated (line), and residual (line below vertical bars) diffraction profiles.

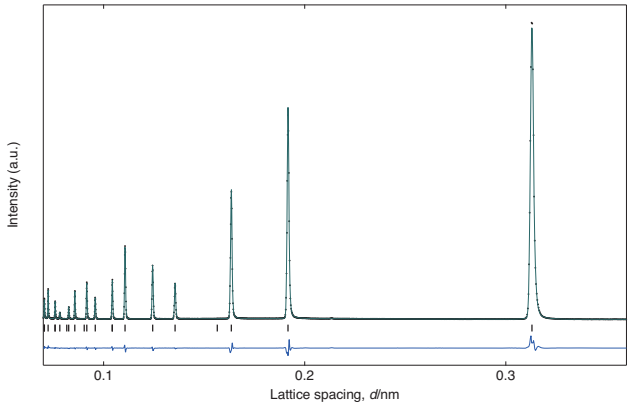

Fig. 10: Rietveld refinement of Si measured by 90-deg bank: observed (cross), calculated (line), and residual (line below vertical bars) diffraction profiles.

3.7. Rietveld refinement

Figure 9 and 10 show measured diffraction profile of Si (NIST Standard Reference Material 640d) in linear scale. The neutron diffraction profile is normalized by the profiles of vanadium standard sample, cell, and background. Rietveld refinement result with "ZRietveld" code [7]: observed (cross), calculated (line), and residual (line below vertical bars) diffraction profiles. Bragg-reflection positions are shown for Si. Statistical reliability factors based on the Bragg intensities, R_B, and the structure factor, R_F , of back-scattering and 90 deg bank were 0.62% and 0.65%, 2.40% and 1.98%, respectively.

3.8. Structure of liquid

3.8.1. Structure of THF

Investigation of structure of tetrahydrofuran (THF)-water (10 mol% THF) solution was started on NOVA. Hydrogenous liquids are most difficult cases to obtain reliable $S(Q)$because of its large self-term effect. null-H_2O (H_2O:D_2O=64:36, $\bar{b}_{H/D} = 0$) method was applied to correct the self-term effect. Isotopic substitution was applied to resolve partial correlation function, $g(r)$. In this case, only 20-deg bank was used to analyze. Figure 11 shows the resulted partial $g(r)$. The first three peaks at 1.09 Å, 1.72 Å and 2.20 Å are corresponding to intra molecular H-C, H···H, and H···C & H···O correlations, respectively. It was confirmed that null-H_2O method was appropriately correct the self-term effect.

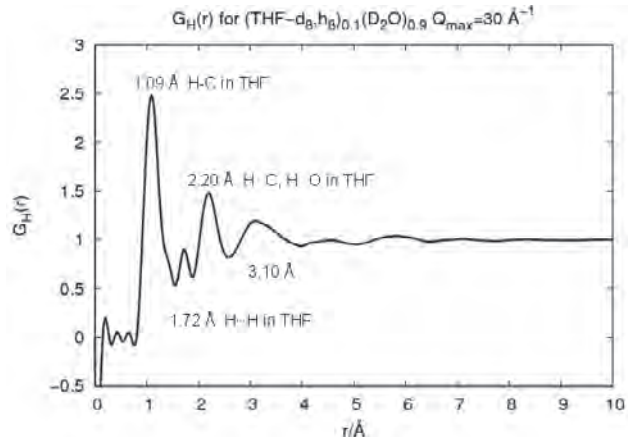

Fig. 11: Partial pair correlation function of THF. This shows atomic arrangement around hydrogen atom.

Besides the partial $g(r)$, structural modeling with Empirical Potential Structure Refinement (EPSR) was started. By this modeling, spatial coordinates of each atom can be obtained and snap shots can be drawn as depicted in Fig. 12. Aggregation of THF molecules were observed and it was found that concentration fluctuation exists consequently. Water molecules are mainly located around oxygen atom of THF. These are consistent with previously reported results of pure-THF liquid and 23 mol% THF solution.

3.8.2. Structure of propanol-solution

To establish meso-scale structure analysis on NOVA, propanol water solution was chosen as a model sample. This system already investigated by Misawa with "corse graining" Reverse Monte-Carlo (RMC) method and by combining quasi-elastic scattering measurement, he suggested the existing of nearest and secondary nearest water molecules around propanol. This model explains peculiar partial molar volume of the system. However, orientation of water molecules are unknown which is important to understand its hydrophobic hydration mechanism. Introduction of quasi-lattice algorithm enables to reproduce longer distance fluctuations and analysis of molecular orientation in the model. Fig. 13 shows orientation of water molecule obtained by adopting the algorithm. The algorithm is working properly and analysis of propanol solutions are on-going.

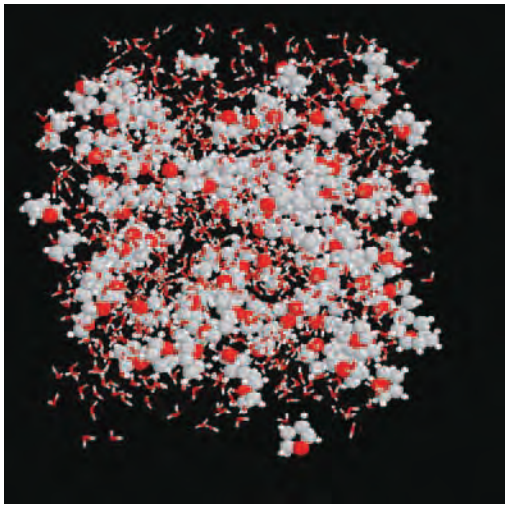

Fig. 12: Snap shot of THF obtained by EPSR method. Water and THF molecules are described by wireframe model and CPK model, respectively.

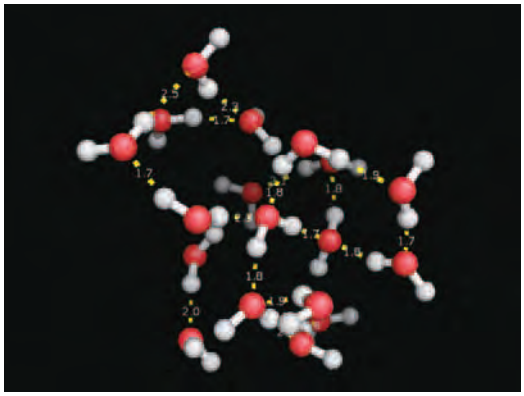

Fig. 13: Snap shot of water molecules obtained by Reverse Monte Carlo method modified to reproduce molecular orientation.

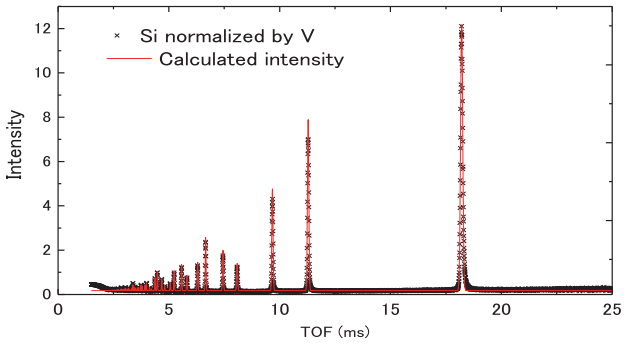

Fig. 14: Observed $S(Q)$of standard silion on NOVA.

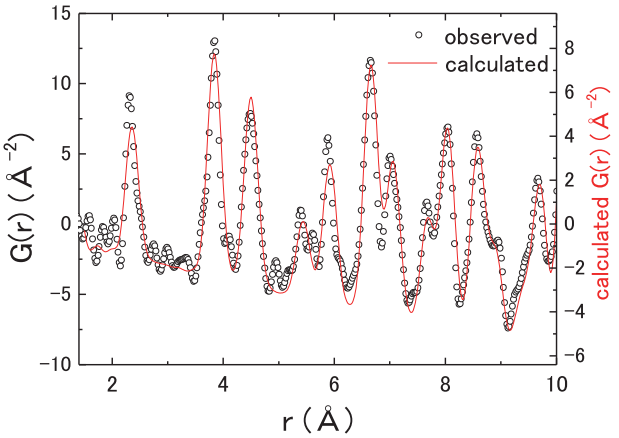

Fig. 15: Obtained $G(r)$of standard silicon. Red line shows calclated $G(r)$from crystalline parameters.

3.9. Pair Density Function of crystalline powder

For crystalline materials study, PDF measurement is essential as a total diffractometer. PDF is defined as follow.

$$\begin{aligned} G(r) &= 4\pi r\rho(g(r) - 1) \\ &= \frac{2}{\pi}\int_0^{Q_{max}} Q(S(Q) - 1)\sin(Qr)dQ \end{aligned} \tag{5}$$

Standard Silicon power was used to compare with LAN-LNPDF instrument. Observed $S(Q)$on NOVA and $G(r)$were depicted in Figures 14 and 15. Red line in Fig. 15 is calculated $G(r)$with crystallographic parameter, i.e. averaged structure. $G(r)$obtained by NOVA is consistent with the calculated one. To compare Q resolution effect, $G(r)$upto 200 Å^{-1} of NOVA and NPDF were compared in Fig. 16 with almost same Q_{max}. The Q resolution inversely proportional to the longest accessible r value in $G(r)$. At present, 90-deg bank was used to obtain $G(r)$whereas NPDF uses back-scattering bank. In this case, the resolution of NOVA is about 6 times worse than NPDF's one. Under this resolution difference, $G(r)$is almost coincident below 50 Å. Above 50 Å, dumps of oscillation was seen but position of peaks are almost consistent upto 200 Å. This dumping was caused by the resolution effect. Even the back-scattering bank's resolution is about 3 time worse than NPDF's one.

3.10. Sample Environments

Besides these high-performance of NOVA as a highintensity neutron diffractometer, equipment's for hydrogen study has been fabricated and installed:

1. Sample exchanger which can load 10 samples,
2. Equipment for an in-situ experiment for H_2/D_2 gas atmosphere (max pressure is 10 MPa and temperature range is 50K $\sim$ 473K),
3. Furnace of vanadium foil heater (room temperature to 1373 K).

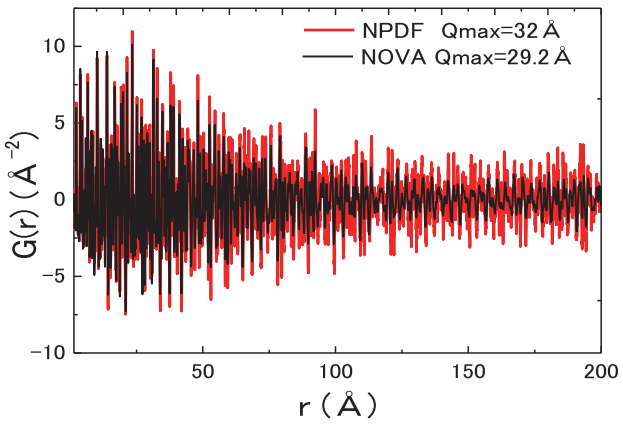

Fig. 16: Comparison of $G(r)$of standard silicon with NOVA and NPDF.

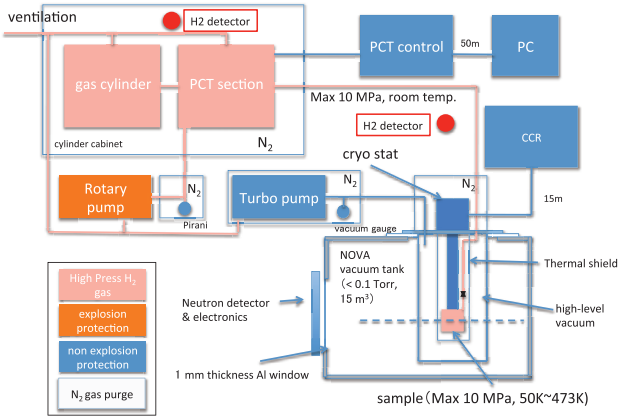

Fig. 17: PCT system on NOVA.

3.10.1. Hydrogen gas atomosphere

An in-situ H_2/D_2 gas equipment can control hydrogen content in hydrogen storage materials by hydrogen gas pressure and temperature. In another words, the phase of hydrogen storage materials can be fixed by the pressure and the temperature. The equipment can measure pressure-composition-temperature (PCT) during neutron diffraction on NOVA. PCT curve at room temp. of $LaNi_5$-D_x was measured by the in-situ environment on NOVA and confirmed that the curve is reasonably consisted with literature (Fig. 18). At three hydrogen composition pointed in Fig. 18, neutron diffraction were performed as shown in Fig. 19. According to hydrogen content increasing, peak shift to longer dvalue and new peaks were observed. As the sample cell, single crystal sapphire was chosen and another material will be tested in 2011.

3.10.2. Measurement of time-transient phenomena

A test measurement of time-transient phenomena on NOVA. Increasing of temperature according to time, the changing of diffraction pattern of $Li^{11}BD_4$ was successfully observed (Fig. 20). $Li^{11}BD_4$ is hydrogen storage and also shows super ionic conductivity at 108 degree Celsius. The temperature of $Li^{11}BD_4$ was gradually changed during the measurement. Fig. 20 was produced by plotting patterns every one minutes for 3

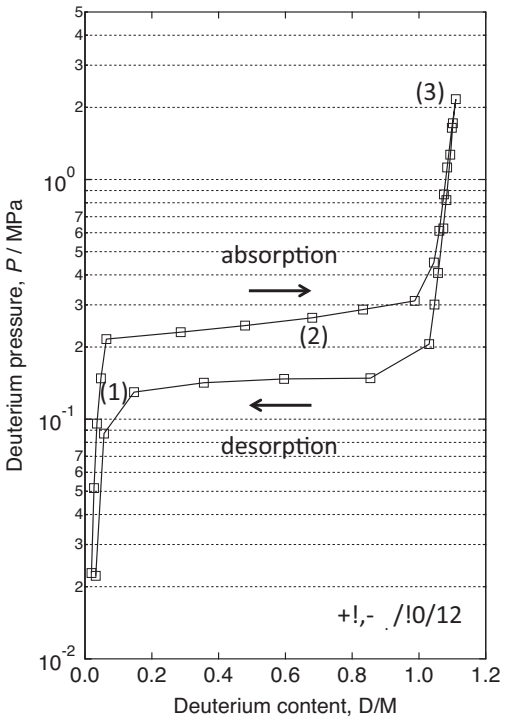

Fig. 18: PCT curve of $LaNi_5$-Dx measured on NOVA.

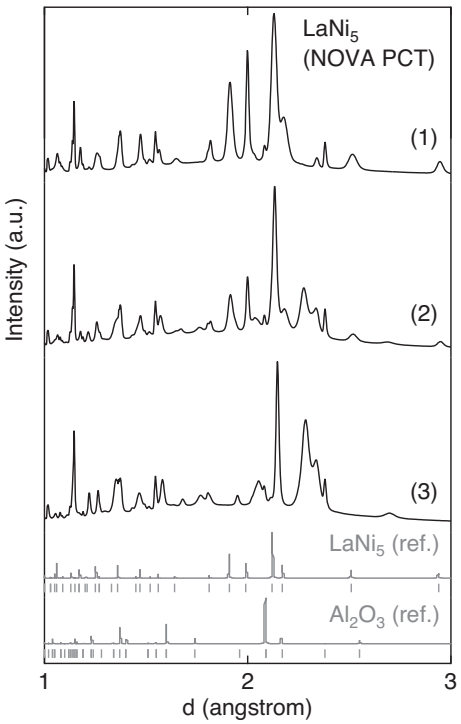

Fig. 19: Diffraction pattern of $LaNi_5$-Dx measured on NOVA.

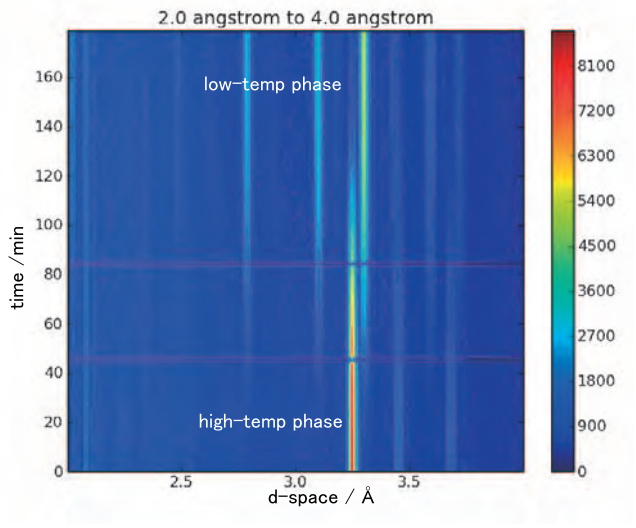

Fig. 20: Time transient measurement of NOVA.

hrs measurement (14 hrs experiment). Time for slice can be chosen flexibly after the experiment and it can be varied. This is the sake of event mode recording system of DAQ.

3.10.3. Inelastic measurement on NOVA

With Fermi chopper, inelastic scattering experiments were performed on NOVA. Studies of incoherent-inelastic corrections of hydrogen atoms will be progressed to improve accuracy of hydrogen position information. It is expected that full-scale research of hydrogen storage materials will be starting soon.

4. Hydrogenous materials study

4.1. Structure analysis of AlD_3

Aluminium trihydride (AlH_3, alane) is of interest as a possible hydrogen storage material because of its high gravimetric and volumetric hydrogen densities (10.1 mass% and 149 kgH_2/m^3, respectively) and its simple hydrogen desorption reaction of AlH_3 to Al ($AlH_3 \rightarrow Al + 3/2H_2$) at 370 $\sim$ 470K. Recently, it is revealed *in-situ* microscopic observations and *in-situ* X-ray photoelectron spectroscopy that AlH_3 particles (size 100 nm $\sim$ 1 mm) are covered by Al_2O_3 layer (thickness 3 $\sim$ 5 nm) and, at room temperature, the hydrogen desorption reaction is prevented by the oxide layer on the surface of AlH_3; reaction begins only when the layer breaks up by thermal volume expansion of the underlying bulk AlH_3. The layer apparently forms after thermal desorption of the solvated ether from AlH_3 etherate, which is prepared by the following reaction between $LiAlH_4$ and $AlCl_3$ in ether solution.

$$\begin{aligned} 3LiAlH_4 + AlCl_3 + n[(C_2H_5)_2O] \\ \rightarrow 4AlH_3 + n[(C_2H_5)_2O] + 3LiCl \\ \rightarrow 4AlH_3 + 3LiCl + n[(C_2H_5)_2O] \end{aligned}$$

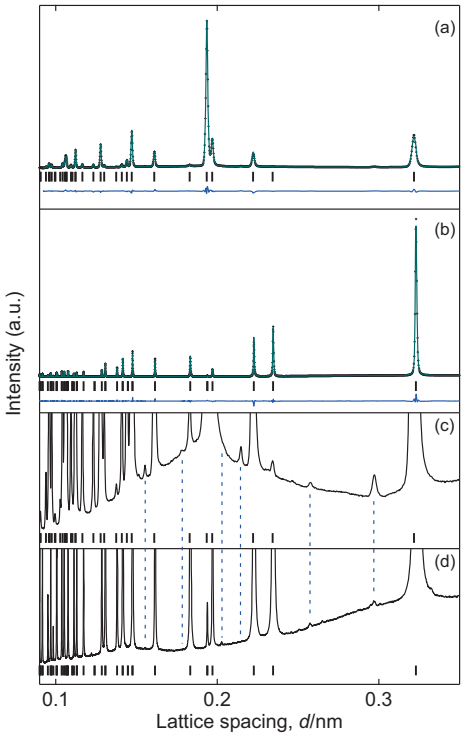

Fig. 21: High-intensity (a) neutron diffraction profile of α-AlD_3 and (b) X-ray diffraction profile of α- AlD_3 in linear scale. Rietveld refinement results: observed (cross), calculated (line), and residual (line below vertical bars) diffraction profiles. Tick marks show Bragg-reflection positions of α-AlD_3 and α-AlH_3. Vertical enlargements by 70 times of the diffraction profiles are shown in (c) for (a) α-AlD_3, and in (d) for (b) α-AlH_3, respectively. Positions except for α-AlD_3 and α-AlH_3 are shown by dashed lines.

To obtain precise structural information regarding the surface layer, we performed high-intensity neutron diffraction measurements by NOVA at 120 kW and Rietveld analysis of α-AlD_3 [8]. The diffraction profiles show small diffraction peaks in addition to the peaks of α-AlD_3 in Fig. 21. These lattice spacing values for neutron and X-ray diffraction profiles are close to those of χ-Al_2O_3 (corresponding to 101 $\sim$ 107% of the values in the literature). Therefore, the present result suggests that χ-Al_2O_3 forms on the surface of AlH_3 (AlD_3) by desorption of solvated ether. Furthermore, the shortrange order (0.18 $\pm$ 0.021 nm for Al-O; 0.28 $\pm$ 0.058 nm for O-O; 0.32 $\pm$ 0.055 nm for Al-Al) of amorphous Al_2O_3 suggested by electron-energy-loss spectroscopy (EELS) may be observed under diffraction peaks of the crystal structures in Fig. 21.

High-intensity (a) neutron diffraction profile of α-AlD_3 and (b) X-ray diffraction profile of α-AlH_3 in linear scale. Rietveld refinement results: observed (cross), calculated (line), and residual (line below vertical bars) diffraction profiles. Tick marks show Bragg-reflection

positions of α-AlD_3 and α-AlH_3. Vertical enlargements by 70 times of the diffraction profiles are shown in (c) for (a) α-AlD_3, and in (d) for (b) α-AlH_3, respectively. Positions except for α-AlD_3 and α-AlH_3 are shown by dashed lines.

4.2. Structure analysis of $LiAl(ND_2)_4$

$LiAl(ND_2)_4$ also has high gravimetric and volumetric hydrogen densities. The decomposition process of NH_3 is not clear and the structure becomes amorphous. Because of the difficulty of synthesis of the sample, total amount of the sample was limited to ∼50 mg. It was tried to obtain $S(Q)$with such small amount on NOVA. As the result, $S(Q)$and $G(r)$was successfully obtained (Fig. 22).

4.3. Phase separation of LaD_2 under high pressure

Phase separation of LaD_2 under high pressure, up to 17 GPa was observed. It was reported that rare earth metal dihydride shows spontaneous two phase separation occurs [9]. These two phases are different in their hydrogen density and it was expected that hydrogen moves in the metal lattice during the phase separation. By neutron scattering on NOVA, positions of hydrogen (deuterium) were observed under the high pressure. A Paris-Edinburgh cell had been chosen. The highest pressere, 17 GPa, is the highest in Japanese neutron facilities. It is necessary to reduce the sample volume to achieve such high pressure: the volume is 15 mm^3 at 17 GPa. Combining with synchrotron radiation results, interesting results were obtained. Back ground reduction and high power of J-PARC (200 kW at this experiment) realizes this success. The publication is in preparation.

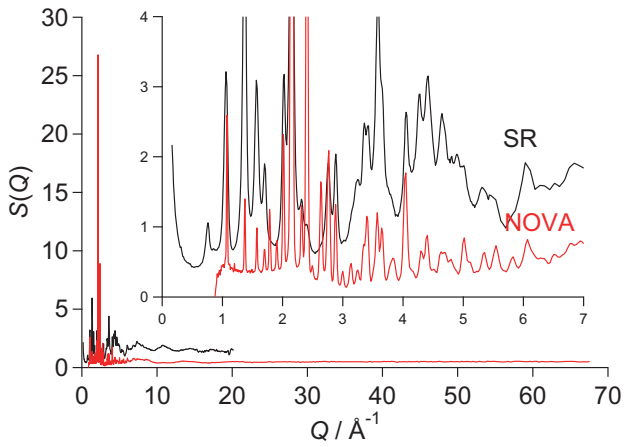

Fig. 22: $S(Q)$of $LiAl(ND_2)_4$ by NOVA (red line) and synchrotron (black line).

5. Acknowledgement

NOVA is supported by a NEDO project “Advanced Fundamental Research Project on Hydrogen Storage Materials (Hydro-Star)”. Under this project, authors thanks to Prof. E. Akiba (Kyushu Univ.), Y. Nakamura, H. Kim, K. Asano, K. Sakaki (AIST), A. Machida, K. Aoki, T. Hattori M. Honda and Y. Katayama (JAEA), Y. Kojima (Hiroshima Univ.), H. Ogawa (AIST), Th. Proffen (SNS) and S. Orimo (IMR, Tohoku Univ.). For analysis software developments, supports from Y. Inamura (JAEA) and T. Itoh (CROSS). We are also grateful to H. Oki and T. Iwase for their dedicated contributions.

References

[1] K. Suzuki, M. Misawa, K. Kai, N. Watanabe, Nuclear Instruments and Methods **147** (1977) 519.
[2] J.M. Carpenter, J. Non-Cryst. Solids **76** (1985) 1.
[3] T. Egami, S.L.J. Billinge, Underneath the Bragg Peaks - Structural Analysis of Complex Materials, (Pergamon, 2003).
[4] K. Nakayoshi, *et al.*, Nucl. Instrum. Methods Phys. Res., Sect. **A623** (2010) 537.
[5] H. Ohshita, *et al.*, Nucl. Instrum. Methods Phys. Res. **A623** (2010) 126.
[6] J. Suzuki, *et al.*, Nucl. Instrum. Methods Phys. Res., Sect. **A 600** (2009) 123.
[7] R. Oishi, *et al.*: Nucl. Instr. Meth. **600** (2009) 9496
[8] K. Ikeda, *et al.*, Mater. Trans., JIM **52** (2011) 598.
[9] A. Machida, T. Watanuki, D. Kawana, K. Aoki, Phys. Rev. B **83** (2011).

Development of Advanced Neutron Optical Devices and VIllage of Neutron Spin Echo Spectrometers (VIN ROSE)

M.Hino[1], M.Kitaguchi[1], T.Ebisawa[2], M.Bleuel[1,4], N.Achiwa[2], M.Katagiri[2], F.Maekawa[2], K.Oikawa[2], H.Seto[3], N.L.Yamada[3], Y.Kawabata[1]

[1]*Research Reactor Institute, Kyoto University, Kumatori, Osaka 590-0494, Japan*
[2]*J-PARC Center, Japan Atomic Energy Agency, Tokai, Ibaraki 319-1195, Japan*
[3]*Neutron Science Laboratory, High Energy Accelerator Research Organization (KEK), 1-1 Oho, Tsukuba, Ibaraki, 305-0801, Japan*
[4]*Reactor Institut Delft, TU Delft, Mekelweg15, 2629 JB Delft, The Netherlands*

Neutron spin echo (NSE) method is very powerful tool to investigate slow dynamics. It was proposed by F. Mezei [1] and is an essential spectrometer with very high neutron energy resolution. New types of neutron spin echo using Resonance Spin Flippers (RSFs) have been developed which are called Modulated IntEnsity of Zero Effort (MIEZE) and Neutron Resonance Spin Echo (NRSE). The basic idea of MIEZE and NRSE was proposed by R. Gähler and R. Golub [2,3]. In NRSE, two RSFs replace a homogeneous static magnetic field for spin precession in the Mezei-type NSE spectrometer. The RSF consists of a static magnetic field and an oscillating magnetic field. The static field is proportional to the frequency of the oscillating field. The energy resolution of MIEZE and NRSE spectrometer is proportional to the frequency of the oscillating field (Fig. 1).

By using new type of RSF with iron yoke dipole magnets, the strong static fields was realized and solves problem of cooling and power consumption for RSFs as well as reducing the material in the beam. MIEZE and NRSE signals have been demonstrated with high frequency at MINE1 port at JRR3 at JAEA [4]. At MINE1, we used monochromatic beam. Spin echo instruments have no principle limitation for type of the neutron source, but so far all of them including classical NSE have been installed at continuous neutron sources. In classic type NSE and NRSE, the benefit of using a pulsed neutron source is the same with conventional neutron spectrometers: The combination of neutron spin echo and time-of-flight (TOF) method makes it possible to scan a wide dynamic range of Fourier times at once. In order to maximize this benefit, a project proposed by D. Richter et. al. and the installation of a Mezei-type NSE spectrometer at the SNS, USA has launched [5]. In parallel a project to develop MIEZE and NRSE for pulsed neutron sources is under way in Japan [6]. We call the MIEZE and NRSE spectrometers 'VIN ROSE'.

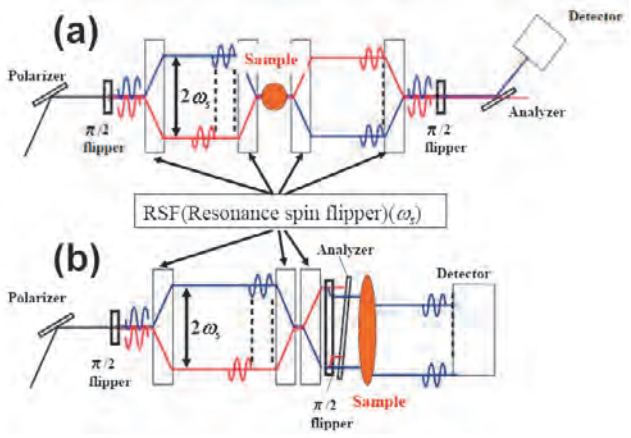

Fig. 1: Schematic view and energy diagram of (a) MIEZE and (b) NRSE spectrometer.

Like classic NSE, MIEZE spectrometers measure the intermediate scattering function of samples and the experimental arrangement is similar to those of TOF spectrometers. Unlike classical NSE spectrometers, the sample is placed after the analyzer in the MIEZE instruments and because of that there are no optical components between the sample and the detector. This enables the MIEZE spectrometer to measure small-angle neutron scattering and neutron reflectometry [7,8]. Even in case of magnetic scattering, the contrast of MIEZE signal is not reduced, whereas the signal of NSE and NRSE spectrometers becomes very small in that case. We proposed a new MIEZE technique, which involves inserting a second analyzer and an additional π-flipper, that is able to distinguish between the magnetic and nonmagnetic quasielastic scattering intensities. Superparamagnetic fluctuations of magnetite particles in a ferrofluid were observed by using this new technique [9]. It is possible to combine MIEZE with a polarimetry analysis instrument. MIEZE signal is measured as a function of time of flight which means at a pulsed source that resolution function is scanned every neutron pulse. This also means that a complete

MIEZE measurement can be done with one neutron pulse if neutron flux is strong enough. Actually, it will be very difficult to do one pulse measurements even with very high intensity sources like JSNS/J-PARC. However, it is feasible to synchronize with the sample environment (i.e. pulse magnetic field and laser excitation). This method uses the benefit of pulse neutron source and we expect to open new frontiers for investigation of dynamics in material.

At first, we have installed a small MIEZE spectrometer at the BL10(NOBORU) at J-PARC and succeeded in observing MIEZE signal and verified TOF-MIEZE spectroscopy derived by us. NOBORU is very useful port but there is narrow experimental space, and it is very difficult to test the VIN ROSE with high resolution. As next step, fortunately, we installed MIEZE spectrometer to BL05(NOP) at J-PARC (Fig. 2).

Figure 3 shows 600kHz MIEZE signal with $\pi/2$-π-π-$\pi/2$ coil system at BL05. The first and second π flipperswere iron yoke type and operatec with 300 and 600 kHz, respectively. The inset shows enlarged figure of MIEZE signal from 13 to 13.02 ms and the period was estimated to be about 1.6 us. MIEZE spectrometer is ready to measure sample though we have to improve the contrast.

It is possible for NRSE to get higher resolution than MIEZE spectrometer if beam divergence effect is small. Especially in NRSE spectrometer, divergent beam provides the deviation of the flight length, which makes the phase difference between neutron spin states and also decreases the contrast of the spin echo signals. The flight length can be adjusted by using ellipsoidal focusing mirrors. Recently, one of authors has founded a fabricating method of neutron supermirror on flexible sheet (Fig. 4)

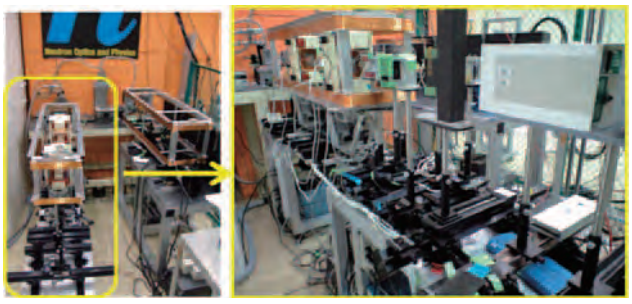

Fig. 2: The photograph of MIEZE spectrometer installed at BL05(NOP) at MLF of J-PARC.

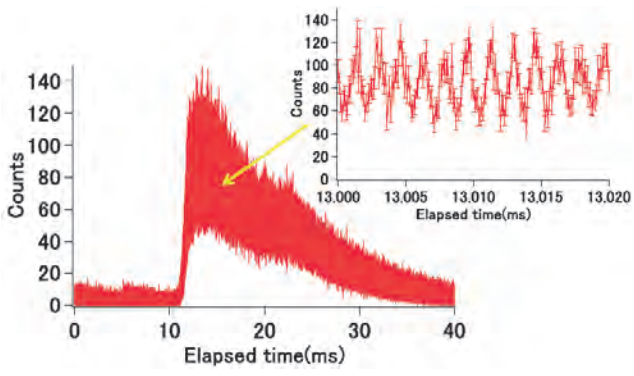

Fig. 3: The measured MIEZE signal with effective frequency of 600 kHz.

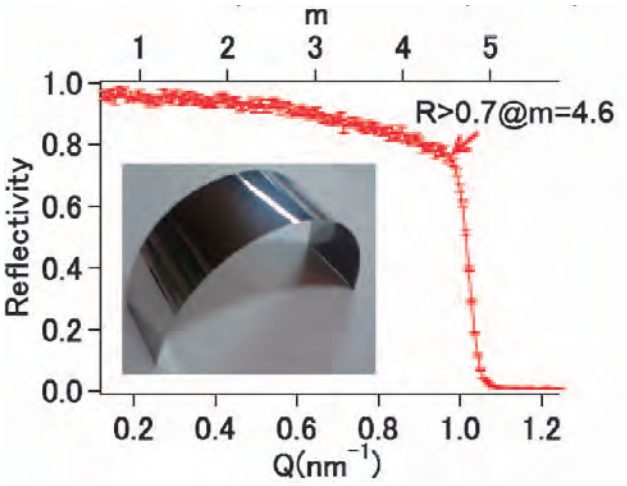

Fig. 4: The photograph of m=4.6 supermirror sheet and the measured reflectivity.

Correction for beam divergence effect using 2D-focusing supermirrors has been numerical simulated. The clear spin echo signal was calculated and neutron intensity increased with the wide acceptance of beam divergence [10]. We also have prepared shape adjusting jig and start to make 2D focusing mirror for VIN ROSE.

References

[1] F.Mezei, Z.Phys 255(1972)146.
[2] R. Golub and R. Gähler, Z. Phys.B65(1987) 269.
[3] R. Gähler, R. Golub and T. Keller, Physica B 180-181 (1992) 899.
[4] M.Kitaguchi, *et al.*,Physica B404(2009) 2594.
[5] M. Ohl, *et al*, Physica B350(2004) 147.
[6] Y.Kawabata, *et al.*,PhysicaB385-386(2006) 1122.
[7] M. Bleuel, *et al.*, Physica B 356(2005) 213
[8] M.Hino, *et al.*, Physica B 385-386(2006) 1125.
[9] H.Hayashida, *et al.*, Meas. Sci. Technol. 19 (2008) 034006, ibid Nucl.Inst.Meth. A**600**(2009) 56.
[10] M.Kitaguchi, *et al.*,Physica B4(2011), in press.

Structural Analysis of Nano Interface of Functional Soft Matter Using Neutron Reflectometer at BL16 in J-PARC/MLF

K.Mitamura[1,2], N.L.Yamada[3], N.Torikai[4], H.Sagehashi[3], T.Sugita[5], M.Furusaka[5], M.Hino[6],T.Fujiwara[7], H.Takahashi[8], H.Seto[3], M.Kobayashi[1,2], R.Inoue[9], K.Kawashima[9], K.Matsui[9],T.Kanaya[9], K.Nishida[9], A.Horinouchi[10], Y.Fujii[10], K.Tanaka[10], D.Kawaguchi[11], Y.Matsushita[11], M.Inutsuka[12], K.Ito[12], H.Yokoyama[12], N.Hariyama[4], A.Takahara[1,2]

[1]*JST, ERATO*
[2]*IMCE, Kyushu University, Fukuoka, Japan*
[3]*Neutron Science Laboratory, KEK, Tsukuba, Ibaraki, Japan*
[4]*Graduate School of Engineering, Mie University, Tsu, Mie, Japan*
[5]*Department of Quantum Science and Engineering, Hokkaido University, Sapporo, Japan*
[6]*Research Reactor Institute, Kyoto University, Kumatori, Osaka, Japan*
[7]*Nuclear Professional School, The University of Tokyo, Tokyo, Japan*
[8]*Department of Nuclear Engineering and Management, The University of Tokyo, Tokyo, Japan*
[9]*Institute for Chemical Research, Kyoto University, Gokasho, Uji, Kyoto, Japan*
[10]*Department of Applied Chemistry, Kyushu University, Fukuoka, Japan*
[11]*Department of Applied Chemistry, Nagoya University, Nagoya, Japan*
[12]*Department of Advanced Materials Science, University of Tokyo, Chiba, Japan*

1. Instrumentation

1.1 Upgrade of reflectometer

Neutron reflectometry (NR) is greatly valid for investigations on structures of surfaces and buried interfaces composed of soft materials. A beam line (BL) 16 in J-PARC/MLF is dedicated for a horizontal type neutron reflectometer. At BL16, two downward neutron beams (2.22° and 5.71°) are transported from a coupled hydrogen moderator to irradiate free surface such as air/water interface. In order to realize neutron reflectivity measurement with high flux neutron beam at J-PARC/MLF as early as possible, we started to accept the neutron beam with "ARISA-II" reflectometer relocated from KENS facility in 2008. But the background was very high because only minimum components, that is, slits, sample stage, and detector, had been installed at this time.

In 2009, a disk chopper was installed so as to suppress the background due to slow neutrons generated at earlier pulses. To check the effect of this chopper, the reflection from a standard Ni mirror with known film thickness was observed with the incident angle of 0.6°. As shown in Fig. 1, the background is drastically suppressed by this chopper. In addition, a T0 chopper to cut fast neutrons, Ni/C mirror to cut further slow neutrons in 2010. Thanks to these components, observable reflectivity reached around 10^{-7}.

In January 2011, ARISA-II has been replaced with a brand-new reflectometer because the vertical strokes of the slits, sample and detector stages were too short to receive both the two downward beam lines at BL16 [1]. The novel reflectometer "SOFIA (SOFt-Interface Analyzer)" started running from the end of January. Figure 2 shows a drawing of SOFIA in the experimental hutch. SOFIA reutilizes the same T0 chopper, disk chopper, Ni/C mirror, and 2-dimensional scintillation detector (^{6}LiF/ZnS) as ARISA-II. With the new slit, sample, and detector stages, we can accept the 5.71° beam line as well as the 2.22° beam line. This enables us to measure NR over wide scattering vector (q) region on free liquid surfaces. Also, the slit system can finely collimate to irradiate an area of 10 mm square,

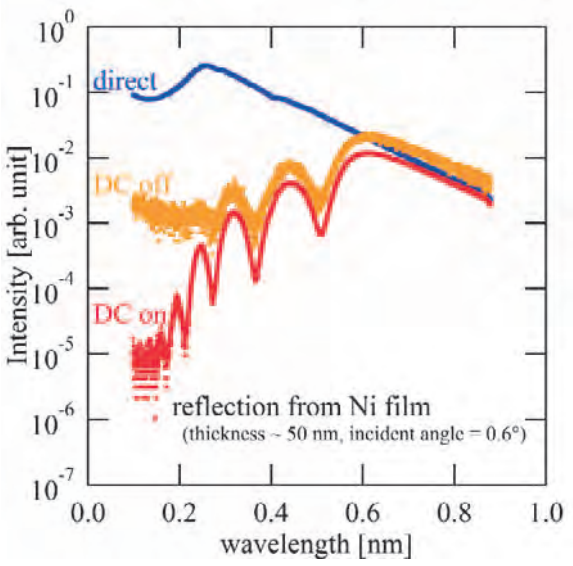

Fig. 1: TOF profiles of direct beam and reflection beam from with and without disk chopper.

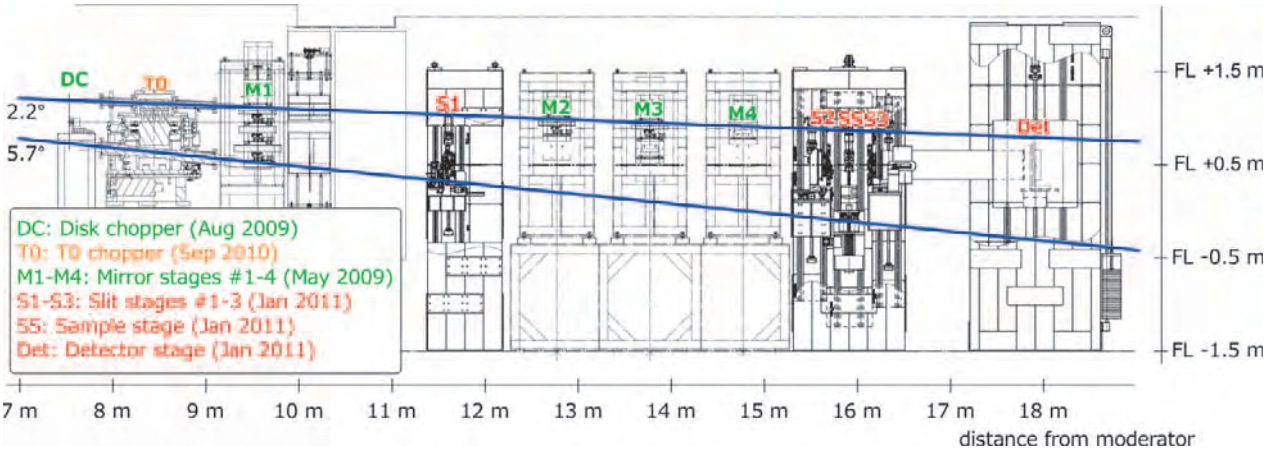

Fig. 2: Side view of SOFIA reflectometer placed at BL16 in J-PARC/MLF.

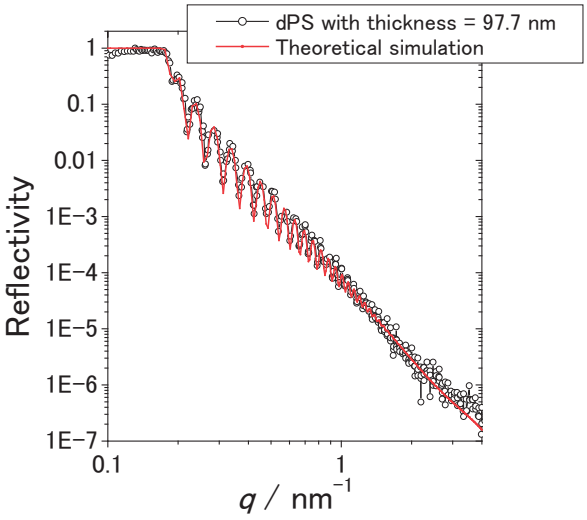

Fig. 3: NR profile of deuterated polystyrene (d-PS) thin film on a Si substrate with a theoretical profile (red line).

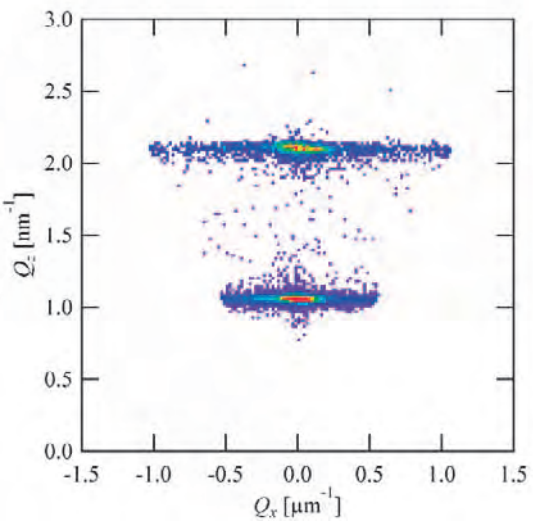

Fig. 4: Reflectivity map of d-DPPC depending on the momentum transfer in the direction of parallel (Q_x) and normal (Q_z) to the substrate.

typical sample size in the latest frontiers, with the angular resolution of 3%.

To check the performance of SOFIA, we performed NR measurement using a deuterated polystyrene (d-PS) thin film spun-cast on a silicon substrate. Figure 3 shows the obtained NR profile. The NR profile was well reproduced up to $q \sim 4.0$ nm^{-1} by a theoretical curve considering a plausible scattering length density of d-PS (6.46×10^{-4} nm^{-2}) and thickness evaluated by ellipsometery (98 nm). The typical duration times for the specular reflectivity measurement with 3-inch diameter substrates are follows.

- 5 minutes for Q<1 nm^{-1} with deuterated film.
- 20 minutes for Q<2 nm^{-1} with deuterated film.
- 1 hour for Q<4 nm^{-1} with deuterated film.
- 2 hours for Q<2 nm^{-1} with hydrogenated film.

Since SOFIA equips 2-dimensional detector, we can simultaneously measure the off-specular reflection as well as the specular reflection at the same time. For the test measurement, we used a stacking of deuterated dipalmitoylphosphatidyl- choline (d-DPPC) bilayers on a Si wafer. According to literatures, this sample shows the off-specular reflection due to the thermal undulation of bilayers [2] as well as the surface roughness [3]. Figure 4 shows the reflectivity map depending on Q_x and Q_z, the momentum transfer in the direction of parallel and normal to the substrate respectively. The conversion was successfully performed and the streaks due to the off-specular reflection extend in the direction of Q_x from the Bragg peaks of the bilayer stacking.

1.2 Development of focusing mirror [4]

A grazing-incidence small-angle scattering (GISAS) technique can observe in-plane nm-scale structure em-

bedded in thin films or adsorbed at interfaces [5, 6]. In practice, the number of GISAS study is, however, very limited with neutrons, since it requires high flux and high angular resolution for the incident beam. Thus, GISAS measurements so far with neutron have been conducted only on conventional small-angle neutron scattering instruments with a long flight path at high-intensity reactor sources [7-9]. To overcome this problem and realize a GISAS measurement on a pulsed neutron reflectometer with SOFIA reflectometer, we are developing focusing mirror system. By focusing neutron beam on detector, we can obtain a small beam spot with large beam divergence, that is, high density neutron in real space. This enables us to perform small-angle scattering measurement with a relatively short length of about 2 m between the sample and detector positions. Also, the mirror optics is suitable for focusing pulsed neutrons with a broad wavelength band due to no effect of chromatic aberration.

There are two possible ways to fabricate elliptically-shaped cylindroid supermirrors. One is to fabricate a substrate that has an elliptical surface by mechanical polishing or chemical wet etching, followed by formation of a supermirror using sputtering technique. Another way is to start with a conventional supermirror on a flat substrate and bend it accordingly. If this bending method is accomplished, it is really cost effective compared with the former method. In this study, the cylindroid supermirrors with an elliptical arc along its long sides for vertical and horizontal beam focusing are developed by physically bending the mirror prepared on a flat substrate, and their focusing performance was tested with ARISA-II.

The bending device is illustrated in Figure 5. It is a channel made of an aluminum block, and two ends of it have two parallel brims of 10 mm width, as shown in the gray stripes in the figure, that had a shape of a part of an elliptical arc with major and minor axes of 4,300 mm and 35.8 mm, respectively. The $2.5Q_c$ supermirror was put on the brims to form the focusing mirror surface without imposing extra load such as screw tightening, to bend it following the elliptical shape only by its weight, and its mirror-coated plane was set face down to reflect the neutron downward. The maximum height difference of the elliptical arc between the edge and center of the device is as small as 120 μm over 250 mm length.

The bent cylindroid mirror was arranged at the position of 2,150 mm, which is half of the designed focal distance, 4,300 mm, of the cylindroid mirror, separating from the first slit on the ARISA-II beam line. Its angle relative to the downward neutron beam of the ARISA-II was adjusted to be 0.24°, resulting in that the reflected beam possesses about 2.7° as a downward angle relative to the horizontal. Figure 6 compares spatial distribution of the neutron intensity along the vertical direction with and without the bent mirror. It

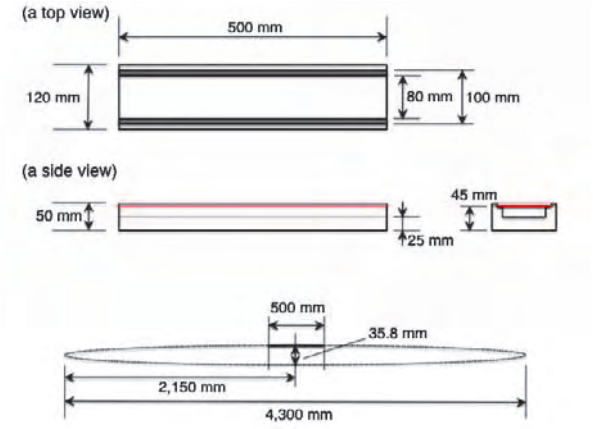

Fig. 5: Illustration of a bending device. An elliptical arc was prepared on the two parallel brims, shown in the gray stripes, along the long sides.

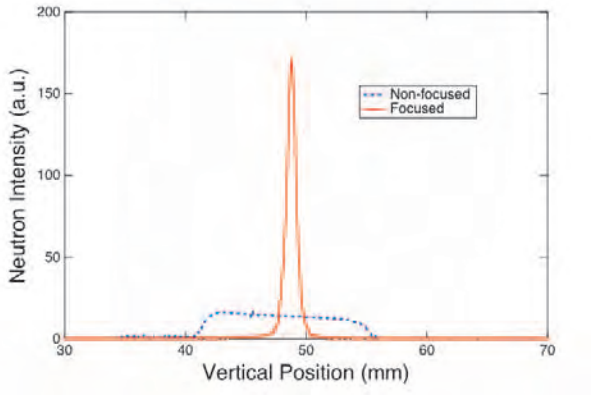

Fig. 6: The spatial distribution of the neutron intensity along the vertical direction with and without the bent mirror.

should be noted that the position of the direct beam measured without the mirror was shifted in the figure for ease in comparison. The opening width (S1) of the first slit was set to 0.4 mm. As shown clearly in the figure, the highly focused beam was obtained with the bent cylindroid mirror even though the detector was not strictly positioned at the exact focal position, that is, 66 mm shorter than the exact focal distance, since a sample stage of ARISA-II does not have enough space to place the relatively large detector component at the exact focal position. The peak intensity of the focused neutron beam was almost 10 times higher than that without the bent mirror. The full-width at half maximum (FWHM) of the focused beam was estimated to be 0.9 mm, which is almost the same to a spatial resolution of the detector, that is, about 1 mm.

To measure the beam size without the smearing effect of the detector, the second slit was placed at the precise focal position, and the detector was set 276 mm behind this second slit. The slit scan along the vertical

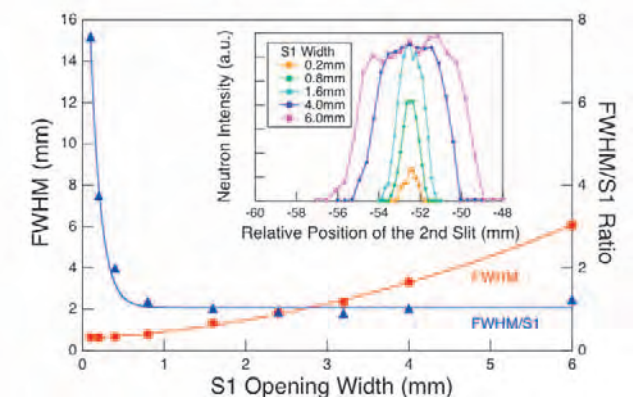

Fig. 7: The FWHM values and their ratio to the opening width (S1) of the first slit for the reflected beam as a function of S1. The inset shows the spatial distribution of each reflected beam.

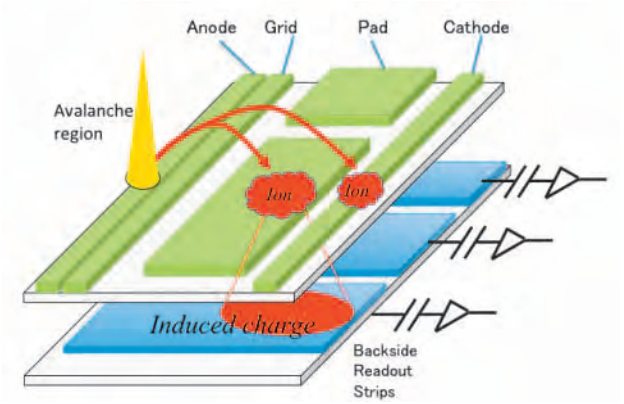

Fig. 8: Illustration of a 2-D floating pad readout. An electrode in green describes the top layer, and blue is the backside layer. When avalanche occurs, ions are collected to the nearest pad. At the same time, induced charge appears in backside strips.

direction was made for the second slit with the opening width of 0.05 mm without moving the detector, to have much better spatial resolution than the detector itself. Figure 7 shows the variation in the FWHM values estimated from the spatial distribution of the reflected beam, some of which are shown in the inset, and their ratio to S1 with changing the opening width (S1) of the first slit from 0.1 to 6.0 mm. When the S1 value is larger than 1.6 mm, peak neutron intensity profiles showed flat tops as shown in the inset, and FWHM value increased with increasing the S1 value. On the other hand, when the S1 value is smaller than 0.8 mm, the peak intensity rapidly decreased without changing the FWHM value much, that is, the ratio of FWHM to S1 became abruptly larger than unity as shown in the figure. This is attributed to that the elliptical shape of the bent mirror is not precisely achieved as designed enough to focus the neutron with the beam width less than 0.8 mm.

After this measurement, we also try to focus neutron in horizontal direction with the same mirror holder. To erect a supermirror without unnecessary load, a soft spongy material was used as a spacer between the mirror and a lid of the holder. A test experiment was performed at a cold neutron beam line in Hokkaido University (HUNS), and almost the same focusing performance can be achieved in horizontal direction too.

1.3 Development of ^{3}He detector

A MicroStrip Gas Chamber (MSGC) has been introduced by Oed [10]; however, this detector suffers from discharges due to surface streamers and resulting in poor gas gains. Recently, a new patterning approach to this type of detector has been proposed which utilizes a complicated electrode geometry on the surface of the detector [11]. This new multi-grid type MSGC (M-MSGC) is equipped with intermediate grid electrodes placed between the anode and the cathode. This

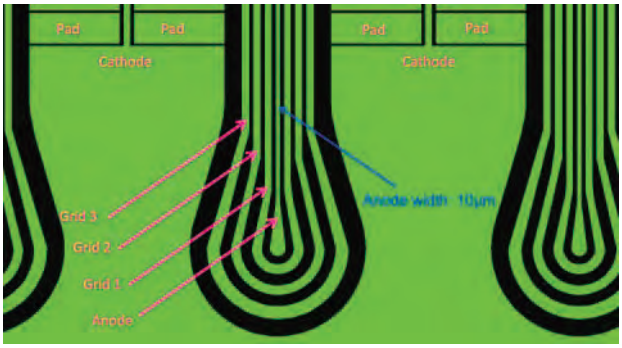

Fig. 9: CAD design layout of M-MSGC. Electrodes are curved and smoothed in order to avoid the concentrated electric field in the corner.

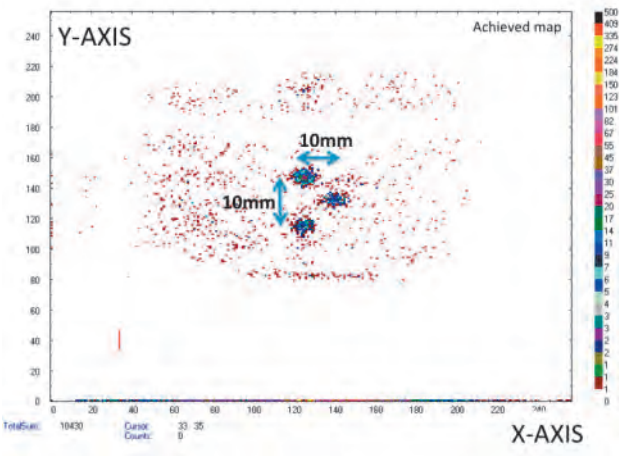

Fig. 10: The spatial distribution of the neutron beam with 1mm collimated beam. So far, 1.8mm spatial resolution is obtained with M-MSGC.

structure is useful for stabilizing the surface charge. The intermediate grid electrodes also isolate the anode

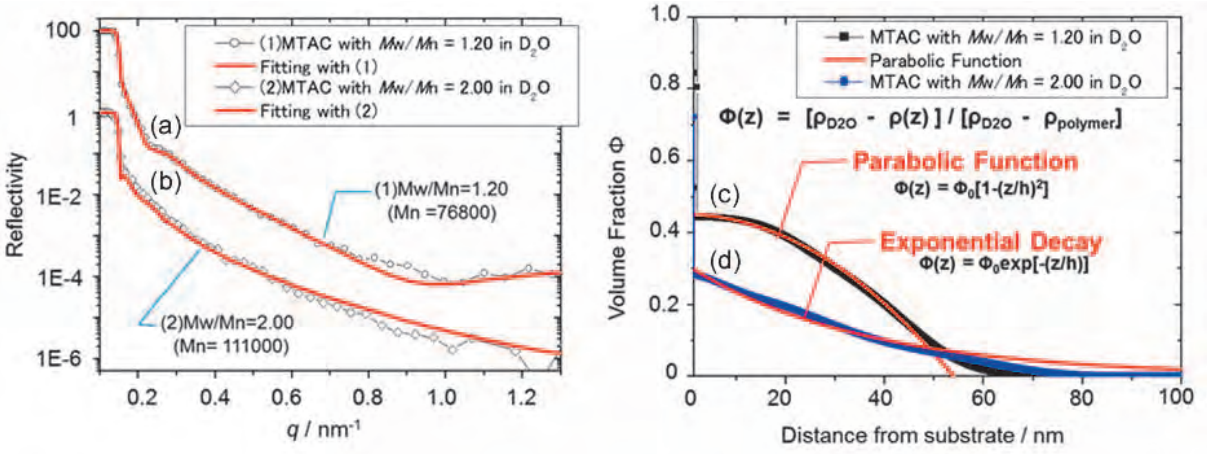

Fig. 11: NR and the corresponding volume fraction profiles of PMTAC brush (a), (b) at MWD (Mw/Mn = 1.20) and (c), (d) at MWD (Mw/Mn = 2.00) in pure D_2O with theoretical fitting curves (red line), respectively.

and the cathode and realize a favorable electric field for avoiding the surface streamer development. The multi-grid type MSGC can offer very narrow gap between neighboring electrodes that might reduce a surface charge effect considerably. The present MSGC may be applied to the field where both the high gain and the stable operation required. A new large size multi-grid-type ^{3}He MSGC (M-MSGC) has been designed and fabricated for SOFIA reflectometer.

Here a new double layered new M-MSGC, which made out of two layers of glass material which enables 2-dimensional (100×100mm^2 size) position readout is described. In the top layer, MSGC made out of very thin glass material with floating pad electrode pattern is layered. These floating pads are placed close to the cathode strip in MSGC on the surface of the M-MSGC and induced charges are read out via the pads. In the multi-grid-type MSGC, 3 grid electrodes are inserted between narrow anode strips and wide cathode strips. The role of grid electrodes is to virtually reduce the surface resistance and to stabilize the electric field. This MSGC is made out of thin glass plate (0.3mm thick) and patterned with oxide chromium material. The layout of the MSGC is shown in Fig. 8 and Fig. 9. Floating pads are placed close to the cathode strip on the surface of the M-MSGC and induced charges are read out via the pads. Since the area of pads is sufficiently large and the positive charges are moving toward the pads, backside electrodes can sense the induced charge. Collected charges on the pads are leaked through the surface resistivity. The basic experiment has been performed at ARISA-II, and the read out of the position along the both layer is successfully ensured (Fig. 10). We gained 1.8mm spatial resolution in FWHM. Now 200×200mm^2 size in fabricating process.

2. Scientific topics

2.1 Chain dimension of polyelectrolyte brush with heterogeneous chain length in water

Polymer brush, which is a polymer layer with an end tethered on solid substrate, has swollen structure in a good solvent, and its chain dimension largely affects physical characteristics such as adhesion, anti-fouling effect etc. Chain dimensions of polymer brushes with homogeneous chain length can be predicted theoretically and also confirmed by NR measurements [12, 13]. However, chain dimensions with heterogeneous chain length have not been confirmed experimentally, while the theoretical prediction was submitted [14].

Here, we examined polyelectrolyte brushes, poly [2-(methacryloyloxy) ethyltrimethylammonium chloride] (PMTAC) brushes at different molecular weight distributions (MWDs) (i) Mn = 76800 with Mw/Mn = 1.20, (ii) Mn = 111000 with Mw/Mn = 2.00, which were prepared on silicon substrates by atomic transfer radical polymerization [15]. Figure 11 (a) and (b) represent NR profiles of PMTAC brushes at the low and high MWDs in pure D_2O, respectively, and Figure 11 (c) and (d) show the corresponding volume fraction (Φ) profiles along with distance from substrate (z) of the brushes at low and high MWDs evaluated by fitting, respectively. The volume fraction profile of PMTAC at low MWD was well described by a theoretical equation, so-called "parabolic function" $\Phi(z) = \Phi_0[1-(z/h)^2]$ ($\Phi_0 = \Phi(0)$, $\Phi(h) = 0$), representing chain dimension or expansion of polymer brush with uniform chain length in a good solvent, which was derived from a self-consistent field theory [12]. The layer thickness of the polymer brush can be estimated to 53 nm from the value of h, which was around triple of dry thickness (ca. 18 nm) obtained by NR. These results indicated the PMTAC brush had swollen structure in pure D_2O as predicted

by the theory.

On the other hand, in case of the PMTAC brush at high MWD, the volume fraction profile was not represented by a parabolic function but exponential decay function $\Phi(z) = \Phi_0 \exp(-[(z/h')])$ ($\Phi_0 = \Phi(0)$, $\Phi(h') = 1/e$). The value of h' assumed as a brush thickness was ca. 36 nm. Since the dry thickness of the brush was ca. 22 nm, the brush in pure D_2O was also in swollen state.

The shift in the form of the volume fraction profiles into the monotonous decay with increase of the Mw/Mn value should be resulted from heterogeneity of chain length of the brush. Indeed, W. M. de Vos *et al.* [14] have theoretically predicted the monotonous decay of volume fraction profile of polymer brush with Mw/Mn = 2.0 in a good solvent [13]. However, its experimental verification has not been done. The result obtained by the NR experiment was consistent with the prediction, and could provide a validity of the theory.

We confirmed that the effect of MWD of polymer brush in a good solvent appeared as difference in how the brushes are expanded in liquid media. The relationship between chain dimension and the physical properties will be revealed in the future, using the new reflectometer SOFIA and other characterization.

2.2 Interfacial glass transition temperature of polymer thin films

It was reported that the thermal and mechanical properties of polymer thin films were totally different from those of bulk. Glass transition temperature (T_g) of polymer thin films is extensively studied by various methods including X-ray/neutron reflectivity [16, 17], dielectric relaxation [18, 19], positron annihilation lifetime spectroscopy (PALS) [20], ellipsometry [21, 22] and so on. For polystyrene thin films supported on Si substrate, the decrease of T_g with thickness was observed and this finding is normally interrupted in terms of a mobile surface layer at the free surface. On the contrary, an increase of T_g with decreasing film thickness was observed for poly(methyl methacrylate) (PMMA) thin film supported on Si substrate, implying an interfacial interaction between PMMA thin film [22] and substrate. Summarizing so far reported experimental results, the anomalous physical properties of the free surface or the interfacial region are related to the physical properties of polymer thin films and we have to understand the heterogeneous dynamics of polymer thin films along depth direction. Compared to the investigation of physical properties of polymer thin at the free surface, the studies concerning the physical properties near the interface between polymer thin film and the substrate is still lacking due to the experimental difficulty.

In this report, we studied T_g of polymer thin films near the interface between polymer thin film and substrate (interfacial T_g) with bi-layer PS thin films consisting of the surface h-PS layer and the bottom d-PS layer using neutron reflectivity (NR).

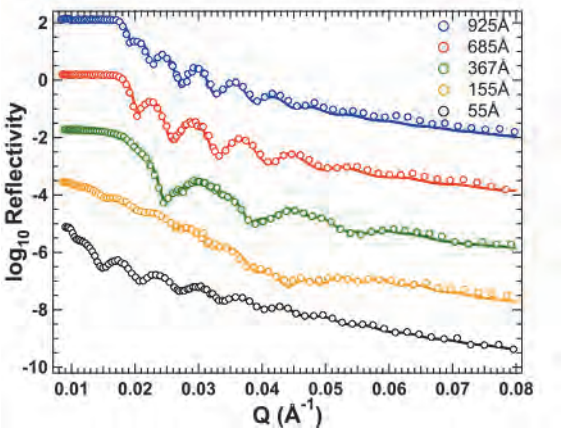

Fig. 12: Neutron reflectivity profiles from bi-layer thin films consisting of surface h-PS layer ∼890Å thick and bottom d-PS layer with various thicknesses at 313K and solid lines were the results of fit using a bi-layer model.

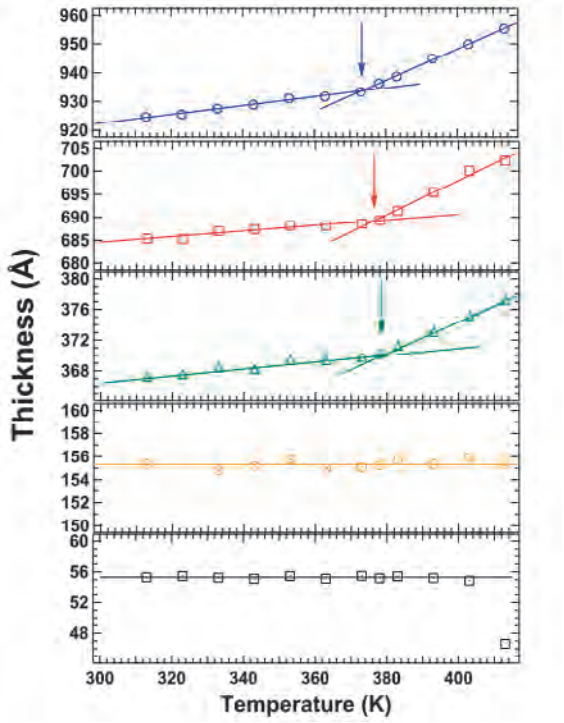

Fig. 13: Temperature dependence of thickness of bottom d-PS layer and solid arrows correspond to the evaluated T_g's of bottom layers.

Figure 12 shows the NR profiles from bi-layer films consisting of surface h-PS layer ∼880Å thick and the bottom d-PS with various film thicknesses at 313K. The solid curves, which are the results of fits with bi-layer model, could describe the experimental results

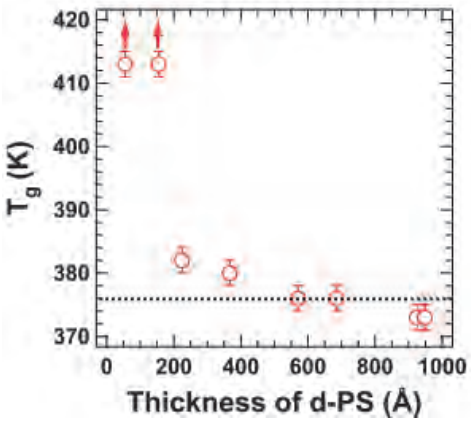

Fig. 14: Evaluated interfacial T_g as a function of thickness of bottom d-PS layer.

fairly well. The temperature dependence of the thickness of bottom d-PS layer is shown in Figure 13 and the evaluated T_g shown by solid arrows shifted to high temperature with decreasing film thickness, implying an onset of the interfacial effect between polymer thin film and substrate. For the bi-layer film with the bottom d-PS layer 155Å thick, we observed thermal zero thermal expansivity and it is considered that interfacial T_g shifted out of the experimental temperature range (T>413K). As for the bi-layer film with the bottom d-PS layer 55Å thick, the negative thermal expansivity was observed. Referring to the works performed by Miyazaki *et al.* [23], who studied the annealing effect on polymer thin films, the lack of annealing is related to the negative thermal expansivity. The detailed physical origin of negative thermal expansivity observed for the bottom d-PS layer ∼55Å is still under consideration, however at least we could point out that the interfacial T_g of the bottom d-PS ∼55Å thick was above experimentally accessible temperature range (>413K), too.

The evaluated interfacial T_g as a function of the thickness of bottom d-PS layer was summarized in Figure 14 and only the low limit was shown for the bottom d-PS layer below 155 Å thick. We observed the onset of the interfacial effect was at around ∼500Å from the substrate and this thickness was reasonable compared to so far reported values [24].

We confirmed that combination of multi-layer consisting of deuterated polymer and hydrogenated polymer and NR was powerful tool for the selective evaluation of T_g or related physical properties of polymer thin films along the depth direction precisely.

2.3 Surface Reorganization of Poly(methyl methacrylate) Films by Water [25]

In the future, the quantity of polymeric materials used for medical diagnosis and treatment will continue to increase. [26] New tools for tailor-made diagnostics, such as DNA arrays and tips for micro-total-analysis systems, are generally made from polymers. [27] Ultimately, we can expect that polymers will be buried in the human body as a part of organs and in-situ diagnostic or treatment equipment. [28, 29] In these applications, the polymer surface is in contact with a water phase. However, despite the importance of detailed knowledge of the fundamental interactions of polymer interfaces with liquids, such studies are very limited.

We have recently studied the density profiles of a deuterated poly(methyl methacrylate) (dPMMA) film spin-coated on a substrate in some non-solvents along the direction normal to the interface by neutron reflectivity (NR). [30, 31] NR measurement clarified that dPMMA film was swollen in water, which is a typical non-solvent, and the interface with water was diffuse in comparison with the pristine surface, probably due to the partial dissolution of segments into the water. If this is the case, the surface aggregation states of dPMMA should be changed in a relatively large scale by water. However, such cannot be experimentally demonstrated without using a selective label at the surface. In this study, a dPMMA monolayer was mounted onto a poly(methyl methacrylate) (PMMA) film to confer contrast between the surface and internal regions, resulting in a dPMMA/PMMA bilayer film. NR was then applied to the bilayer films to demonstrate whether the surface reorganizes by water.

Monodisperse PMMA and dPMMA with number-average molecular weight of 300 k and 296 k, respectively, were used. A dPMMA monolayer was transferred onto a PMMA spin-coated film, which was pre-annealed under vacuum for 2h at 423 K, resulting in a bilayer film. It was dried under vacuum for 1h at room temperature. The top dPMMA layer possessed the root-mean-square roughness of ca. 0.15 nm and the thickness of approximately 1 nm. The density profile of the bilayer film along the direction normal to the surface was examined by NR measurement with ARISA-II reflectometer. Reflectivity was also calculated on the basis of a model scattering length density (b/V) profile using Parratt32 software, which is a freeware program from the Hahn-Meitner Institute. [32] The (b/V) values of SiO_2, Si, dPMMA, and PMMA used for the calculations were 4.15×10^{-4}, 2.07×10^{-4}, 6.62×10^{-4}, and 1.04×10^{-4} nm^{-2}, respectively.

Figure 15 (a) shows the scattering vector ($q=(4\pi/\lambda)\cdot\sin\theta$, where λ and θ are the wavelength and the incident angle of the neutrons, respectively) dependence of NR for the bilayer films before and after annealing for 2h at 423 K. Open symbols denote experimental data. Solid curves are calculated reflectivity based on model scattering length density (b/V) profiles shown in the panel (b). The data after the annealing was offset by two decades for the sake of clarity. Since the calculated reflectivities were in good agreement with the experimental data, it can be claimed that the model

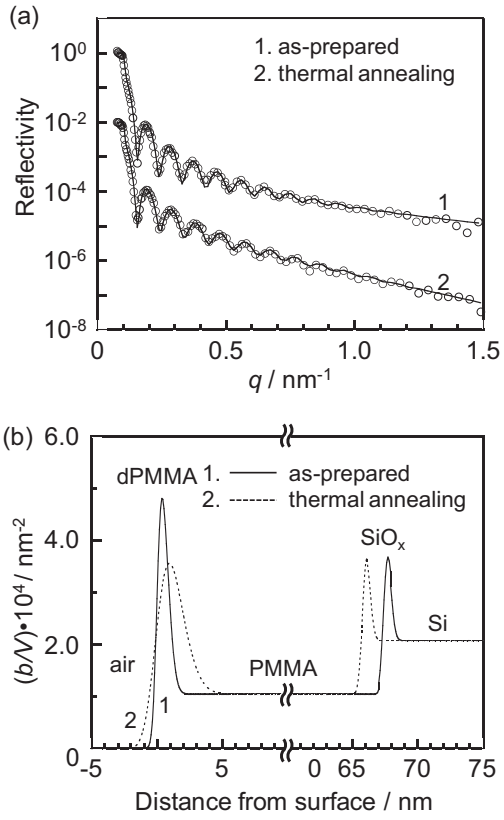

Fig. 15: (a) NR for dPMMA/PMMA bilayer films before and after the annealing. Open symbols denote experimental data. Solid curves are calculated reflectivities based on model scattering length density (b/V) profiles shown in the panel (b).

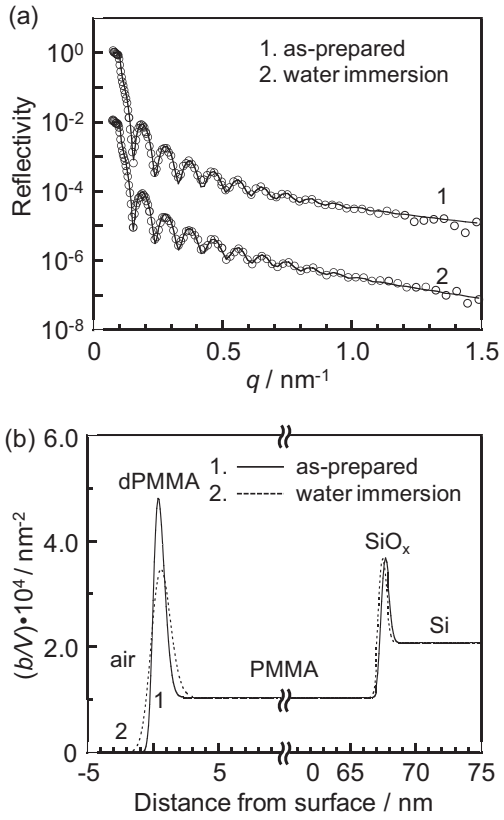

Fig. 16: (a) NR for dPMMA/PMMA bilayer films before and after water immersion. Open symbols denote experimental data. Solid curves are calculated reflectivity based on model scattering length density (b/V) profiles shown in the panel (b).

(b/V) profiles well reflect the density profiles of the bilayer along the direction normal to the interface. In this study, two independent bilayer films were used as before and after annealing. The thickness of the top dPMMA layer prepared by Langmuir-Blodgett method was identical in the two samples. However, the bottom PMMA layer prepared by a spin-coating method was not the case. The bottom layer as after annealing was slightly thinner than that as before annealing, as shown in the panel (b). However, this should not be crucial for our discussion because the top dPMMA layer was our interest. The annealing induced two clear structural changes for the bilayer; the (b/V) value decreased at the middle of the top dPMMA layer and the interface between dPMMA and PMMA became broader. This means that dPMMA segments diffused toward the interior region. The current annealing conditions should be good enough to fully relax dPMMA chains and thus to delete the preparation history. Nevertheless, dPMMA segments still existed at the top of the bilayer. Although this may not be explained in terms of the bulk diffusion coefficient of PMMA chains, similar slow diffusion, along the direction normal to the surface, has been reported. [33, 34]

To study to what extent the aggregation states of PMMA at the surface can be altered by water molecules, NR was applied to similar bilayer films. Figure 16 shows the q dependence of NR for the two bilayer films before and after water immersion for 2h at room temperature. Open symbols and solid curves have the same meaning as before. The data after the water immersion was offset by two decades for clarity. Surprisingly, the (b/V) profile shown in the panel (b) was discernibly changed after the water immersion. That is, the (b/V) value decreased at the middle of the top dPMMA layer and the interface between dPMMA and PMMA became broader. Although the extent was not so striking in comparison with the previous thermal annealing, it is clear that dPMMA segments in the top layer diffused into the internal dPMMA phase. Taking into account that water has been regarded as a typical non-solvent of PMMA, the results shown in Figure 16 are quite intriguing. This result is quite reasonable for our parallel experiment to examine interfacial relaxation of PMMA by lateral force microscopy, [35] showing that the segmental mobility of PMMA at the water

interface was much faster than that at the sir-facing surface, and local conformation of PMMA at the water interface by sum-frequency generation spectroscopy. [36]

In conclusion, surface aggregation states of PMMA were altered by water, which is a typical non-solvent. This is because water molecules could penetrate into the PMMA film. More conclusive study for the surface reorganization of PMMA by water will be reported shortly showing how fast it attains on the basis of in-situ NR measurements.

2.4 In situ neutron reflectivity measurements of asymmetric polystyrene interface

Understanding the mobility of polymers at interfaces is crucial to the optimization of adhesion, welding, crack healing, etc. Neutron reflectivity (NR) measurement is a powerful tool for investigation of polymer interdiffusion because of its superior depth resolution. However, the fitting process of NR profiles is not examined in detail. Since the simple Fickian model (symmetric error function) has been used for the analyses even in the asymmetric bilayer films in terms of molecular weights, accurate diffusion coefficients cannot be obtained. The objective of this study is to elucidate the interdiffusion behavior of polystyrene bilayer films with different molecular weights by time-resolved neutron reflectivity (TR-NR) measurements. We demonstrate the utility of the combination of TR-NR measurements and analyzing those based on the concentration profiles obtained by solving diffusion equation.

Linear deuterated polystyrene (l-dPS) was prepared by a living anionic polymerization. Linear normal polystyrene (l-hPS) was purchased from Tosoh Corp. Weight-average molecular weights, M_ws, of l-dPS and l-hPS were evaluated to be 127k and 427k, respectively, by multi-angle laser light scattering (MALLS) measurements.

l-hPS/l-dPS bilayer films were prepared by floating method. TR-NR experiments were performed on ARISA-II, with polychromic wavelengths ranging from 0.20 to 0.88 nm, $D_{s\text{-}d}$ = 1777 mm. For TR-NR measurements, the high-temperature cell was maintained at 405 K and the incident angle was fixed at 0.6° before putting a sample. After checking the temperature of the cell, a bilayer sample was put onto the cell.

Neutron reflectivity profiles were analyzed based on a model of interdiffusion with different physical properties proposed by Jabbari and Peppas [37]. This model was developed for describing the interdiffusion at an interface with different physical properties. In this model, diffusion coefficients are governed by the frictional coefficients in matrix. When the polymer species are identical, the interdiffusion behavior can be treated properly.

The partial differential equation describing the diffusion process at the interface between two compatible polymers can be expressed in the following form after differentiation with respect to the z axis:

$$\frac{\partial \phi_s}{\partial t} = D\frac{\partial^2 \phi_s}{\partial z^2} + \frac{\partial D}{\partial \phi}\left(\frac{\partial \phi_s}{\partial z}\right)^2 \quad (1)$$

$$D = D_0\left(\frac{1-\phi_s}{N_s}+\frac{\phi_s}{N_f}\right)\left(\frac{1-\phi_s}{N_s}+\frac{\phi_s}{N_f}+2\chi_{sf}\phi_s(1-\phi_s)\right) \quad (2)$$

where φ_s, N_s, N_f, and χ_{sf} are the volume fraction of slower component, the degree of polymerization of slower and faster components and the Flory-Huggins interaction parameter, respectively. D_0 is the diffusion coefficient for the entanglement segment and can be described as

$$D_0 = \frac{RTN_e}{f_m} \quad (3)$$

where N_e and f_m and T are the degree of polymerization of entanglement segment, the friction coefficient of the monomeric unit and temperature, respectively. D_0 is the fitting parameter in this analysis. The initial and boundary conditions for solving the above diffusion equations are:

$$t = 0 \quad \varphi_f = 0 \quad \text{for } 0 \le z < d_s \quad (4)$$
$$t = 0 \quad \varphi_f = 1 \quad \text{for } d_s \le z \le d_s + d_f \quad (5)$$
$$z = 0 \quad \partial\varphi_f/\partial z = 0 \quad \text{for } t > 0 \quad (6)$$
$$z = d_s + d_f \quad \partial\varphi_f/\partial z = 0 \quad \text{for } t > 0 \quad (7)$$

where d_s and d_f are the film thicknesses of slower and faster components, respectively. It is important to recognize the importance of each term on the right-hand side of equation (2). The first term represents interdiffusion at the interface between the two polymers while the second term represents the swelling of the slower-moving component by the faster-moving component [37].

Figure 17 shows the selected NR profiles and the calculated reflectivities based on symmetric and asymmetric interfaces. If the flux of hPS is equal to that of dPS, the scattering length density, (b/V), profile is symmetric at the interface. In this case, the top of the fringes of the calculated reflectivity profiles simply decays with increasing time and the position of the fringe top is maintained as shown in Figure 17a. On the other hand, the (b/V) profile obtained by solving partial differential equation of (1) was asymmetric at the interface. The calculated reflectivities based on the asymmetric interface are shown in Figure 17b. Since the χ^2 values of the reflectivies for asymmetric interfaces (Figure 17b) are smaller than those for symmetric ones (Figure 17a), the (b/V) profile obtained by solving the diffusion equation reproduce more an accurate re-

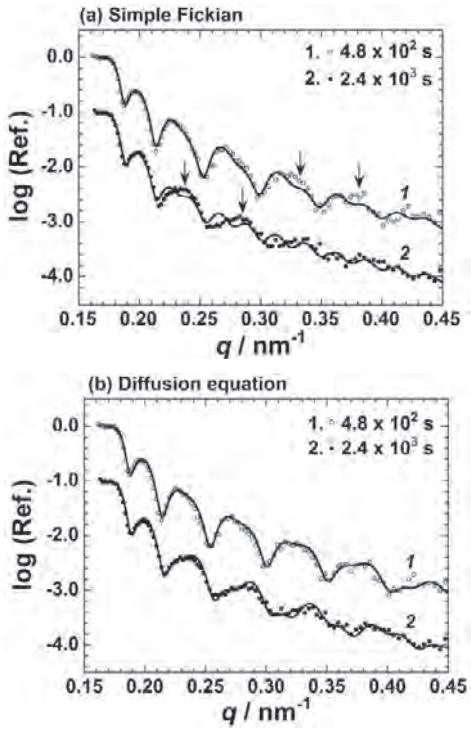

Fig. 17: Selected neutron reflectivity profiles and those analyzed by (a) simple Fickian (symmetric error function) and by (b) solving diffusion equation (eq.1). The symbols represent the experimental values and the solid lines denote the calculated ones.

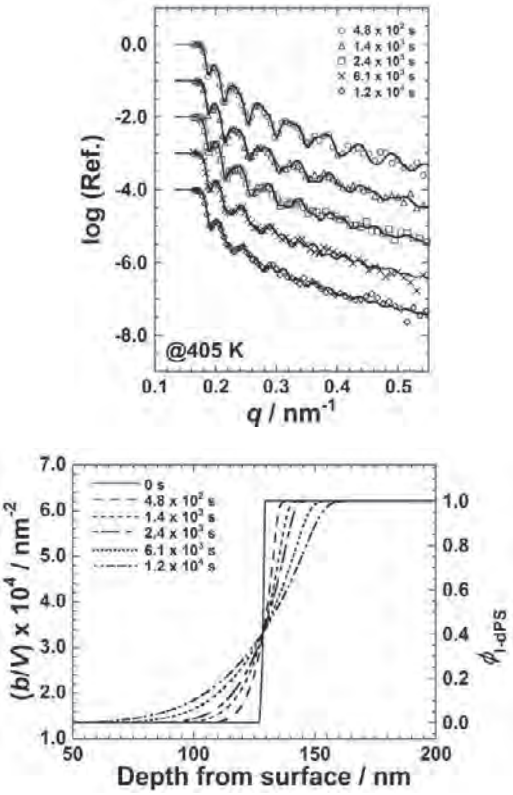

Fig. 18: Selected TR-NR profiles and the model (b/V) profiles near l-hPS-427k/l-dPS-127k interface.

flectivity profile than that done by the simple Fickian equation.

Figure 18a shows the selected neutron reflectivity profiles of l-hPS-427k/l-dPS-127k bilayer film annealed at 405 K for 4.8×10^2 s, 1.4×10^3 s, 2.4×10^3 s, 6.1×10^3 s, and 1.2×10^4 s. The symbols represent the experimental values and the solid lines are the calculated reflectivities based on the model (b/V) profiles shown in Figure 18b. The initial interface is located at 127.3 nm from the surface drawn by the dotted line. The (b/V) profiles gradually broaden with increasing time. The shapes of the (b/V) profiles are asymmetric; the (b/V) profiles in l-hPS side are very broad but those in the l-dPS side are relatively sharp. Furthermore, the value at the intersection of (b/V) profiles is 3.35×10^{-4} nm^{-2}, which corresponds to φ of l-dPS $=$ 0.41. Thus, these results clearly indicate that the flux of low molecular weight component (l-dPS) is larger than the high molecular weight one (l-hPS) at the interface.

The D_0 values gradually decreased with increasing time and reach the constant value of 4.4×10^{-2} `m s^{-1} around the critical time, τ_c, of 6×10^3 s. This means that steady-state interdiffusion proceeds at $t > \tau_c$ while segmental diffusion is dominant at short-time region.

In conclusion, TR-NR profiles of an asymmetric bilayer film are analyzed by the (b/V) profiles obtained by solving partial differential equation and diffusion coefficients can be obtained.

2.5 Spontaneously formed polymer brush at water/polymer interfaces

It is well known that surfaces covered with water-soluble polymers such as poly(ethylene glycol) (PEG) shows anti-fouling property and blood compatibility [38]. Such a surface architecture is often called polymer brush, and its unique properties have been attracting a lot of attention. In general, polymer brush is fabricated either by attaching functional polymers to surfaces (grafting-to) or by synthesizing polymers initiated from surfaces (grafting-from).

The spontaneous surface segregation phenomena of copolymers with surface-active blocks should be useful for preparing such a brush layer in spontaneous process [39]. We report hydrophilic polymer brushes formed at the interface between water and hydrophobic polymer matrix by the segregation of amphiphilic diblock copolymers blended in the matrix. In this system, while the hydrophilic block with high surface energy avoids air surface it segregate to cover the interface between hy-

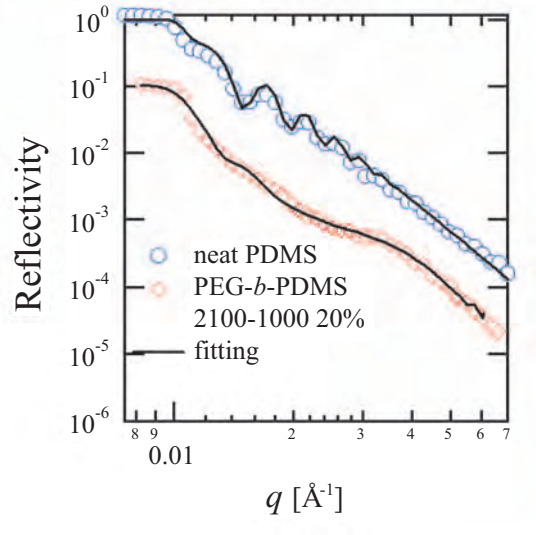

Fig. 19: Neutron Reflectivities of sample films containing no copolymers (neat PDMS) and 20 wt% of PEG-*b*-PDMS (M_n = 2100-1000).

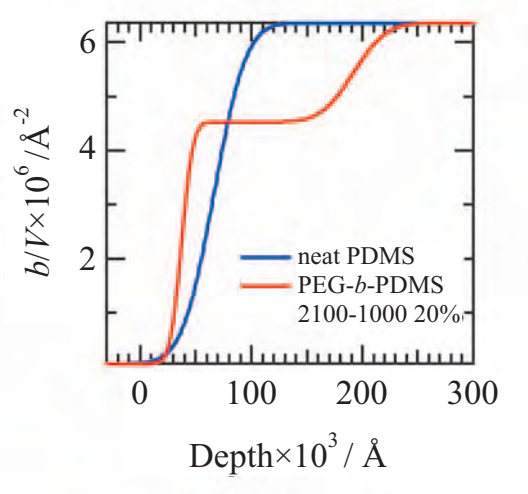

Fig. 20: Scattering length density profiles at D_2O/sample interfaces obtained by the fitting the reflectivity curves.

drophobic PDMS and water. The structures of spontaneously formed brush layers at D_2O/polymer interfaces were observed by NR.

We have conducted NR studies using an ARISA-II on BL16 at MLF, J-PARC. We have tested several kinds of amphiphilic block copolymers in various copolymer concentrations. Figure 19 shows neutron reflectivity curves at the D_2O/PDMS films containing 20 wt% of PEG-*b*-PDMS (M_n = 2100-1000) and at D_2O/ neat PDMS. The formation of a clear brush layer was suggested by the appearance of fringe at around q = 0.04 Å^{-1}. The scattering length density profiles obtained by fitting with box models are shown in Figure 20. The brush density was calculated to be as high as 0.2 chains/nm^2 from the profile which is surprisingly comparable to polymer brushes fabricated by the grafting-from method.

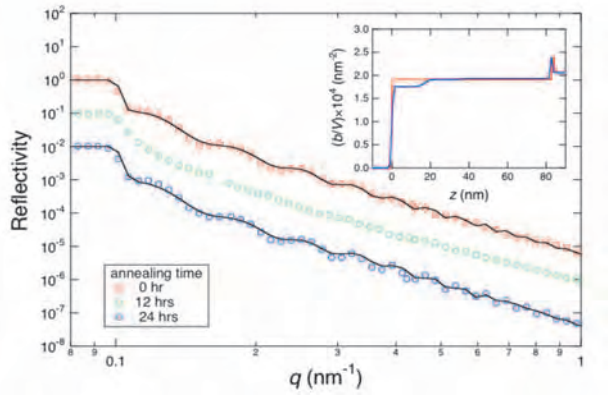

Fig. 21: Specular neutron reflectivity profiles for d-PS/h-PS blend thin films after annealing for different time at 120°C. The solid lines on the reflectivity profiles are calculated ones from depth profiles of (b/V) shown in the inset.

2.6 De-wetting suppression of a polymer thin film by blending a high molecular weight component

Polymers are nowadays utilized as a form of thin film in a variety of industrial applications such as coating, paint, adhesion, and so on. The contribution of interfacial interaction with air or a substrate is enhanced with decreasing the film thickness. As a result, polymer thin films are unstable and often encounter de-wetting from a substrate. Thus many attempts have been made so far to suppress the de-wetting of polymer thin film.

Here, depth distribution of component polymers was investigated for thin films of binary polystyrene blends with different molecular weights by neutron reflectometry, to understand the mechanism of de-wetting suppression effect by adding small amount of high molecular weight component. The samples used were a poly(styrene-h_8) (h-PS) with number-averaged molecular weight M_n=10×10^3, and a poly(styrene-d_8) (d-PS) with M_n=60×10^3. The weight fraction of d-PS, that is, the higher molecular weight component, in the blend was 0.1. Thin film specimens were prepared by spin-coating from dilute toluene solution of the blend on silicon substrates, used as received from a manufacturer, with a native oxide layer.

Figure 21 compares specular neutron reflectivity profiles for d-PS/h-PS blend thin films annealed at 120°C for different times: 0, 12, and 24 hours. It was confirmed by an optical microscope that no de-wetting occurred for all the blend thin films examined here. The as-prepared blend film, that is, without annealing, shows regular Kiessig fringes in the reflectivity profile,

though they are not so clear since scattering length density, (b/V), of the film is not high. It was evaluated by a model fitting with a depth profile of (b/V), shown in the inset, that the film exhibits constant (b/V) value, that is, 1.9×10^{-4} nm^{-2}, through the film thickness of about 80 distributed in the as-prepared film. However, the Kiessig fringes almost disappeared after annealing for 12 hours. Further annealing of the film brought about appearance of the Kiessig fringes in the reflectivity profile. The corresponding depth profile of (b/V) in the inset represents lower value at the film surface than the inside, suggesting that h-PS with the lower molecular weight was preferentially segregated to the film surface due to its less penalty in conformational entropy compared with a higher molecular weight component.

3. Conclusion

At BL16 in J-PARC/MLF, we have constructed a horizontal type neutron reflectometer ARISA-II and SOFIA. Thanks to the high flux beam and instrumental upgrades, the specular reflectivity can be measured up to 10^{-7} within a few hours for a 3 inch substrate at 220 kW. Also, time resolved measurement with the slice of a few minutes, and off-specular reflectivity measurement with a position sensitive detector were possible. Using the reflectometers, we have investigated the chain dimensions of polyelectrolyte brushes in contact with water, the surface and interface effects on the glass transition and non-solvent immersion using deuterium labeling, interdiffusion behavior of asymmetric polymer/polymer interfaces with time-resolved measurement, self-assembled polymer brush at water/polymer interfaces, polymer distribution depending on molecular weight in a polymer blend thin film, and so on.

For further upgrade, we developed a focusing mirror system and succeeded in the specular reflectivity measurement with sample focusing geometry. Beside this, we are developing a 2-dimensional M-MSGC with ^{3}He gas for high throughput measurement, and planning to install MIEZE type NSE system for slow dynamics measurement in ns order [40, 41].

References

[1] K. Mitamura *et al.*, *J. Phys. Conf. Ser.* **272**, 012017 (2011).
[2] M. C. Rheinstödter *et al.*, *Phys. Rev. Lett.* **97**, 048103 (2006).
[3] M. Hishida *et al.*, *Phys. Rev. E* **80**, 051407 (2009).
[4] N. Torikai *et al.*, *J. Phys. Conf. Ser.*,in press.
[5] B. Lee *et al.*, *Macromolecules* **38**, 4311 (2005).
[6] C. M. Papadakis *et al.*, *Langmuir* **24**, 13815 (2008).
[7] W. A. Hamilton *et al.*, *J. Chem Phys.* **116**, 8533 (2002).
[8] M. Wolff *et al.*, *Phys. Rev. Lett.* **92**, 255501 (2004).
[9] P. Muller-Buschbaum *et al.*, *Langmuir* **22**, 9295 (2006).
[10] A. Oed, *Nucl. Instr. and Meth. A* **263**, 351 (1988).
[11] H. Takahashi *et al.*, *Nucl. Instr. and Meth. A* **458**, 375 (2001).
[12] S. T. Milner et al., *Macromolecules* **21**, 2610 (1998).
[13] A. Karim *et al.*, *Phys. Rev. Lett.* **73**, 3470 (1994).
[14] W. M. Vos *et al.*, *Polymer* **50**, 305 (2009).
[15] M. Kobayashi *et al.*, *Macromolecules* **43**, 8409 (2010).
[16] T. Miyazaki *et al.*, *Phys. Rev. E* **69**, 061803 (2004).
[17] T. Kanaya *et al.*, *Polymer* **44**, 3769 (2003).
[18] K. Fukao, and Y. Miyamoto, *Phys. Rev. E* **61**, 1743 (2001).
[19] A. Serghei *et al.*, *Macromolecules* **39**, 9385 (2006).
[20] G. B. DeMaggio *et al.*, *Phys. Rev. Lett.* **78**, 1524 (1997).
[21] S. Kawana, and R. A. L. Jones, *Phys. Rev. E* **63**, 21501 (2001).
[22] J. L. Keddie, *et al.*, *Faraday. Discuss.* **98**, 219 (1994).
[23] T. Miyazaki *et al.*, *Phys. Rev. E* **69**, 022801 (2004).
[24] K. Tanaka *et al.*, *J. Phys. Chem. B* **113**, 4571 (2009).
[25] A. Horinouchi *et al.*, *Chem. Lett.* **39**, 810 (2010).
[26] M. A. Wheatley, in Polymer-Based Nanostructures Medical Applications, ed. by P. Broz, Royal Society of Chemistry, Cambridge (2010) Chap. 7.
[27] Y. Sun and Y. C. Kwok, *Anal. Chim. Acta* **556**, 80 (2006).
[28] J. Jagur-Grodzinski, *Polym. Adv. Technol.* **17**, 395 (2006).
[29] P. S. Dittrich *et al.*, *Anal. Chem.* **78**, 3887 (2006).
[30] K. Tanaka *et al.*, *Langmuir* **24**, 296 (2008).
[31] H. Atarashi, *et al.*, *J. Phys. Chem. Lett.* **1**, 881 (2010).
[32] Berlin Neutron Scattering Center (BENSC) Parratt32 Program. http://www.hmi.de/bensc/ instrumentation/instrumente/v6/refl/parratt˙en.htm (accessed February 2004).
[33] S. K. Kumar *et al.*, *Macromolecules* **23**, 2189 (1990).
[34] Y. Pu *et al.*, *Phys. Rev. Lett.* **87**, 20 (2001).
[35] Y. Fujii *et al., J. Phys. Chem. B* **114**, 3457 (2010).
[36] Y. Tateishi *et al.*, *Polym. Chem* **1**, 303 (2010).
[37] E. Jabbari, N. A. Peppas, *Polymer* **36**, 575 (1995).
[38] A. Halperin, *Langmuir* **15**, 2525 (1999).
[39] H. Yokoyama *et al.*, *Macromolecules* **26** 5180 (2005).
[40] M. Hino *et al.*, *Physica B* **385-386**, 1125 (2006).
[41] H. Hayashida, *et al.*, *Nucl. Inst. Meth. A* **600**, 56 (2009).

Polarization Analysis Neutron Spectrometer Project in J-PARC

K.Ohoyama, K.Iwasa[1], T.Yokoo[2], S.Itoh[2], H.Hiraka, M.Fujita, M.Matsuura, H.Kimura[5], T.J.Sato[3], H.Seto[2], K.Tomiyasu[1], K.Kaneko[4], T.Arima[5], T.Ino[2], T.Oku[4], H.M.Shimizu[2], M.Takada[4], J.Suzuki[4], M.Hino[6], T.Muto[2], J.Suzuki[2]

Institute for Materials Research, Tohoku Univ., Sendai, Miyagi, 980-8577, Japan
[1]Department of Physics, Tohoku Univ. Sendai, Miyagi, 980-8578, Japan
[2]Neutron Science Laboratory, High Energy Accelerator Research Organization (KEK), 1-1 Oho, Tsukuba, Ibaraki, 305-0801, Japan
[3]Institute for Solid State Physics, Univ. of Tokyo, Kashiwa, Chiba, 277-8581, Japan
[4]Quantum Beam Science Directorate, Japan Atomic Energy Agency, Tokai, Ibaraki, 319-1195, Japan
[5]Institute of Multidisciplinary Research for Advanced Materials, Tohoku Univ., Sendai, 980-8577, Japan
[6]Research Reactor Institute, Kyoto Univ., Kumatori, 590-0494, Osaka, Japan

This project is aiming at constructing a neutron polarization analysis spectrometer based on a collaboration between universities and KEK, which will make it possible to investigate complicated spin correlations in novel magnetism, in particular, strongly correlated electron systems. The proposal was accepted by the first stage panel of J-PAPC Center on 15-May-2011; now preparations for the final panel are under progress.

The polarization analysis technique is indispensable for investigations of mechanism of multipolar orderings, high-T_C superconductivity, and multiferroics systems. The instrument in this project is a high-intensity and middle-resolution chopper spectrometer with short L2; as a polarizer, a ^{3}He spin filter-type will be installed. Since many technical developments will be needed, flexibilities of the alignment are highly required. For such developments of novel neutron experiments techniques, in particular, the polarized neutron method, strong supports of KEK through the S-type project, which has high ability of neutron instrumentations and generation of polarized neutrons, are indispensable to achieve the ambition.

Designs of the spectrometer

The project team has applied to install this spectrometer at the BL23 beamline, though it is not authorized yet. Fig. 1 is a schematic rendering view of the spectrometer, drawn by Mr. J. Suzuki of KEK through this S-type project. The flight pass are L1=17m, L2=2m, and L3=2m, respectively. Since a space for the polarizer system is needed between the chopper and the sample position, L3 becomes longer than conventional chopper spectrometers. The PSD detector bank is a rotary type; covering scattering angle is about 60°, which is determined by the limit size of ^{3}He filter analyzer which will be installed between the sample position and detectors. In 2010FY, we purchased 18 PSD of 3/4 inch (14M Yen) as detectors of this spectrometer, which will be used for tests, as well as experiments after the construction.

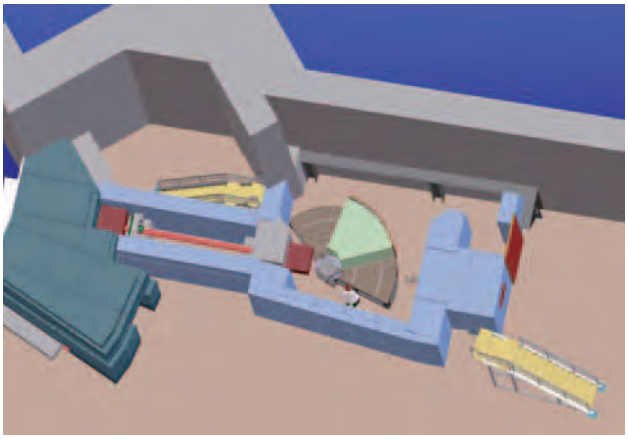

Fig. 1: Schematic rendering view of the spectrometer, at BL23. (drawn by J. Suzuki of KEK)

An important point of this project is the beam flux, because for polarization analysis, flux becomes 1/4 of the unpolarized beam in principle, or ∼1/25 for ^{3}He spin filters as the polarizer and analyzer. Thus, effective focusing in the guide tubes is indispensable. In 2010FY, we succeeded in finding a focusing model which gives six times enhancement. Fig. 2 shows a result of simulation calculations of the model with McStas. This result indicates that the flux at 100meV is expected to be $5*10^5$ (n/sec/cm2/meV/1MW) for m=4(red). Based on the S-type project of KEK, we estimated performance of shields of this specrometer by simulation calculations of amount of radiation of neutron and photon; the simulation calculated was done by RIST. Basically, we succeeded in finding a good model of the shield structure of the spectrometer.

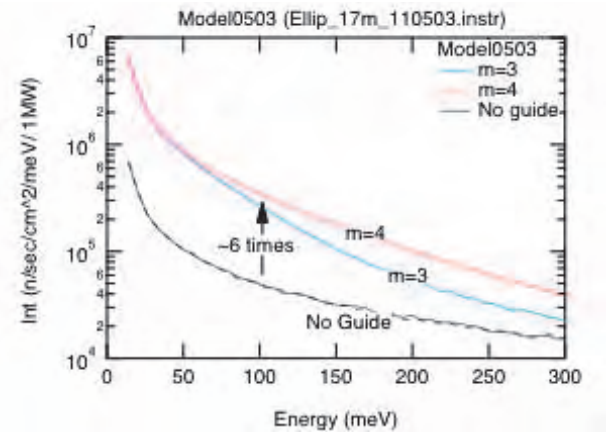

Fig. 2: Expected flux of white beam at the sample position for L1=17m calculated with McStas. At E=100meV, $5*10^5$ (n/sec/cm2/meV/1MW) is expected for m=4(red).

Fig. 3: Workshop of S-type project held in Tokai on April-2010. In 2010 FY, two domestic workshop and one international workshop were held to discuss science and concept of this project.

Polarizer (SEOP, Proton Filter)

The most important device in this project is polarizer/analyzer. In the present project, a SEOP type 3He filter polarizer will be used, because this technique shows most high performance and feasibility at present. The SEOP system is developed under a JEAE-KEK-Tohoku Univ. collaborative project and this S-type project. Moreover, in this project, another technique is also developing: the dynamic proton filter method, in which development of a highly polarized proton filter is indispensable. By using the proton filter technique, higher neutron polarization over 90% is realized in the thermal neutron region. Moreover, an important advantage of the proton filter technique for material science is that superconducting magnets can be used for sample accessaries, while it is quite difficult or almost impossible for the SEOP system. In this S-type project, thus, the dynamic proton filter method is developing for the future technique.

On theother hand, as the first stage of this project, supermirror packages will be used as the analyzer. Thus, in 2010FY, we purchased test pieces of polarization supermirrors (12M Yen), which will be used for feasibility studies for thermal neutrons.

Workshops

In 2010FY, two domestic workshops and one international workshop were held to discuss science themes and the detailed designs of the spectrometer (fig. 3); these workshops were partly supported by the S-type project of KEK. In particular, on 6-8, January, International workshop on novel material science using polarized neutrons was held in Institute for Materials Research, Tohoku Univ. We had 55 participants, including 6 participants from abroad. In the international workshop, many important suggestions and advice were given from the participants.

Plan in 2011FY

In 2011FY, we should pass the final panel of J-PARC Center as soon as possible to start construction process. Moreover, We develop a test device of suppermirror, and will have test experiments using neutron beam simultaneously. In 2011 FY, we are going to have some workshops to discuss science themes using polarized neutron and ideas of the spectrometer more details.

Development of an Advanced Special Diffractometer under Extreme Environment for Materials

T.Fukunaga[1], K.Mori[1],
T.Kamiyama[2], M.Yonemura[2], K.Kino[2], S.Torii[2], M.Kawai[2]

[1]*Research Reactor Institute, Kyoto University, Asashiro-nishi, Kumatori, Sennan, Osaka 590-0494, Japan*
[2]*Institute of Materials Structure Science, High Energy Accelerator Research Organization, Oho, Tsukuba, Ibaraki 301-8501, Japan*

A new neutron diffractometer, SPICA, at the ninth beamline (BL09) are designed for the study of materials under special environments, such as battery research. Lithium ion batteries (LIB) are promising power sources such as cell phones and laptop computers because of the high energy density. If the power capability could be improved, new applications such as a battery of electrical vehicles will spread out. In order to improve or innovate the battery characteristics, the clarification of the structure in materials of the positive and negative electrodes and their solid electrolyte interface at the atomic level will be very important and its information becomes a technological lodestar. a

The design concept of SPICA is to investigate the atom configuration of materials under special environments. In order to measure the atom location or the change of the atomic configuration precisely under special environments, SPICA diffractometer was designed to have the high resolution and high intensity. Therefore, the BL09 beamline for SPICA diffractometer views the decoupled-poisoned moderator. Moreover, SPICA diffractometer will be set with the flight path of L_1=52 m, which is the distance from the moderator to the sample position. The guide line was designed to keep the high intensity at the sample position. The high-performance focusing system with elliptic supermirrors was adopted to suppress diffuse intensity. According to the preliminary simulation of the guide line, the elliptic guide has an excellent performance over a wide range of wavelengths, in particular at short wavelength. Since in the beam line we have three disk choppers and one T_0 chopper, the guide line is divided by nine sections.

The flight path of 52 m from the moderator to sample position means that SPICA is located outside of the main hall of the Materials and Life Science Facility (MLF). Then we constructed an experiment building for SPICA as shown in Fig. 1 and Photo.1. The experiment building with about the size of 12(w) x 32(l) x 10(h) meters was designed to consist of two areas, that is, an experiment room and experimental preparation room.

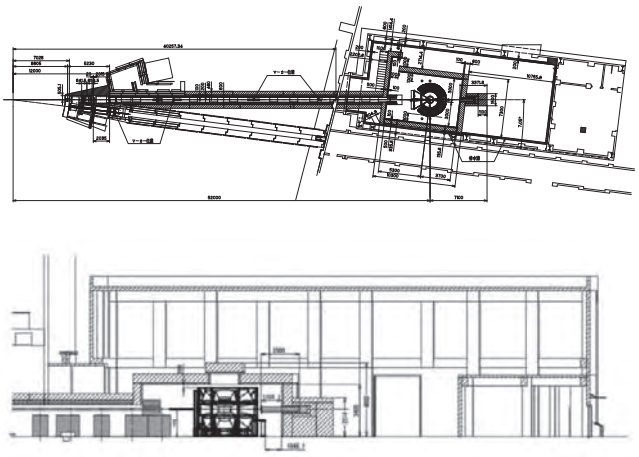

Fig. 1: The ground plan of BL09 and the cross-section drawing of the experiment building for SPICA.

Photo. 1: The view of the experiment building of BL09.

SPICA diffractometer was designed to consist of three detector banks that are the backward detector bank (150-175 degrees), the multipurpose detector bank (13-140 degrees) and the forward (small angle) detector bank (1-25 degrees) as shown in Fig. 2. The distance L_2 from the sample to detectors is about 2 m for all banks. Specially, the backward detector bank is used

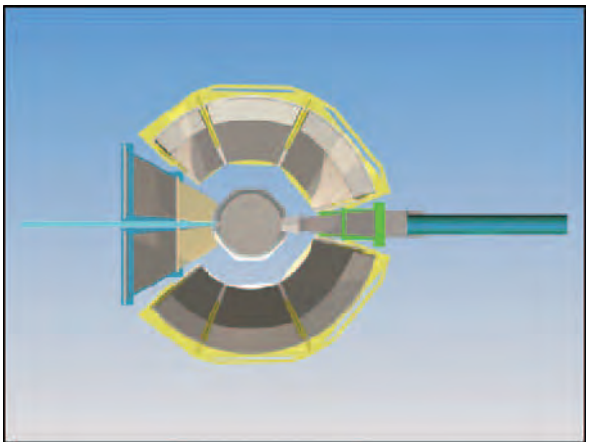

Fig. 2: Three detector banks (blue: backward detector bank of 150-175 degrees, yellow: multipurpose detector bank of 13-140 degrees, green: forward detector bank of 1-25 degrees) of SPICA diffractometer.

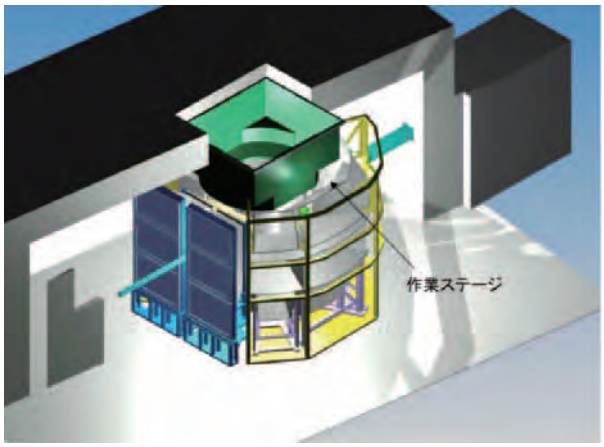

Fig. 3: Partially schematic perspective view of SPICA diffractometer.

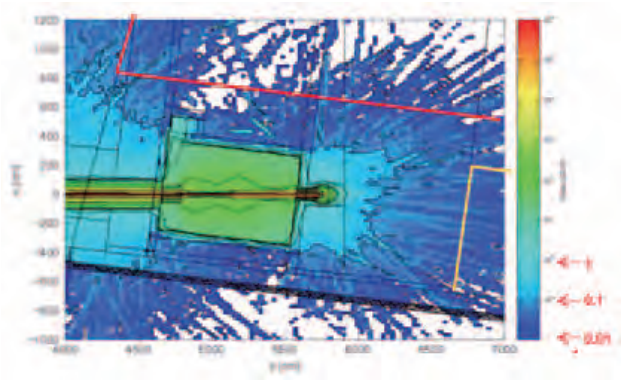

Fig. 4: An example of radiation calculation of the SPICA.

to realize the high-resolution measurement of lattice parameters because of reducing a $\cot\theta\Delta\theta$ contribution to the overall resolution. To cover this large detector area, about 1500 one-dimensional ^{3}He position-sensitive detectors (PSD's: 64 cm in length x half inch in dia meter) will be used.

The wide angle detector system with the backward detector bank, the multipurpose detector bank and the forward detector bank allows us to measure the diffraction data in the wide scattering vector Q range or wide lattice space d range. More importantly, an in-situ observation of the atomic structure can be carried out under various special conditions. Therefore, all detectors of the three banks play an important role to detect tiny change and time-dependent change in structure on charging/discharging process of the battery.

In order to fulfill the role and aim of the detector banks, the chamber of the backward detector bank is evacuated for the high-resolution measurement on lattice space and the chamber of the forward detector bank is also evacuated to reduce the background due to the downstream neutron beam. In contrast, the multipurpose detector bank has air scattering chambers in order to make it a snap to handle the various specialized equipment around the sample.

Kino et al.[1)] have reported the loss of neutron and contamination of scattered neutrons obtained by numerical calculation and simulation to materialize the air scattering chamber. The loss of neutrons is 6 to 11 % although it is almost double compared to that of the vacuum scattering chamber. The contamination of the scattered neutrons by air is less than 1% by placing blades made of B_4C resin in the chamber as dense as possible. The contamination is seen on the TOF spectrum as continuous backgrounds between diffraction peaks. The air scattering chamber with the blades is acceptable for the multipurpose detector bank of SPICA diffractometer. A partially schematic perspective view of SPICA diffractometer is shown in Fig. 3. In Fig. 4, an example of radiation calculation of the SPICA and the BL09 building is shown.

Reference

1) K. Kino, K. Mori, M. Yonemura, S. Torii, M. Kawai, T. Fukunaga, T. Kamiyama, J. Phys. Soc. Jpn. **80** (2011) accepted.

Neutron Transmission Imaging

Y.Kiyanagi, T.Kamiyama, S.Muto*, S.Satoh*, J.Haba*, H.M.Shimizu*,
T.Tanimori**, M.Ooi***, T.Shinohara***

Graduate School of Engineering, Hokkaido University
Kita 13, Nishi 8, Kita-ku, Sapporo, Hokkaido, 060-8628, Japan
**Neutron Science Laboratory, High Energy Accelerator Research Organization (KEK),*
1-1 Oho, Tsukuba, Ibaraki, 305-0801, Japan
***Division of Physics, Graduate School of Science, Kyoto University*
Oiwake-cho, Kita Shirakawa, Sakyo-ku, Kyoto, 606-8502, Japan
****J-PARC Center, Japan Atomic Energy Agency*
Shirakata Shirane 2-4, Naka-gun, Tokai, Ibaraki, 319-1195, Japan

Neutron transmission imaging is a useful method for inspecting inside of objects. So far, reactor based steady neutron sources are used for neutron imaging. On the other hand, pulsed neutron imaging has been proved to give images of crystal texture information of inside of materials, magnetic field and so on. This project is aiming at promoting the neutron transmission imaging not only at large facilities but also medium and small facilities. Here, we present new results on imaging using a pulsed source and detector developments for the imaging.

We performed experiments on energy resolved imaging at J-PARC. The effect of the multiple scattering and the diverse of the beam on the obtained image is one of items to be studied. We measured transmission through 20 mm thick iron rod having heat treatment at surface area with the aid of MCP detector [1]. A multichannel plate (MCP) collimator was placed just after the sample. The thickness of Fig. 1 Transmission of iron rods with and without a collimator indicating the scattering and diverse of beam.

MCP is 1mm and the diameter of the hole is 10 micro m. Figure 1 shows a transmission images around 4.5A with and without the collimator. 1/4 parts of two samples were measured at once. The transmission without the collimator was about 30% and that with the collimator is about 15% while the values slightly changed depending on the layers. This indicates that the multiple scattering effect appeared in the transmission. In the case with the collimator the image shows smooth change of the boundary of two layers. Furthermore, enhancement of the boundary of two layers was observed in the case without the collimator. This may be attributed to the phase contrast effect usually appeared at the boundary where the density changes. We need further investigation on this problem.

At the JSNS, *Au-In-Cd* alloy is developed as a new decoupler material [2]. In general, the alloy is used to be made by a melting method. However, we made it with a diffusing method at the maximum temperature of 850°C (Melting point of Au is 1063°C). We can see the surface of the alloy with SEM/EDX but observing inside is still difficult. We have to confirm uniformity of the alloy. Then, we measured the atomic distribution of the alloy with the neutron resonance imaging technique with the MCP detector [2]. Measured samples and results are shown in Fig 2. The samples are *Au-In-Cd* alloy composing of *Au* 74.9, *In* 0.5, and *Cd* 24.6 at% (t=0.9mm), *Au* (t=500μm and t=1000μm) and *In* (t=10μm). The measurement was performed at J-PARC BL10 (NOBORU). Distance from the moderator to the MCP detector was 14m. Samples were set on the detector. Time resolution of the detector was 1μsec and time bins are 1500 channels. Neutron trans-

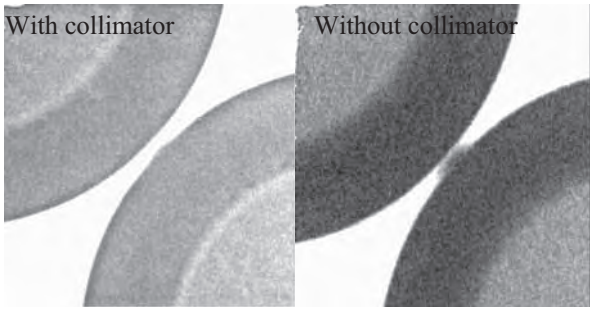

Fig. 1:

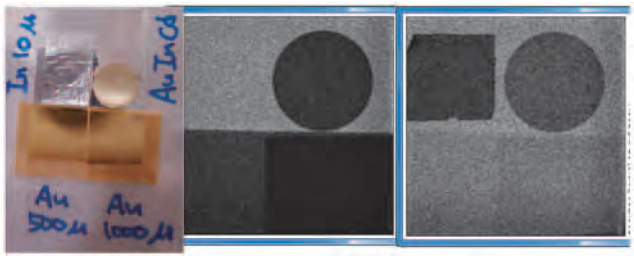

Fig. 2: Sample (left) and neutron resonance images for *Au* (center) and *In* (right).

mission curves are shown in Fig. 2. Center figure of the Fig. 2 shows neutron resonance image of Au (T=480 to 500 μsec), In (T=830 to 850 μsec). From these results, we can see Au and In are distributed in the whole area of the Au-In-Cd alloy without large grain or lack. We can see the difference of the thickness of Au or In even in the Au-In-Cd alloy. But we need more study to define the thickness of the materials from these data.

A new neutron imaging detector system has been developed in collaboration with the KEK Detector Technology Project (KEKDTP) for better spatial resolution. The detector is HAMAMATSU F2225 based on the micro channel plate (MCP) technology. To detect a neutron by MCP, natural boron is contained in base material of MCP (B-MCP). At the B-MCP, amplified electrons illuminate phosphor screen as same as normal MCP. Pictures are reflected by a mirror and captured by a high flame speed camera with an image intensifier tube. A test experiment for evaluating characteristics of B-MCP, such as sensitivity, gain, resolution and so on, was performed at the LINAC based pulsed neutron source at Hokkaido University. Pulse-by-pulse image pictures were obtained successfully by above setup. Figure 4 shows an integrated picture of a sample image. Further improvements of the detector system for TOF imaging are in progress.

The μ-pic detector was tested at 2 times higher intensity of J-PARC compared with last year. An external gate equipped enabled stable transmission measurements with high efficiency under such a high intensity condition. Transmission of a powder iron sample to get transmission without texture was measured, and also a welded iron was measured. The strain distribution was obtained and the result is shown in Fig. 5. It is indicated that larger strain appeared at the welded area than others. Furthermore, as shown in Fig. 6 the spatial resolution more than 0.2 mm, which corresponds to the resolution of an imaging plate, was demonstrated, which is remarkably high resolution of this type detector. This is due to an improved method to analyze the trace of decay particles of ^{3}He.

The small accelerator based neutron source for imaging was installed at Kyoto University, and the test experiments on industrial materials were also performed.

Reference

1) O. H. Siegmund *et al*, Nucl. Inst. Meth., **A 576** (2007) p.178.
2) M. Ooi *et al*, IWSMT-10 Beijing, China Oct. 18-22 2010, J. Nucl. Mat., under reviewing.

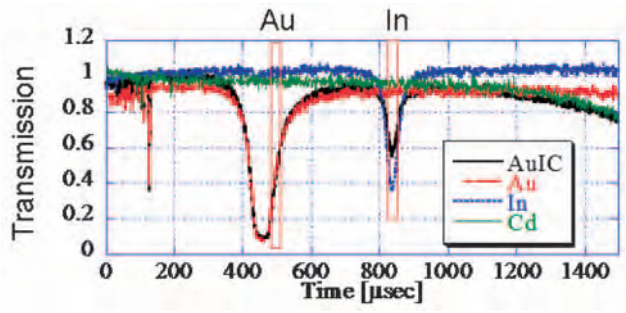

Fig. 3: Transmission curve of the sample.

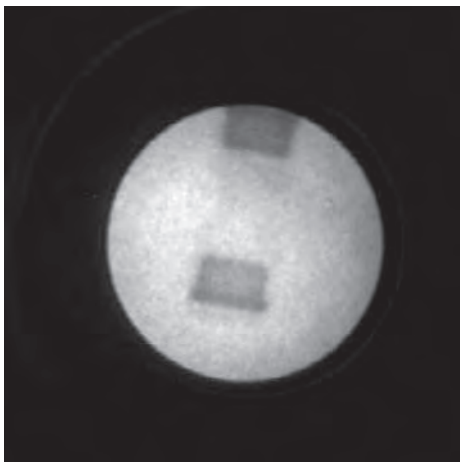

Fig. 4: Integrated image of neutron permeation of sample (a tube fitting).

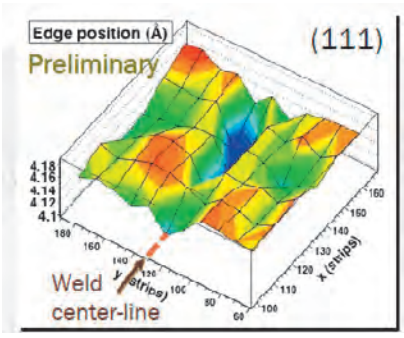

Fig. 5: Variation of lattice space of a welded iron plate deduced from Bragg edge analysis.

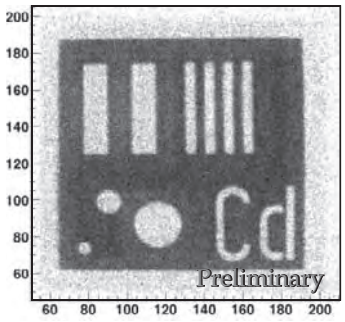

Fig. 6: Image indicating spatial resolution. 0.5mm gap in 'd' was observed.

KENS REPORT XVII

2009-2010

PUBLICATION LIST

List of Publications

2009

Development of Data Processing Softwave for a New TOF Sigle Crystal Neutron Diffractoweter at J-PARC
T. Ohhara, K. Kusaka, T. Hosoya, K. Kurihara, K. Tomoyori, N. Niimura, I. Tanaka, J. Suzuki, T. Nakatani, T. Otomo, S. Matsuoka, K. Tomita, Y. Nishimaki, T. Ajima, and S. Ryufuku
NIM A **600** 195 2009

14C年代測定を利用した縄紋中期竪穴住居の実態の把握
小林謙一
国立歴史民俗博物館研究報告 **149** 113-133 2009

A CCD-based Pixel Detector with Micron Spatial Resolution for Ultra Cold Neutrons
G. Ichikawa, S. Kawasaki, S. Komamiya, Y. Kamiya, T. Sanuki, H. M. Shimizu, M. Hino, and M. Kitaguchi
IEEE Nuclear Science Symposium Conference Record **5402255** 1619 2009

A Small Angle Neutron Scattering (SANS) Experiment using Very Cold Neutrons (VCN)
M. Bleuel, J. M. Carpenter, B. J. Micklich, P. Geltenbort, K. Mishima, H. M. Shimizu, Y. Iwashita, K. Hirota, M. Hino, S. J. Kennedy, and J. Lal
Physica B **404** 2629 2009

Aluminum Hydride for Hydrogen Storage
K. Ikeda, S. Orimo, S. Muto, and K. Tatsumi
Proceeding of Eighteenth International Symposium on Processing and Fabrication of Advanced Materials XVIII (PFAM XVIII) **1** 81 2009

Assembly State of Proteasome Activator 28 in an Aqueous Solution as Studied by Small-Angle Neutron Scattering
M. Sugiyama, E. Kutimoto, Y. Morimoto, H. Sahashi, E. Sakata, K. Hamada, K. Itoh, K. Mori, T. Fukunaga, Y. Minami, and K. Kato
J. Phys. Soc. Jpn., **78** 124802 2009.

B4Cレジンのアウトガス測定
横尾哲也、金子直勝、伊藤晋一、大友季哉、末次祐介、白井満、鈴谷賢太郎
KEK Report **2009-4** 2009

BL12高分解能チョッパー分光器 (HRC)
横尾哲也、伊藤晋一
波紋 Vol. **19** 118-119 2009.

Characterization of Swollen Structure of High-density Polyelectrolyte Brushes in Salt Solution by Neutron Reflectivity
M. Kobayashi, Y. Terayama, M. Hino, K. Ishihara, and A. Takahara
J. Phys. Conf. Ser. **184** 184 012010 2009

Construction of Ibaraki Prefectural Neutron Spectrometers
M. Hayashi, T. Ishigaki, T. Kamiyama, and I. Tanaka
Nuclear Instruments and Methods in Physics Research A **600** 14 2009

Crystal Structure of Fe-doped Lanthanum Gallate for Oxygen Partial Pressures Studied by Neutron Powder Diffraction
K. Mori, R. Kiyanagi, J. W. Richardson Jr., J. Fieramosca, Y. Onodera, K. Itoh, M. Sugiyama, T. Kamiyama, and T. Fukunaga
Solid State Ionics, **180** 541-545 2009

Dehydriding Process of a-AlH3 Observed by Transmission Electron Microscopy and Electron Energy-loss Spectroscopy
S. Muto, K. Tatsumi, K. Ikeda and S. Orimo
Journal of Applied Physics **105** 123514(1) 2009

Dehydriding Reaction of AlH3: in-situ Microscopic Observations Combined with Thermal and Surface Analyses
K. Ikeda, S. Muto, K. Tatsumi, M. Menjo, S. Kato, M. Bielmann, A. Z'ttel, C. M. Jensen, and S. Orimo
Nanotechnology **20** 204004 2009

Density Functional Study of a Photo-induced Phase in Graphite
H. Ohnishi and K. Nasu
J. Physics: Conference Series **148** 012059 2009

Design and Performance Analyses of the New Time-of-flight smaller-angle Neutron Scattering Instrument at J-PARC
T. Shinohara, S. I. Takata, J. I. Suzuki, T. Oku, K. Suzuya, K. Aizawa, M. Arai, T. Otomo, and M. Sugiyama
NIM A **600** 111 2009

Design of a Neutron Polarizer Using Polarizing Super Mirrors for the TOF-SANS Instrument at the J-PARC
T. Shinohara, J. I. Suzuki, T. Oku, S. I. Takata, H. Kira, K. Suzuya, K. Aizawa, M. Arai, T. Otomo, and M. Sugiyama
Physica B **404** 2640 2009

Design of Neutron Beamline for Fundamental Physics at J-PARC BL05
K. Mishima, T. Ino, K. Sakai, T. Shinohara, K. Hirota, K. Ikeda, H. Sato, Y. Otake, H. Ohmori, S. Muto, N. Higashi, T. Morishima, M. Kitaguchi, M. Hino, H. Funahashi, T. Shima, J. -i. Suzuki, K. Niita, K. Taketani, Y. Seki, and H. M. Shimizu
Nucl. Instrum. Methods Phys. Res. **A600** 342 2009

Detector Area Expansion at iNSE Neutron Spin Echo Spectrometer
N. L. Yamada, H. Endo, N. Osaka, Y. Kawabata, M. Nagao, T. Takeda, H. Seto, and M. Shibayama
Physica B **404** 2607 2009

Development of a Compact on-beam SEOP Neutron Spin Filter
T. Ino, M. Nakamura, T. Oku, T. Shinohara, K. Ohoyama, and H. Hiraka
Physica B **404** 2667 2009

Development of a Data Acquisition Sub-system Using DAQ-Middleware
K. Nakayoshi, Y. Yasu, E. Inoue, H. Sendai, M. Tanaka, S. Satoh, S. Muto, N. Kaneko, T. Otomo, T. Nakatani, and T. Uchida
NIM A **600** 173 2009

Development of a Readout System Employing High-speed Network for J-PARC
S. Satoh, S. Muto, N. Kaneko, T. Uchida, M. Tanaka, Y. Yasu, K. Nakayoshi, E. Inoue, H. Sendai, T. Nakatani, and T. Otomo
NIM A **600** 103 2009

Development of an Automatic Sample Changer for iMATERIA
A. Hoshikawa, T. Ishigaki, M. Nagai, Y. Kobayashi, H. Sagehashi, T. Kamiyama, M. Yonemura, K. Aizawa, T. Sakuma, Y. Tomota, M. Arai, M. Hayashi, K. Ebata, Y. Takano, and T. Kasao
Nuclear Instruments and Methods **600** 203 2009

Development of an Automatic Sample Chnger for iMATERIA
A. Hoshikawa, T. Ishigaki, M. Nagai, Y. Kobayashi, H. Sagehashi, T. Kamiyama, M. Yonemura, K. Aizawa, T. Sakuma, and Y. Tomota
Nuclear Instruments & Methods in Physics Research, Section A: Accelerators, Spectrometers, Detectors, and Associated **600** 189 2009

Development of Modulating Permanent Magnet Sextupole Lens for Focusing of Pulsed Cold Neutrons
M. Yamada, Y. Iwashita, M. Ichikawa, T. Sugimoto, H. Tongu, H. Fujisawa, H. M. Shimizu, T. Ino, K. Mishima, K. Taketani, T. Yoshioka, S. Muto, T. Morishima, T. Oku, J. -i. Suzuki, T. Shinohara, K. Sakai, H. Sato, K. Hirota, Y. Otake, Y. Seki, S. Kawasaki, S. Komamiya, and Y. Kamiya
Physica B **404** 2646 2009

Diffuse and Doubly Split Atom Occupation in Hexagonal LiBH4
T. Ikeshoji, E. Tsuchida, K. Ikeda, M. Matsuo, H. -W. Li, Y. Kawazoe, and S. Orimo
Applied Physics Letters **95** 221901 2009

Direct Dry Syntheses and Thermal Analyses of a Series of Aluminum Complex Hydrides
T. Sato, K. Ikeda, H. -W. Li, and S. Orimo
Materials Transactions **50** 182 2009

Direct Observation of the Critical Relaxation of Polarization Clusters in BaTiO3 Using a Pulsed X-Ray Laser Technique

K. Namikawa, M. Kishimoto, K. Nasu, E. Matsushita, R. Z. Tai, K. Sukegawa, Yamatani, H. Hasegawa, M. Nishikino, M. Tanaka, and K. Nagashima
Phys. Rev. Lett. **103** 197401 2009

Distribution of Glass Transition Temperature Tg in a Polymer Thin Film by Neutron Refrectivity
K. Kawashima, R. Inoue, T. Kanaya, G. Matsuba, K. Nishida, and M. Hino
J. Phys.: Conference Series **184** 012004 2009

Early-stage real-time Dynamics of Interlayer Sp3-bond Formation by Visible-light Irradiation of Graphite
K. Nishioka, and K. Nasu
Phys. Rev. B **80** 235420 2009

First Demonstration of Novel Method for Inelastic Neutron Scattering Measurement Utilizing the Multiple Incident Energies
M. Nakamura, R. Kajimoto, Y. Inamura, F. Mizuno, M. Fujita, T. Yokoo, and M. Arai
J. Phys. Soc. Jpn. **78** 093002-1 2009

First Demonstration of Novel Method for Inelastic Neutron Scattering Measurement Utilizing the Multiple Incident Energies
M. Nakamura, R. Kajimoto, Y. Inamura, F. Mizuno, M. Fujita, T. Yokoo, and M. Arai
J. Phys. Soc. Jpn. **78** 093002 2009

Formation of sp3-bonded Carbon Nanostructures by Femtosecond Laser Excitation of Graphite
J. Kanasaki, E. Inami, K. Tanimura, H. Ohnishi, and K. Nasu
Phys. Rev. Lett. **102** 087402 2009

Full Fitting Analysis of the Relative Intermediate Form Factor Measured by Neutron Spin Echo
M. Nagao, and H. Seto
Physica B **404** 2603 2009

Generation and Growth of Sp3-bonded Domains by Visible Photon Irradiation of Graphite
H. Ohnishi, and K. Nasu
Phys. Rev B **80** 014112 2009

Glass Transition and Molecular Mobility in Polymer Thin Films
R. Inoue, T. Kanaya, K. Nishida, I. Tsukushi, M. T. F. Telling, B. J. Gabrys, M. Tyagi, C. Soles, and W. -1 Wu
Phys. Rev. E **80** 031802 2009

Glassy Dynamics and Heterogeneity of Polymer Thin Films
T. Kanaya, R. Inoue, K. Kawashima, T. Miyazaki, I. Tsukushi, K. Shibata, G. Matsuba, K. Nishida, and H. Hino
J. Phys. Soc. Jan. **78** 041004 2009

High Pressure Neutron Scattering Experiments on Hydrogen Storage Materials
A. Machida, T. Otomo, T. Hattori, and H. Fukazawa
Review of High Pressure Science and Technology/Koatsuryoku No Kagaku To Gijutsu **19** 24 2009

High-intensity and Versatile Chopper Spectrometer Project for J-PARC,
T. J. Sato, O. Yamamuro, K. Hirota, M. Shibayama, H. Yoshizawa, S. Itoh, S. Watanabe, T. Asami, K. Kindo, Y. Uwatoko, and T. Kanaya
J. Neutron Res. **16** 113-119 2009

Highly Polarized Very Cold Neutrons through a Permanent Magnet Quadrupole
K. Taketani, K. Mishima, T. Ino, T. Yoshioka, S. Muto, T. Morishima, H. M. Shimizu, T. Oku, J. Suzuki, T. Shinohara, K. Sakai, H. Sato, K. Hirota, Y. Otake, M. Kitaguchi, M. Hino, Y. Seki, Y. Iwashita, M. Yamada, M. Ichikawa, T. Sugimoto, S. Kawasaki, S. Komamiya, Y. Kamiya, and H. O
Physica B **404** 2643 2009

Hydration Structure around the Nitrogen Atom of the Pyridine Molecule
Y. Kameda, A. Maki, Y. Amo, and T. Usuki
Activity Report on Neutron Scattering Research, **16** 682 2009

Hydrogen Storage in Aluminum Hydride
K. Ikeda, K. Tatsumi, S. Muto, S. Sato, M. Menjo, S. Kato, M. Bielmann, A. Zttel, K. Hashi, H. Itoh, T. Kabutomori, C. M. Jensen, and S. Orimo
Proceeding of The Seventeenth Annual International Conference on COMPOSITES/NANO ENGINEERING (ICCE-17) 393 2009

IBARAKI Materials Design Diffractometer (iMATERIA)-Versatile Neutron Diffractometer at J-PARC
T. Ishigaki, A. Hoshikawa, M. Yonemura, T. Morishima, T. Kamiyama, R. Oishi, K. Aizawa, T. Sakuma, Y. Tomota, and M. Arai
Nuclear Instruments & Methods in Physics Research, Section A: Accelerators, Spectrometers, Detectors, and Associated **600** 189 2009

IBARAKI Materials Design Diffractometer(iMATERIA)-Versatile Neutron Diffractometer at J-PARC
T. Ishigaki, A. Hoshikawa, M. Yonemura, T. Morishima, T. Kamiyama, R. Oishi, K. Aizawa, T. Sakuma, Y. Tomota, M. Arai, M. Hayashi, K. Ebata, Y. Takano, K. Komatsuzaki, H. Asano, Y. Takano, and T. Kasao
Nuclear Instruments and Methods **600** 189 2009

In Situ TOF Neutron Diffraction During Phase Transformation in an Engineering Steel
Y. Tomota, P. G. Xu, T. Kamiyama, and E. C. Oliver
Instruments and Methods **600** 313 2009

Influence of Salt Concentration on Swelling States of Poly (sulfobetaine) Brush at Aqueous Solution Interface
Y. Terayama, M. Kikuchi, M. Kobayashi, M. Hino, and A. Takahara
J. Phys. Conf. Ser. **184** 012011 2009

Ionic Dynamics of Molten Cuprous Iodide
Y. Kawakita, Y. Kato, H. Shigeta, K. Shibata and S. Takeda
J. Alloys and Compounds **452** (2009) 136-139.

J-PARC/MLFの超高分解能粉末構造解析装置「SuperHRPD」
神山崇，鳥居周輝
中性子産業利用促進協議会季報「四季」**2** 2 2009

Local Structure Around the Amino Group of Glycine Carbamate in Concentrated Aqueous Solutions
Y. Kameda, Y. Amo, and T. Usuki
Bull. Chem. Soc. Jpn., **82** 1485-1490 2009

Morphological Development of Multilamellar Phospholipid Film Depending on Drying Kinetics
M. Hishida, N. L. Yamada, K. Yoshikawa, and H. Seto
Phys. Rev. E **80** 51407 2009

Nano-scale sp2-sp3 Conversion by Visible Lights Irradiation and Photoinduced Phase Transitions
L. Radosinski, K. Nasu, J. Kanazaki, K. Tanimura, A. Radosz, and T. Luty
Molecular electronic and related materials- Control and probe with light, ed by Naito Toshio, (2010, Trans-world Research Network Publisher, Trivandrum, Kerala, India) 281-303, 2009.

Nanopore Formation on Unilamellar Vesicles of Long- and short-chain Lipids
N. L. Yamada, M. Hishida, and N. Torikai
Phys. Rev. E **79** 32902 2009

Nanopore Formation on Unilamellar Vesicles of Long- and short-chain Lipids
N. L. Yamada, M. Hishida, and N. Torikai
Phys. Rev. E **79** 032902 2009

Nanopore Formation on Unilamellar Vesicles of Long- and short-chain Lipids
N. L. Yamada, M. Hishida, and N. Torikai
Vir. J. Nan. Sci. & Tech. **19** 2009

Nanopore Formation on Unilamellar Vesicles of Long- and short-chain Lipids
N. L. Yamada, M. Hishida, and N. Torikai
Vir. J. Bio. Phys. Res. **17** 2009

Neutron Interferometric Search for Short-range Gravity
Vladimir Gudkov, Geoffery Greene, and Hirohiko M. Shimizu
Nucl. Instrum. Methods Phys. Res. A**611** 153 2009

Neutron Powder Diffraction Under High Pressure at J-PARC
W. Utsumi, H. Kagi, K. Komatsu, H. Arima, T. Nagai, T. Okuchi, T. Kamiyama, Y. Uwatoko, K. Matsubayashi, and T. Yagi
Nuclear Instruments and Methods in Physics Research A **600** 50 2009

Neutron Reflectometry for Observation of Machined Surface Roughness
K. Inoue, T. Hirayama, T. Uno, T. Ebisawa, K. Ikeda, H. Honda, and H. Shimizu
Jpn. J. Appl. Phys. **48** 126504-1 2009

Neutron magneticscattering studiesonferromagnetisminpotassium nanoclustersarrayedinzeoliteA Trialexperiments
T. Nakano, T. Takase, S. Araki, T. Kamiyama, Y. Nozue, and S. Ikeda
Nuclear Instruments and Methods in Physics Research A **600** 240 2009

Newly Designed Neutron Diffraction Cell for Fluids at High Temperatures and High Pressures
H. Iwase, N. Matubayasi, Y. Kameda, K. Itoh, T. Otomo, and M. Nakahara
J. J. Appl. Phys, **49** 16602 2009

Numerical Simulation on the Dynamics of Photo-induced Cooperative Phenomena in Molecular Crystals
K. Ishida, and K. Nasu
Computer Physics Communications (Elsevier) **180** 1489-1494 2009

Object-oriented Data Analysis Framework for Neutron Scattering Experiments
J. Suzuki, T. Nakatani, T. Ohhara, Y. Inamura, M. Yonemura, T. Morishima, T. Aoyagi, A. Manabe, and T. Otomo
NIM A **600** 123 2009

Partial Structures of molten AgBr
H. Ueno, S. Tahara, Y. Kawakita, S. Kohara, and S. Takeda
Nucl. Instr. Meth. Phys. Res. A **600** 322-324 2009

Photo-induced Domain Type Collective Structural Changes with Inter-layer σ-bonds in the Visible Region of Graphite
H. Ohnishi, and K. Nasu
Phys. Rev. B **79** 054111 2009

Photo-induced domain-type Collective Structural Changes with Interlayer σ-bonds in the Visible Region of Graphite
H. Ohnishi and K. Nasu
Virtual Journal of Nano-scale Science & Technology (APS)-March 9 **19** 2009

Pulsed Neutron Beam Control using a Magnetic Multiplet Lens
T. Oku, T. Shinohara, J.-i. Suzuki, R. Pynn, and H. M. Shimizu
Nucl. Instrum. Methods Phys. Res. A**600** 100 2009

Pulsed Neutron Beam Control using a Magnetic Multiplet Lens
T. Oku, T. Shinohara, J.-i. Suzuki, R. Pynn, and H. M. Shimizu
Nucl. Instrum. Methods Phys. Res. A**600** 100 2009

Quantum Monte Carlo Study on Speckle Variation Due to Photo-relaxation of Ferroelectric Clusters in Para-electric Barium Titanate
K. Ji, K. Namikawa, H. Zheng, and K. Nasu
Phys. Rev. B **79** 144304 2009

Quantum Monte Carlo Study on Speckle Variation Due to Photo-relaxation of Ferroelectric Clusters in Para-electric Barium Titanate
K. Ji, K. Namikawa, H. Zheng, and K. Nasu
Virtual Journal of Ultra-fast Science (APS), **8** 2009

Quasielastic Neutron Scattering Investigation of Motion of Water Molecules in N-propyl alcohol-water Mixture
M. Nakada, K. Maruyama, O. Yamamuro, and M. Misawa
J. Chem. Phys. **130** 074503 2009

Reversible Hydriding/Dehydriding Properties of New Y3Al2 Hydrides
K. Ikeda, N. Watanabe, S. Kato, T. Sato, Y. Nakamori, and S. Orimo
Journal of Alloys and Compounds **471** L13 2009

Riertveld Analysis Software for J-PARC
R. Oishi, M. Yonemura, Y. Nishimaki, S. Torii, A. Hoshikawa, T. Ishigaki, T. Morishima, K. Mori, and T. Kamiyama
Nuclear Instruments & Methods in Physics Research, Section A: Accelerators, Spectrometers, Detectors, and Associated **600** 94 2009

SANS Simulation of Aggregated Protein in Aqueous Solution
M. Sugiyama, K. Hamada, K. Kato, E. Kurimoto, K. Okamoto, Y. Morimoto, S. Ikeda, S. Naito, M. Furusaka, K. Itoh, K. Mori, and T. Fukunaga
Nucl. Instr. Meth. Phys. Res. A **600** 272-274 2009

Simulation Study of a Pulsed Neutron Focusing using a Pulsed Electromagnetic Lens Coupled with a Permanent Magnet
H. Iwashita, H. Iwasa, F. Hiraga, T. Kamiyama, Y. Kiyanagi, J. Suzuki, T. Shinohara, T. Oku and H. M. Shimizu
Nucl. Instrum. Methods Phys. Res. A**600** 129 2009

Single-Length-Scaling Analysis for Antiferromagnetic Fractons in Dilute Heisenberg System RbMn0.4Mg0.6F3
S. Itoh, T. Nakayama, R. Kajimoto and M. A. Adams
J. Phys. Soc. Jpn. **78** 013707-1 2009

Single-Length-Scaling Analysis for Antiferromagnetic Fractons in Dilute Heisenberg System RbMn0.4Mg0.6F3
S. Itoh, T. Nakayama, R. Kajimoto, and M. A. Adams
J. Phys. Soc. Jpn. **78** 013707 2009

Site-dependent Lattice Dynamics of Photo-Induced Structural Change
K. Ishida and K. Nasu
Phys. Rev. B **80** 140301(R) 2009

Spontaneous Deformation of an Oil Droplet Induced by the Cooperative Transport of Cationic and Anionic Surfactants Through the Interface
Y. Sumino, H. Kitahata, H. Seto, S. Nakata, and K. Yoshikawa
Journal of Physical Chemistry B **113** (48) 15709 2009

Structural Analysis of Lithium Lanthanum Titanate Perovskite Structure
K. Ohara, Y. Kawakita, L. Temleitner, L. Pusztai, S. Kohara, A. Jono, H. Shimakura, N. Inoue, and S. Takeda
Phys. Status Solidi C **6** 1004-1007 2009

Structural and Electrochemical Properties of La0.8Sr0.2Ga1 xFexO3
K. Mori, Y. Onodera, R. Kiyanagi, J. W. Richardson Jr., K. Itoh, M. Sugiyama, T. Kamiyama, and T. Fukunaga
Methods in Physics Research A **600** 328 2009

Structural Investigation on Supercritical Carbon Dioxide and its Mixture with Alcohol
T. Sato, M. Sugiyama, M. Misawa, K. Hamada, K. Itoh, K. Mori, and T. Fukunaga
Journal of Molecular Liquids, **147** 102-109 2009

Structural Study of Amorphous LaNi5Dx: In Situ Neutron and X-ray Diffraction Experiments in Deuterium gas
K. Itoh, T. Shoumura, M. Sugiyama, K. Mori, and T. Fukunaga
J. Alloys and Compounds **474** 4-8 2009

Structural Study on Zr0.39 Ni0.61 and (Zr0.39 Ni0.61)D0.59 Amorphous Alloys by Neutron and X-ray Diffraction
K. Itoh, T. Watanabe, T. Otomo, M. Sugiyama, K. Mori, and T. Fukunaga
Journal of Alloys and Compounds, **483** 213–216 2009

Structural Study on Zr0.39Ni0.61 and (Zr0.39Ni0.61)D0.59 Amorphous Alloys by Neutron and X-ray Diffraction
K. Itoh, T. Watanabe, T. Otomo, M. Sugiyama, K. Mori, and T. Fukunaga
J. Alloys Compd. **483** 213 2009

Structure and Dynamics of Water on a Wide Length and Time Scale T. Yamaguchi
Fukuoka University Science Reports, **38** 95-104 2009

Structure and Surface Properties of High-density Polyelectrolyte Brushes at the Interface of Aqueous Solution
M. Kobayashi, H. Yamaguchi, Y. Terayama, Z. Wang, K. Ishihara, M. Hino, and A. Takahara

Macromolecular Symposia **279** 79–87 2009

Structure of Mg50Ni50 Amorphous Alloy Studied by Using X-ray Diffraction and Reverse Monte Carlo Modeling.
K. Itoh, T. Otomo, M. Sugiyama, K. Mori, and T. Fukunaga
Journal of Physics:Conference Series **144** 012107 2009

Structure of Na2S-GeS2 Glasses Studied by Using Neutron and X-ray Diffraction and Reverse Monte Carlo modeling
K. Itoh and T. Fukunaga
Solid State Ionics, **180** 351–355 2009

Strucutre-property Relationships of Fast Copper ion Conductor Cubic CuI
D. S. Adipranoto, F. Shikanai, M. Yonemura, K. Mori, J. G. Park, K. Itoh, and T. Kamiyama
Solid State Ionics **180** 492 2009

Study of the Neutron Guide Design of the 4SEASONS Spectrometer at J-PARC
R. Kajimoto, K. Nakajima, M. Nakamura, K. Soyama, T. Yokoo, K. Oikawa, and M. Arai
Nucl. Instr. and Meth. A **600** 185 2009

Study of the Neutron Guide Design of the 4SEASONS Spectrometer at J-PARC
R. Kajimoto, K. Nakajima, M. Nakamura, K. Soyama, T. Yokoo, K. Oikawa, and M. Arai
Nucl. Instr. and Meth. A **600** 185-188 2009

Study of Thickness Dependent Density in Ultrathin Water Soluble Polymer Films
M. H. Mojammel, M. Mukherjee, K. Kawashima, K. Nishida, and T. Kanaya
Macromolecules, **42** 732-736 2009

Synchrotron Radiation Powder X-ray and Neutron Diffraction Studies on Novel Y3Al2 Hydrides
T. Sato, K. Ikeda, K. Ohoyama, N. Watanabe, and S. Orimo
Journal of Alloys and Compounds **481** 254 2009

Syntheses, Crystal Structures, and Thermal Analyses of Solvent-free Ca(AlD4)2 and CaAlD5
T. Sato, M. H. Srby, K. Ikeda, S. Sato, B. C. Hauback, and S. Orimo
Journal of Alloys and Compounds **487** 472 2009

Synthesis and Partial Dehydrogenation of the Impregnated Lithium Borohydride, LiBH4
M. Menjo, H.-W. Li, M. Matsuo, K. Ikeda, and S. Orimo
Journal of the Ceramic Society of Japan (Proceeding of The First International Symposium on Advanced Synthesis and Processing Technology for Materials (ASPT08)) **117** 457 2009

T0チョッパーの開発（制御）
下ヶ橋秀典
技術交流会報告集 KEK Proceedings **2009-11** 38 2009

Theoretical Study on the Coherent Nonlinear Dynamics of Photo-induced Structural Change
K. Ishida and K. Nasu
J. Physics: Conference Series **148** 012057 2009

Time-resolved Specular and Off-specular Neutron Reflectivity Measurements on Deuterated Polystyrene and Poly (vinylmethylether) Blend Thin Films During Dewetting Process
H. Ogawa, T. Kanaya, K. Nishida, G. Matsuba, J. P. Majewski, and E. Watkins
J. Chem. Phys., **131** 104907 2009

Tribological Behavior of Polymer Brush Prepared by the "Grafting-from" Method
M. Kobayashi, Z. Wang, Y. Matsuda, M. Kaido, A. Suzuki, and A. Takahara
in S. S. Kumar Ed. "Polymer Tribology", Imperial College Press 582-602 2009

Versatile Inelastic Neutron Spectrometer (VINS) Project for J-PARC
T. J. Sato, O. Yamamuro, K. Hirota, M. Shibayama, H. Yoshizawa, S. Itoh, S. Watanabe, T. Asami, K. Kindo, Y. Uwatoko, T. Kanaya, N. Higashi, and K. Ueno
Nuclear Instruments and Methods in Physics Research A **600** 143 2009

Versatile Inelastic Neutron Spectrometer (VINS) Project for J-PARC
T. J. Sato, O. Yamamuro, K. Hirota, M. Shibayama, H. Yoshizawa, S. Itoh, S. Watanabe, T. Asami, K. Kindo, Y. Uwatoko, T. Kanaya, N. Higashi, and K. Ueno
Nucl. Instr. Methods Phys. Res. Sect. A **600** 143-145 2009

Work Hardening Mechanism in High Nitrogen Austenitic Steel Studied by in Situ Neutron Diffraction and in Situ Electron Backscattering Diffraction
M. Ojima, Y. Adachi, Y. Tomota, K. Ikeda, T. Kamiyama, and Y. Katada Materials
Science and Engineering A **527** 16 2009

ダイヤファイトと可視光誘起グラファイトーダイヤモンド相転移初期過程の理論
大西宏昌、谷村克己 and 那須奎一郎
固体物理 **44** 257-265 2009

フェルミチョッパーの開発
伊藤晋一、上野健治、横尾哲也
日本中性子科学会誌　波紋 **19** 224 2009

愛媛県上黒岩遺跡の研究
春成秀爾、小林謙一編
国立歴史民俗博物館研究報告 **154** 1-620 2009

「何ができる？どこがすごい？」試料水平型反射率計 ARISA-II
鳥飼直也、山田悟史、下ヶ橋秀典 and 瀬戸秀紀
まてりあ **48** 360 2009

学術創成研究「パルス中性子源を活用した量子機能発現機構に関する融合研究」第 8 回研究会
T. Yokoo, and S. Itoh
KEK proceedings **2009-3** 41 2009

高強度全散乱装置　NOVA
大友季哉
日本金属学会報　まてりあ **48** 349 2009

高密度水素貯蔵を目指した水素化物の材料設計と特性評価
池田一貴、李海文 and 折茂慎一
化学工業 **60** 51 2009

次世代新中性子源　J-PARCにより広がる新しい材料科学「何ができる？どこがすごい？」
伊藤晋一、横尾哲也
まてりあ **48** 363-365 2009

水素貯蔵技術とその関連材料
池田一貴、李海文 and 折茂慎一
日本機械学会誌 **112** 289 2009

中性子スピンエコー法による過冷却状態における細孔水の動的挙動
吉田亨次
福岡大学理学集報 **39** 55-62 2009

超高分解能粉末中性子回折装置　SuperHRPD
神山崇、鳥居周輝
まてりあ **48** 353 2009

東大・KEKパルスチョッパー分光器計画とそのサイエンス
横尾哲也、伊藤晋一
NSL News Letter **2009-2** 34 2009

非弾性中性子散乱新手法で実証実験
科学新聞 2009 年 10 月 2 日記事 2009

物構研シンポジウム '09
横尾哲也、その他
KEK proceedings **2009-10** 142 2009

量子ビームが拓く固体物理特集号　II. 中性子線による先端物性研究とJ-PARC大強度パルス中性子への期待　非晶質・液体の静的および動的構造研究
大友季哉
固体物理 **44** 93 2009

Multilamellar Structures Induced by Hydrophilic and Hydrophobic Ions Added to a Binary Mixture of D2O and 3-Methylpyridine
K. Sadakane, A. Onuki, K. Nishida, S. Koizumi, and H. Seto
"Physical Review Letters Virtual Journal of Nanoscale Science

& Technology" **10320** 167803 2009

2010

Aspire To Become TAKUMI - TAKUMI Present Status and Research Topics
Stefanus Harjo, K. Aizawa, T. Ito, H. Arima, J. Abe, A. Moriai, K. Sakasai, T. Nakamura, T. Nakatani, T. Iwahashi, and T. Kamiyama
Materials Science Forum **652** 99 2010

Comissioning of the Fermi-Chopper Spectrometer 4Seasons at J-PARC?Background Study
R. Kajimoto, M. Nakamura, Y. Inamura, F. Mizuno, K. Nakajima, N. Takahashi, S. Ohira, T. Yokoo, R. Maruyama, S. Wakimoto, Y. Ito, T. Iwahashi, W. Kambara, H. Tanaka, N. Yoshida, A. Katabira, K. Aizawa, and M. Arai
"ICANS XIX(19th meeting of International Collaboration on Advanced Neutron Sources) proceedings" 2010

Construction Status of High Resolution Chopper Spectrometer (HRC) at J-PARC
S. Itoh, T. Yokoo, T. J. Sato, S. Satoh, S. Yano, J. Suzuki, K. Ueno, K. Kuwahara, T. Kamiyama, K. Iwasa, K. Ohoyama, T. Otomo, Y. Endoh, J. Akimitsu, S. Kuroda, K. Sato, K. Nasu, K. Iwano, H. Yoshizawa, O. Yamamuro, Y. Ohara, Y. Kawamura, T. Asami, and R. Su
ICANS-XIX (Proceedings of the 19th Meeting of the International Collaboration on Advanced Neutron, Paul Scherrer Institut, PSI-Proceedings **10-01** 079 2010

Crystal Structure of $Li_7P_3S_{11}$ Studied by Neutron and Synchrotron X-ray Powder Diffraction
Y. Onodera, K. Mori, T. Otomo, A. C. Hannon, S. Kohara, K. Itoh, M. Sugiyama, and T. Fukunaga
J. Phys. Soc. Jpn. **79** 87 2010

DAQ-Middleware for MLF/J-PARC
K. Nakayoshi, Y. Yasu, E. Inoue, H. Sendai, M. Tanaka, S. Satoh, S. Muto, J. Suzuki, T. Otomo, T. Nakatani, T. Ito, Y. Inamura, M. Yonemura, T. Hosoya, and T. Uchida
NIM A in press 2010

Development of a Neutron Detector with a GEM
H. Ohshita, S. Uno, T. Otomo, T. Koike, T. Murakami, S. Satoh, M. Sekimoto, and T. Uchida
NIM A in press 2010

Development of Fermi Chopper at KEK
S. Itoh, K. Ueno, T. Yokoo, Y. Funahashi, T. Kamiyama, H. Sato, N. Miyamoto, Y. Kiyanagi, T. J. Sato, T. Otomo, and S. Satoh
ICANS-XIX (Proceedings of the 19th Meeting of the International Collaboration on Advanced Neutron, Paul Scherrer Institut, PSI-Proceedings **10-01** 120 2010

Development of T0 chopper at KEK
S. Itoh, K. Ueno, R. Ohkubo, Y. Funahashi, H. Sagaheshi, T. Yokoo, T. J. Sato, T. Otomo and S. Satoh
ICANS-XIX (Proceedings of the 19th Meeting of the International Collaboration on Advanced Neutron, Paul Scherrer Institut, PSI-Proceedings **10-01** 121 2010

Doping Dependence of Spin-lattice Coupling and Two-dimensional Ordering in Multiferroic Hexagonal Y1 xLuxMnO3 (0x1)
Junghwan Park, Seongsu Lee, Misun Kang, Kwang-Hyun Jang, Changhee Lee, S. V. Streltsov, V. V. Mazurenko, M. V. Valentyuk, J. E. Medvedeva, T. Kamiyama, and J. -G. Park
PHYSICAL REVIEW B **82** 54428 2010

Early-stage real-time Dynamics of Interlayer Sp3-bond Formation by Visible-light Irradiation of Graphite
K. Nishioka and K. Nasu
Virtual Journal of Nanoscale Science & Technology (AIP) **21** 2010

First Neutron Production Utilizing J-PARC Pulsed Spallation Neutron Source JSNS and Neutronic Performance Demonstrated
F. Maekawa, M. Harada, K. Oikawa, M. Teshigawara, T. Kai, S. Meigo, M. Ooi, S. Sakamoto, H. Takada, M. Futakawa, T. Kato, Y. Ikeda, N. Watanabe, T. Kamiyama, S. Torii, and R. Kaj
Nuclear Instruments and Methods in Physics Research A **620** 159 2010

For Hgh-pressure Experiments Using total Scattering Spectrometer NOVA at J-PARC
Hattori, Y. Katayama, A. Machida, T. Otomo, and K. Suzuya
J. Phys.: Conference Series **215** 2010

Gas Desorption Examination of B4C Resin for Neutron Vacuum Chamber
T. Yokoo, N. Kaneko, S. Itoh, T Otomo, Y. Suetsugu, M. Shirai, and K. Suzuya
"ICANS XIX(19th meeting of International Collaboration on Advanced Neutron Sources) proceedings" 2010

High Pressure Raman and Visible Absorption Study of AlH3
N. Shimura, T. Takeichi, T. Kume, S. Sasaki, H. Shimizu, A. Ohmura, K. Ikeda, Y. Nakamori, and S. Orimo
Journal of Physics: Conference Series (Proceeding of the Joint AIRAPT-22 and HPCJ-50 Conference) **215** 012047 2010

Ionic Conductivity and Structural Properties of Lithium Lanthanum Titanate Quenched into Liquid Nitrogen Studied by Neutron Powder Diffraction,
K. Mori, K. Iwase, M. Yonemura, Joan SIEWENIE, Thomas PROFFEN, Y. Onodera, K. Itoh, M. Sugiyama, T. Kamiyama, and T. Fukunaga
Proc. 3rd Int. Conf. Physics of Solid State Ionics (ICPSSI-3). Phys. Soc. Jpn. **79** A 84 2010

Newly Designed High-Temperature and High-Pressure Sample Cell for Neutron Diffraction for Liquids
H. Iwase, N. Matubayasi, Y. Kameda, K. Itoh, T. Otomo, and M. Nakahara
Jpn. J. Appl. Phys. **49** 016602 2010

Partial Pair Correlation Functions of Highly Concentrated Aqueous Urea Solutions Determined by Neutron Diffraction with 14N/15N and H/D Isotopic Substitution Methods
Y. Kameda, A. Maki, Y. Amo, and T. Usuki
Bull. Chem. Soc. Jpn. **20** 131-144 2010

Practical Applications of Permanent Magnet Multipoles
Y. Iwashita, M. Ichikawa, M. Yamada, T. Sugimoto, H. Tongu, H. Fujisawa, M. Masuzawa, T. Tauchi, T. Oku, K. Hirota, H. M. Shimizu, C. Shi, and Y. Zhu
IEEE Trans. Appl. Supercond. **20** 842 2010

Propagating Librations in Ice XI: Model Analysis and Coherent Inelastic Neutron Scattering Experiment
K. Iwano, T. Yokoo, M. Oguro, and S. Ikeda
J. Phys. Soc. Jpn. **79** 063601 2010

Surface Changes on AlH3 During the Hydrogen Desorption
S. Kato, M. Bielmann, K. Ikeda, S. Orimo, A. Borgschulte, and A. Z'ttel
Applied Physics Letters **96** 51912 2010

Surface Reorganization of Thin Poly(Methyl Methacrylate) Films Induced by Water
A. Horinouchi, Y. Fujii, N. L. Yamada, and K. Tanaka
Chem. Lett **39** 810 2010

T0チョッパーの開発 (2)
伊藤晋一、上野健治、大久保隆治、下ケ橋秀典、舟橋義聖
日本中性子科学会誌　波紋 **20** 146 2010

アルミニウム水素化物による水素貯蔵
池田一貴、折茂慎一、齋藤寛之、町田晃彦，片山芳則、青木勝敏
サイエンス&テクノロジー「水素製造・吸蔵・貯蔵・輸送材料と安全化 in press 2010

高分解能チョッパー分光器 (HRC)
横尾哲也、伊藤晋一、佐藤節夫、佐藤卓、矢野真一郎
波紋 **20** 45-48 2010

高分解能チョッパー分光器 HRC
横尾哲也、伊藤晋一、佐藤節夫、佐藤卓、矢野真一郎
日本中性子科学会誌　波紋 **20** 45 2010

高分解能チョッパー分光器の花
横尾哲也、伊藤晋一
波紋 **20** 2010

試料水平型中性子反射率計 ARISA-II
山田悟史、鳥飼直也、下ヶ橋秀典 and 瀬戸秀紀
波紋 **20** 58 2010

動き出した J-PARC 中性子非弾性散乱装置「四季」 - 非弾性中性子散乱実験の新規手法の実証 -
梶本亮一、中村充孝、稲村泰弘、水野文夫、横尾哲也、中谷健、新井正敏、藤田全基
固体物理 **45** 79 2010

T0 チョッパー制御・計測システムの開発
下ヶ橋秀典
平成 21 年度 KEK 技術賞 受賞論文集 KEK Internal **2010-2** 2010